AD-A174 494 HEAT AND MOISTURE BUDGETS OF AN EXTRATROPICAL CYCLONE BASED ON NAVY OPERA (U) NAVAL POSTGRADUATE SCHOOL MONTEREY CA R E RAU JUN 86 1/2

UNCLASSIFIED F/G 4/2 NL

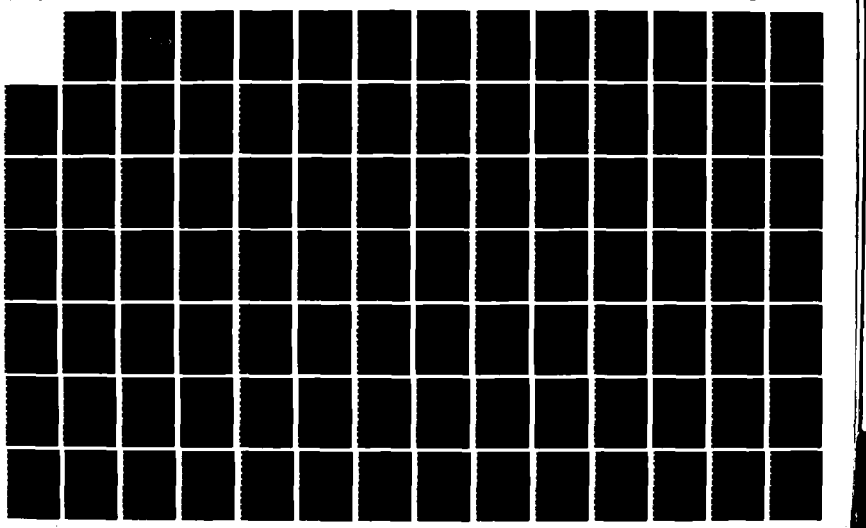

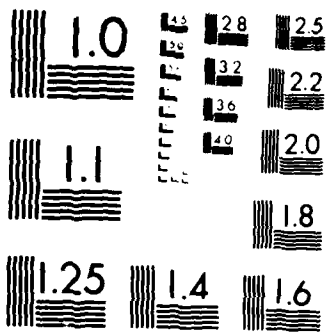

(2)

NAVAL POSTGRADUATE SCHOOL
Monterey, California

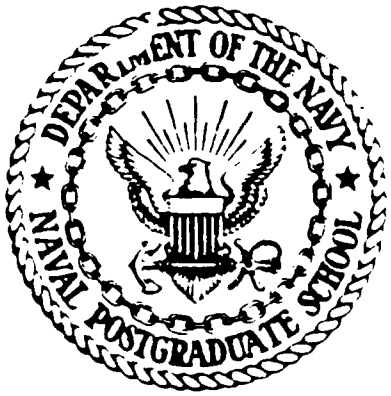

THESIS

HEAT AND MOISTURE BUDGETS OF AN EXTRATROPICAL CYCLONE BASED ON NAVY OPERATIONAL REGIONAL ATMOSPHERIC PREDICTION SYSTEM (NORAPS) ANALYSES AND FORECASTS

by

Robert E. Rau Jr.

June 1986

Thesis Advisor: R. L. Elsberry
Co-Advisor: C.-S. Liou

Approved for public release; distribution unlimited

SECURITY CLASSIFICATION OF THIS PAGE

REPORT DOCUMENTATION PAGE

1a REPORT SECURITY CLASSIFICATION	1b RESTRICTIVE MARKINGS
2a SECURITY CLASSIFICATION AUTHORITY UNCLASSIFIED	3 DISTRIBUTION/AVAILABILITY OF REPORT Approved for public release; Distribution Unlimited
2b DECLASSIFICATION / DOWNGRADING SCHEDULE	
4 PERFORMING ORGANIZATION REPORT NUMBER(S)	5 MONITORING ORGANIZATION REPORT NUMBER(S)
6a NAME OF PERFORMING ORGANIZATION Naval Postgraduate School	6b OFFICE SYMBOL (If applicable) 35
7a NAME OF MONITORING ORGANIZATION Naval Postgraduate School	
6c ADDRESS (City, State, and ZIP Code) Monterey, California 93943-5100	7b ADDRESS (City, State, and ZIP Code) Monterey, California 93943-5100
8a NAME OF FUNDING / SPONSORING ORGANIZATION	8b OFFICE SYMBOL (If applicable)
9 PROCUREMENT INSTRUMENT IDENTIFICATION NUMBER	
8c ADDRESS (City, State, and ZIP Code)	10 SOURCE OF FUNDING NUMBERS

PROGRAM ELEMENT NO	PROJECT NO	TASK NO	WORK UNIT ACCESSION NO

11 TITLE (Include Security Classification)
HEAT AND MOISTURE BUDGETS OF AN EXTRATROPICAL CYCLONE BASED ON NAVY OPERATIONAL REGIONAL ATMOSPHERIC PREDICTION SYSTEM (NORAPS) ANALYSES AND FORECASTS

12 PERSONAL AUTHOR(S)
Rau, Robert E.

13a TYPE OF REPORT	13b TIME COVERED	14 DATE OF REPORT (Year, Month, Day)	15 PAGE COUNT
Master's Thesis	FROM _____ TO _____	1986 June	136

16 SUPPLEMENTARY NOTATION

17 COSATI CODES			18 SUBJECT TERMS (Continue on reverse if necessary and identify by block number)
FIELD	GROUP	SUB-GROUP	Extratropical cyclogenesis, Quasi-Lagrangian Diagnostics (QLD), Heat budget, Moisture Budget

19 ABSTRACT (Continue on reverse if necessary and identify by block number)

Navy Operational Regional Atmospheric Prediction System (NORAPS) analyses and forecasts with 80 km resolution are used to investigate the rapid development of an extratropical cyclone during 28-29 March 1984 over the southeastern United States. The lateral transport of vorticity strongly contributes to the spin-up of the low-level vortex. Diabatic heating and moistening rates are estimated within 500 km of the storm from quasi-Lagrangian heat and moisture budgets and compared with the same rates internally predicted within the NORAPS model. The diagnosed maximum diabatic heating and moistening from analyses agree within 100 mb in elevation and 6 h in time with the model-predicted values. The model-predicted diabatic heating and moistening rates are 50% to 100% greater than diagnosed budget calculations due to an incorrect specification of the moistening and heating rates in NORAPS. Compared to more intense cases of explosive maritime

20 DISTRIBUTION/AVAILABILITY OF ABSTRACT	21 ABSTRACT SECURITY CLASSIFICATION
☒ UNCLASSIFIED/UNLIMITED ☐ SAME AS RPT ☐ DTIC USERS	UNCLASSIFIED
22a NAME OF RESPONSIBLE INDIVIDUAL R. L. Elsberry	22b TELEPHONE (Include Area Code) (408)-646-2373
	22c OFFICE SYMBOL Code 63 Es

DD FORM 1473, 84 MAR 83 APR edition may be used until exhausted
All other editions are obsolete

SECURITY CLASSIFICATION OF THIS PAGE

19. cont.
cyclogenesis, the higher level and lower magnitude of maximum diabatic heating is consistent with the weaker deepening rate and continental nature of this storm.

Approved for pu ic release; distribution is unlimited.

Heat and Moisture Budgets of an Extratropical Cyclone Based on Navy Operational Regional Atmospheric Prediction System (NORAPS) Analyses and Forecasts

by

Robert E. Rau, Jr.
Lieutenant, United States Navy
B.S., St. Louis University, 1977

Submitted in partial fulfillment of the
requirements for the degree of

MASTER OF SCIENCE IN METEOROLOGY AND OCEANOGRAPHY

from the

NAVAL POSTGRADUATE SCHOOL
June 1986

Author: Robert E. Rau, Jr.
Robert E. Rau, Jr.

Approved by: R. L. Elsberry
R. L. Elsberry, Co-Advisor

C. S. Liou
C. S. Liou, Co-Advisor

R. J. Renard
R. J. Renard, Chairman,
Department of Meteorology

John N. Dyer
John N. Dyer,
Dean of Science and Engineering

ABSTRACT

Navy Operational Regional Atmospheric Prediction System (NORAPS) analyses and forecasts with 80 km resolution are used to investigate the rapid development of an extratropical cyclone during 28-29 March 1984 over the southeastern United States. The lateral transport of vorticity strongly contributes to the spin-up of the low-level vortex. Diabatic heating and moistening rates are estimated within 500 km of the storm from quasi-Lagrangian heat and moisture budgets and compared with the same rates internally predicted within the NORAPS model. The diagnosed maximum diabatic heating and moistening from analyses agree within 100 mb in elevation and 6 h in time with the model-predicted values. The model-predicted diabatic heating and moistening rates are 50% to 100% greater than diagnosed budget calculations due to an incorrect specification of the moistening and heating rates in NORAPS. Compared to more intense cases of explosive maritime cyclogenesis, the higher level and lower magnitude of maximum diabatic heating is consistent with the weaker deepening rate and continental nature of this storm.

TABLE OF CONTENTS

LIST OF TABLES

LIST OF FIGURES

ACKNOWLEDGEMENTS

I would like to thank Dr. R. Hodur of the Naval Environmental Prediction and Research Facility (NEPRF), who generously provided the data set. I would like to express my deepest gratitude and heart-felt appreciation to my co-advisor, Prof. C.-S. Liou, who unselfishly spent many long hours helping me sort through various computer coding aspects and guiding me in the right direction. I am truly indebted to my co-advisor, Prof. R. Elsberry, whose superb guidance and constructive criticism made this thesis possible. I especially value the education I have received here at NPS and would like to thank my professors who have taught me to think more critically over the past two years. Last, I would like to mention the special support and patience of my wife, Debbie, and my children, Joseph and Rachel, without whom this thesis would have not been possible.

I. INTRODUCTION

Extratropical maritime cyclones pose extremely hazardous navigational and seaworthiness problems for Naval operations and commercial shipping. To ensure safe maritime operations during heavy weather conditions, advance planning is required to set the heavy weather bill, which includes ballasting the ship, respotting aircraft to the hangar deck, and securing every compartment for heavy weather. An accurate prediction of storm location and intensity is needed 36-48 hours in advance to allow the operational commander time to manuever the task force to avoid the predicted region of high winds and hazardous seas.

While numerical weather prediction models have had considerable success in the prediction of many synoptic-scale systems, they perform rather poorly in predicting the explosive development of maritime cyclones (Sanders and Gyakum, 1980). Explosive cyclogenesis is defined as the decrease of 24 mb per 24 hours in the central sea-level pressure (SLP) before adjusting to a latitude, φ, by multiplying by $\sin \varphi / \sin 60^{o}$. The highest frequency of explosive maritime cyclogenesis cases in the Northern Hemisphere occurs over the western ocean boundary currents (Gulf Stream and Kuroshio) immediately east of continents (Sanders and Gyakum, 1980), where strong sea-surface temperature (SST) gradients enhance the low-level baroclinity. The Navy Operational Regional Atmospheric Prediction System (NORAPS) has shown a better success rate than the Navy Global Atmospheric Prediction System (NOGAPS) in predicting the location and intensity of the cyclone center SLP for a given set of explosive maritime cyclogenesis cases (R. Hodur, NEPRF, personal communication). The reason for this could be that the higher spatial and vertical resolution of the

regional model is able to better resolve the physical processes occurring within the storm environment. However, a need still exists for the improved prediction of these explosive cyclogenesis events.

Maritime cyclones are also very important for air-sea interaction processes. The strong winds around these cyclones may cause a deepening of the oceanic mixed layer due to the downward transfer of momentum from the atmosphere to the ocean. This fact has important implications for acoustic propagation in the upper ocean, which anti-submarine warfare (ASW) and submarine commanders may use to tactically exploit their situation. The strong cold advection to the rear of the maritime cyclone can produce positive temperature gradients (temperature increasing with depth) in the upper ocean and lead to strong surface ducting of acoustic energy which also can be exploited tactically. In the future, regional oceanographic models may need to be coupled to regional atmospheric models to predict correctly the ocean thermal structure response to atmospheric forcing.

This thesis is a study of an extratropical cyclone which formed over the southern United States on 00 GMT 28 March 1984 and moved rapidly off the eastern coast of the United States by 12 GMT 29 March 1984. Although this storm is not purely maritime in nature and barely meets the criterion for explosive cyclogenesis, it can serve as a prototype for future maritime cases that were observed in the Genesis of Atlantic Lows (GALE) field experiment during 1986. GALE, which was jointly sponsored by the Office of Naval Research (ONR), National Science Foundation (NSF) and National Aeronautics and Space Administration (NASA), is expected to provide improved data sets over land and the ocean for study of maritime cyclogenesis. The relatively dense upper-air network over land in GALE will provide observations of the horizontal and vertical structure of the atmosphere. This

pre-GALE cyclone case was previously studied by Toll (1986), who used a linear model to investigate the instability mechanism responsible for the cyclone growth. He concluded that a mixed barotropic-baroclinic instability was responsible for the growth of a mesoscale perturbation imbedded within the larger scale cyclonic circulation.

The emphasis of this thesis will be on the diabatic aspects involved in the cyclone growth and, in particular, the role of thermodynamic and moisture effects. Diabatic processes can provide an additional energy source on the smaller scales that may account for the rapid intensification of the cyclone. The NORAPS analyses and forecasts constitute the data set for various budget calculations. A 00 GMT 28 March 1984 base time is used for the model run. The NORAPS forecast fields are available at six hourly intervals from 00 GMT 28 March until 12 GMT 29 March 1984. The NORAPS analyses are only available every 12 hours during this period.

Quasi-Lagrangian Diagnostics (QLD), which was originally developed by Johnson and Downey (1975) and applied to numerical forecasts of extratropical cyclone cases by Wash (1978), are applied to examine heat, moisture, mass and vorticity budgets. Several previous theses (Calland, 1983; Cook, 1983) have used the QLD technique to explore vorticity and mass budgets of various maritime cyclones. Bosse (1984) studied the role of diabatic effects on explosive maritime cyclogenesis using NOGAPS, which has a coarser spatial and vertical resolution than NORAPS. These budget studies investigate the mean properties of the cyclone both spatially and temporally, and determine the relative contributions of the terms at various stages of cyclone growth. Inherent in this technique is a great amount of areal, vertical and time averaging over the budget volume which is centered on the cyclone. Because subdivisions are not made

within the cyclone, the results of the budget study will not reveal processes within sub-areas of the cyclone.

The QLD technique uses an isobaric spherical coordinate system which is translated with the storm. Since the radius of the storm is small compared to the radius of the earth, the budget volume can be approximated by a cylinder. Horizontal advection associated with storm translation is isolated from the advection in the moving coordinate system, so the divergence of the transport (flux) can be associated with cyclone development processes. Vertical distributions, lateral exchanges and sources and sinks of cyclone properties resulting from purely developmental processes are then analyzed.

This thesis is part of a larger investigation into the nature and physical processes of maritime extratropical cyclogenesis, which has an overall objective of improving numerical weather prediction over the ocean. The objectives of this thesis are:

- Investigate the various properties of the NORAPS model and identify areas where the model does not realistically represent the atmosphere;
- Document the mean thermal and moisture structure of an explosive cyclogenesis case using QLD for both the forecasts and analyses;
- Assess the relative contribution of the terms of the thermodynamic and moisture equations at various stages during cyclone growth, and the horizontal and vertical distributions of those terms;
- Compare the moisture budget estimates of the diabatic heating rates with the heat budget for the forecast case; and
- Compute mass and vorticity budgets during the cyclone's evolution to determine the vertical structure and dynamical contributions to rapid cyclogenesis.

A brief survey of the literature on the role of latent heat release as it affects extratropical cyclones is given in Chapter II. A synoptic overview of the NORAPS analyses and forecasts in conjunction with other Numerical Weather Prediction (NWP) models is presented in Chapter III. Mass and vorticity budget results are discussed in Chapter IV.

The central focus of this thesis is contained in Chapter V where the heat and moisture budget results are discussed. An important discussion is found in Appendix C which summarizes revised heat and moisture budget results after incorporating corrections to a test version of the NORAPS model. Conclusions and recommendations for further study are outlined in Chapter VI.

II. LITERATURE SURVEY

A. GENERAL

Thermal energy and differential vorticity advection are important constituents in the growth of an extratropical cyclone. Concentration of thermal advection forces greater vertical velocities and contributes to storm intensification. This is primarily due to a conservative adiabatic type process. However, the other component of thermal energy is the diabatic heating term, which if concentrated, can promote storm intensification. As diabatic heating is not directly measured in the atmosphere, heat and moisture budgets are a technique of inferring its contribution. Diabatic effects include surface sensible heat fluxes, latent heat release and radiation. How these effects are parameterized in a particular model is critical to the prediction of cyclone development. These physical effects must be studied to gain a clearer understanding of the maritime extratropical cyclone. Maritime cyclones generally have a larger moisture source at the lower boundary which contributes to earlier or more rapid intensification over the ocean than over land. Two different methodologies may be used to study the impact of moisture and latent heating on cyclone growth: sensitivity studies using numerical models and diagnostic studies using real or model-simulated data.

B. NUMERICAL STUDIES

Theories prior to 1960 regarding latent heat release were mainly qualitative in nature. Danard (1964) was one of the first to estimate the effect of latent heat release on vertical velocity through horizontal variations in the static stability. The results indicated the latent heat

release served to increase the vertical velocity of rising air parcels. He conjectured that latent heat release was a mechanism for cyclone intensification rather than initiation, since a pre-existing disturbance had to be present for the deep convection to occur. Danard (1966) later modeled the vertical distribution of latent heat release as a parabolic function with a maximum in the middle of the troposphere. Anthes et al. (1983) and Gyakum (1983b) suggest that a lower tropospheric maximum in the vertical heating profile is more favorable for cyclone intensification. Qualitatively, this is consistent since the lower maximum in vertical velocity equates to a stronger horizontal convergence in the lower levels, which translates into a greater rate of low-level vorticity generation.

Gall (1976) investigated the effects of latent heat release in growing baroclinic waves with dry and moist versions of a general circulation model (GCM). He found the growth rate of the cyclone-scale wave (wavenumber 15) was approximately doubled in the moist experiment compared to the growth rate in the dry experiment. Furthermore, the structure of wavenumber 15 was quite different in the two experiments. At the time wavenumber 15 reached its maximum development, the moist model had maxima of kinetic energy at 500 mb and at the earth's surface, while the dry model had a single maximum at the earth's surface. The difference in the kinetic energy spectrum between the two atmospheres must be explained by the release of latent heat. Gall (1976) attributed this difference to the moist convective adjustment by which the temperatures at the middle and upper levels are increased relative to those at the earth's surface. He also found a difference in the 500 mb temperature perturbations east and west of the most intense surface lows. In the moist experiment, the magnitude of the 500 mb warm temperature perturbation east of these lows exceeded

the magnitude of the cold temperature perturbation west of these lows by 2 to 5°K, whereas the perturbations on either side of these lows were approximately the same in the dry experiment.

Mak (1982) discussed moist quasi-geostrophic (Q-G) baroclinic instability by generalizing the analytic theory of Q-G dynamics in terms of condensational heating. Since the time and length scales of the precipitation pattern associated with a typical extratropical cyclone were comparable to those of the primary circulation, there was likely a close direct feedback between the heating and circulation. This formulation was somewhat similar to the Conditional Instability of the Second Kind (CISK) theory proposed jointly by Charney and Eliassen (1964) and Ooyama (1964). Mak's premise was the moisture supply for the condensational process in a baroclinic wave was sustained by the low-level convergence field of the wave. The condensational heating was parameterized in terms of the vorticity field of the disturbance rather than the vertical velocity. This parameterization was more effective for low frequency disturbances or those with the longer wavelengths. Mak's results revealed that as the heating intensity parameter was increased, the growth rate of the unstable wave significantly increased, the wavelength significantly decreased and the phase speed increased. His results supported the general notion that the baroclinic forcing in a disturbance can organize the condensational heating on a scale comparable to the wave.

Chang et al. (1982) have simulated the cyclone system with and without latent heating using a regional fine mesh (140 km) model encompassing the United States. In the dry simulation, the model failed to predict the formation of a closed circulation throughout the depth of the troposphere and a pronounced northwest-southeast horizontal tilt of the

upper-level trough. The moist simulation produced both of these features which were in good agreement with NMC analyses. The significance of the latent heat release was illustrated by subtracting the predicted dry values from the corresponding moist values. At 500 and 300 mb, the largest positive temperature differences were confined to the areas of large precipitation, which indicates that latent heating was the main factor contributing to this positive temperature difference. However, the moist model had lower 700 mb temperatures than the dry model. Their results indicated that latent heat release stabilized the middle and upper troposphere and reduced the large-scale horizontal temperature gradient or baroclinity. They also postulate that the increased circulation in the lower troposphere caused the formation of a low-level jet.

Chang et al. (1984) also investigated the latent heat induced energy transformations during cyclogenesis. Although condensational processes were not efficient in increasing the total potential energy of the model atmosphere, latent heat acted as a catalyst to enhance the conversion of potential to kinetic energy within the mid-latitude cyclone. The most significant response to heating appeared in the lower troposphere. Latent heating changed the configuration of the motion field from a large-scale pattern with pronounced vertical shear into a small-scale feature with marked horizontal shear which served to reduce the sub-grid scale dissipation below 500 mb. Additionally, the enhancement of ageostrophic generation of kinetic energy provided an important source of energy for the maintenance of the lower tropospheric circulation.

Sardie and Warner (1983) included the effects of latent heating and baroclinity in an analytic three-layer Q-G model to investigate the mechanism of polar low development. This mesoscale phenomenon has wavelengths of 500-1000 km, has a

range of vertical scales and develops within the cold air behind a cold front. They integrated their model for seven real-data cases using three modes, including: a dry baroclinic case (no latent heating); a moist baroclinic case in which diabatic heating is partitioned between the convective and non-convective parts; and the case in which latent heating is solely caused by convective clouds, referred to as CISK. Their results indicate Atlantic polar lows develop due to a CISK type mechanism and shallow baroclinity, while moist baroclinity is the dominant mechanism for Pacific polar lows. Their results on the Atlantic polar lows are consistent with Rasmussen (1979), who argues that some type of CISK mechanism must be operating for these lows which have the smallest horizontal scales.

Anthes et al. (1983) performed a series of numerical simulations using the Queen Elizabeth II storm. The results from the latent heating investigation indicated the evolution of the model storm was not significantly affected by latent heating in the early stages. As the storm intensified and vertical motions became stronger, latent heating played a greater role in enhancing the development. Gyakum (1983) also demonstrated that quasi-geostrophic dynamics could not account for the observed intensity of the cyclone during the explosive stage. He reasoned that the diabatic heating in this case was responsible for the extreme thickness changes in the lower part of the column. He calculated the residual warming of the column over the surface low center to be 16^{o}C in a 12-hour period.

C. BUDGET AND DIAGNOSTIC STUDIES

The purpose of budget studies is to diagnose terms such as diabatic heating and precipitation by properly accounting for all the sources and sinks through the calculation of terms in the thermodynamic and moisture conservation equations. Kuo and Anthes (1984) state that budget calculations

are subject to errors due to sampling, measurement, finite differencing and objective analysis. Errors associated with wind measurements can introduce substantial errors in the calculation of divergence and vertical velocity, which are two of the most crucial terms in the budget calculations. Another factor which can introduce errors is spatial and temporal interpolation performed during the objective analysis. Therefore, a detailed error analysis is of particular importance to budget studies, since the residual of the calculation is influenced by all of the errors mentioned above. The residual also includes real, sub-grid scale physical effects, which can be interpreted only after the contribution of errors is isolated.

Kuo and Anthes (1984) note that the mean divergence removal technique (O' Brien, 1970) generally has a stronger influence on the heat budget than the moisture budget. Because the moisture decreases rapidly with height, erroneous vertical motions at upper levels cause smaller errors in the moisture budget. In their study, they found area-averaged errors in the heat and moisture budgets of about 5^{0}C and 2 g/kg, respectively, for a temporal scale of 6 hours and a spatial scale of 550 x 550 km. The vertically-integrated changes due to radiation, sensible heat flux and moisture changes due to evaporation are small compared to the inherent root mean square (rms) errors in the budget calculation. In general, the above errors are small compared to those due to latent heating during the mature stage of convection, which are typically 20-30^{0}C/day and 10 g/kg/day.

Smith et al. (1984) established the significance of latent heat release in developing extratropical cyclones by separating the vertical motion forced by latent heat release from the total vertical motion. The total vertical motion was calculated using the kinematic method, while the

vertical motion due to latent heat release was determined from the omega equation. The ratio of the vertical motion due to latent heat to the total vertical motion was then calculated. In their case study, a mid-period maximum of 90% below 900 mb suggested the increased latent heat release had a particularly strong influence on below-cloud vertical motions. Additionally, a comparison was made of the vertically-integrated convective and stable latent heat release. The total latent heat release was dominated by the convective components, even though this was a mid-winter storm over the north-central United States. A key finding was that the maximum rate of development occurred after the time of maximum latent heating.

Liou and Elsberry (1985) performed a QLD study of an explosive maritime cyclogenesis case over the northwest Pacific Ocean using a research version of the Univerisity of California at Los Angeles (UCLA) GCM. Their results revealed area-averaged heating rates of 25-30°C/day with the maximum level at 600-700 mb and that diabatic heating was caused by latent heat release from stable condensation and middle-level convection. Additionally, they found that the sea-level pressure (SLP) deepening rate was highly correlated with the diabatic heating rate.

A diagnostic moisture analysis of a meso-β scale thunderstorm environment was performed by Fuelberg et al. (1986). A highly refined rawindsonde network of 75 km spacing (over Oklahoma) with 3 hourly soundings was used. A stationary 15 x 13 budget grid was formed with 25 km horizontal spacing. Data were available every 50 mb from 900 to 150 mb with the exception of specific humidity which was not reported above 350 mb. Coarser resolution (synoptic) data were available from the National Weather Service (NWS) rawinsonde network which allowed a separate budget calculation for comparison with the finer resolution data. Their

results showed that horizontal moisture convergence was the most important term in the budget, especially in the surface to 850 mb layer. Most of the horizontal flux convergence of moisture was attributed to the velocity convergence, with moisture advection being of secondary importance. The horizontal moisture convergence increased an order of magnitude when the storms were occurring. The residuals indicated vapor accumulation prior to the storm activity, but reversed to condensation/precipitation once the storms began. The residuals also increased an order of magnitude as in the horizontal flux term. A comparison with the budget based on the synoptic data showed the magnitude of terms in the mesoscale budget approached an order of magnitude greater than the synoptic-scale values near the time of the storms.

III. SYNOPTIC OVERVIEW AND NWP PERFORMANCE

A. GENERAL

A discussion of various model forecasts and verifying analyses is presented to document the synoptic evolution of the 28-29 March 1984 storm. This storm is frequently referred to as the Carolinas storm as a particularly severe outbreak of tornadoes caused widespread damage in North and South Carolina. Various meteorological aspects will be highlighted and physical mechanisms presented to explain the growth of the cyclone. Significant differences between the model forecast and verifying analyses will be mentioned. For convenience of comparison, the figures are grouped at the end of the chapter. In this study, the NORAPS surface analyses are used as the basis for verifying the corresponding NORAPS forecast. The NORAPS surface analysis procedure includes using an 89 x 89 hemispheric grid (268 km) to interpolate to the higher resolution (80 km) NORAPS grid. A regional update cycle uses the 12 h NORAPS forecast fields to provide the "first guess" for the NORAPS forecast. The National Meteorological Center (NMC) analyses, in particular, provide a different interpretation since they are hand-drawn and subjective in nature as opposed to NORAPS objective analyses. These NMC analyses also depict much more of the mesoscale detail within the larger scale cyclonic circulation. Mesoscale low centers, which have a horizontal scale of 100-200 km, are very evident in the series of NMC analyses for this storm. Toll (1986) used rawindsonde observations and a NORAPS analysis at 00 GMT 29 March 1984 to construct cross-sections for a linear stability analysis to investigate the instability mechanisms associated with cyclone growth.

The tracks of the storm for both the NORAPS forecast (every 6 h) and analyses (every 12 h) from 00 GMT 28 March 1984 until 12 GMT 29 March 1984 are presented in Fig. 3.1a. The model-predicted track of the cyclone agrees well with the analyzed position until 00 GMT 29 March 1984. During the following 12 h, the model-predicted track departs significantly from the analyzed track of the cyclone to the south. The NORAPS predicted cyclone intensity (Fig. 3.1b) agrees quite well with the analyzed intensity, especially at the later time periods.

B. NORAPS ANALYSIS - 00 GMT 28 MARCH 1984

The initial surface analysis (Fig. 3.2a) at 00 GMT 28 March 1984 depicts a broad 990 mb center of low pressure over eastern Texas. The corresponding 1000-500 mb thickness pattern (Fig. 3.2b) reveals moderate warm advection over the southeastern U.S. and strong cold advection across the southwestern U.S. The low-level warm advection patterns at 925 and 850 mb (not shown) have two distinct thermal gradient zones: one along the Gulf Coast and the other is displaced much farther north through the Ohio Valley. This lack of concentrated low-level baroclinity in advance of the storm is consistent with a weak upward vertical motion pattern. A 500 mb pressure trough (Fig. 3.2b) is located along 100°W and a thermal trough lags the height trough by a quarter of a wavelength. This pattern satisfies a necessary condition for baroclinic instability. The broad elongated trough at 500 mb indicates a fairly weak relative vorticity pattern due to curvature effects alone. The 925, 850 and 700 mb analyses (not shown) depict a short-wave trough near 35°N, 110°W (west of the 500 mb trough axis) that rotates through the elongated trough at 500mb. The wind analysis at 300 mb (Fig. 3.3) has a 60 m/s jet streak in the vicinity of western Louisiana. The strong cyclonic shear north of this jet streak contributes heavily to the positive relative

vorticity at 300 mb since the curvature component is weak in this region as noted above. The surface low center is located in the right-rear quadrant of this jet, which is favorable for surface deepening due to upper-level divergence.

C. NWP PERFORMANCE

NORAPS forecasts and verifying analyses will be emphasized in this section. Other models and analyses will be introduced during the discussion to highlight the high degree of variability found in these products. Physical interpretations for the differences among the various models will be given. It is important to note that a 25-point filter is applied eight times to the NORAPS forecast output fields for display purposes, which may tend to smooth out some of the forecast mesoscale structure. A technique called Fields by Information Blending (FIB) is performed to produce the NORAPS surface analyses using an 89 x 89 hemispheric grid. This technique also results in a smoothed analysis.

The NORAPS model forecast (Fig. 3.4a) at 06 GMT 28 March 1984 fills the surface low center 4 mb to 994 mb as it moves northeast to 33°N, 90°W. Although a corresponding NORAPS analysis is not available to verify the filling of the low during this 6 h period, a NMC analysis valid at this time does not indicate this filling tendency (taking into account the diurnal variation in pressure). The low-level warm advection pattern (not shown) is rather diffuse while strong cold air advection continues over Texas. The 500 mb forecast (Fig. 3.4b) depicts a more elongated trough than in the analysis. This is a consequence of the short wave trough discussed above having translated into the western part of the trough. The predicted 300 mb wind maximum (not shown) has weakened by about 10 m/s from the analysis. The filling tendency predicted by the NORAPS forecast may be attributed

to adjustments in the initial mass and momentum fields which occur in the first few hours after the time integration of the model.

At 12 GMT 28 March 1984, the NORAPS surface forecast (Fig. 3.5a) depicts a 990 mb low center near 36°N, 87°W, whereas the corresponding analysis (Fig. 3.5b) has a 987 mb center near 36°N, 89°W. This 3 mb pressure difference between the analysis and forecast is the largest difference during the forecast. Both the model and analyzed low tropospheric fields depict two distinct thermal gradient regions in advance of the low center which form into a single zone to the rear of the low. The NORAPS 500 mb forecast (Fig. 3.6a) underestimates the intensity of the trough by 60 m. The 300 mb wind field (not shown) verifies well with a 60 m/s jet over southern Louisiana in both the forecast and analysis.

In the 18 GMT 28 March 1984 NORAPS forecast (Fig. 3.7a), the surface low deepens to 987 mb and translates eastward to 36°N, 85°W. Greater organization is seen in the low-level thermal field (not shown) in advance of the low which indicates the formation of a warm front in the lower troposphere. The 500 mb trough axis translates to 95°W with 60 m height falls occurring at the base of the trough (Fig. 3.7b). The 300 mb wind field (Fig. 3.8) indicates an interesting pattern of an intensifying jet streak (in the northwesterly flow) associated with an upper-level trough downstream of the major upper-level trough being investigated. Another 60 m/s jet streak is associated with the major upper-level trough over the Gulf of Mexico. The developing surface low is in the right-rear and left-front quadrants of the two jet streaks previously mentioned. The expected divergence in these quadrants of the jets can enhance the surface development through removal of mass aloft.

In the 00 GMT 29 March 1984 NORAPS forecast (Fig. 3.9a), the surface low deepens to 983 mb and tracks eastward to 81°W. The verifying analysis (Fig. 3.9b) shows excellent agreement with the model with respect to position and intensity (Fig. 3.1). The 1000-500 mb thickness pattern (Fig. 3.9a and Fig. 3.9b) indicates strong cold advection along the Gulf Coast and strong warm advection along the eastern seaboard north of Cape Hatteras in both the forecast and analysis. The predicted 500 mb trough does not verify well as the central value is 60 m too high and the formation of a closed low is not predicted (Fig. 3.10a). Whereas a 60 m/s jet streak is predicted (Fig. 3.11a) along the Gulf Coast, the analyzed maximum is actually 80 m/s (Fig. 3.11b). The extensive outbreak of severe weather, including 22 tornadoes, in the Carolinas occurs within a 6 h period centered on 00 GMT 29 March 1984, as outlined by Ferguson et. al. (1986).

Another model, the Mesoscale Atmospheric Simulation System (MASS), developed by NASA, was used by Kocin et al. (1984) to simulate the severe weather outbreak across the Carolinas. This model's smaller grid size (50 km) and extensive physics package can sometimes capture the dynamical interactions and diabatic processes which force mesoscale features. The model was initialized at 12 GMT 28 March 1984 and integrated 15 hours (to 03 GMT 29 March 1984) to study the evolution of a mesoscale low that was involved in triggering the severe weather. Forecasts are available every 3 hours. A time series of the MASS forecast and NMC analyses is presented in Fig. 3.12. A significant feature of this model prediction was the formation of a mesoscale low center between 18-21 GMT 28 March 1984 over eastern Alabama, which moved rapidly northeast and was associated with the severe weather event in the Carolinas. Although this model prediction was 3 h too slow in the prediction of

this mesoscale feature and lagged the analyzed low center by 250 km, it more accurately modeled the observed state than NORAPS. The possible reasons why MASS produced a more accurate forecast than NORAPS are that its extensive physics package and smaller grid size enabled it to capture some of the low-level forcing mechanisms such as the surface heat fluxes and latent heat release on the smaller scales, which could not be adequately resolved in the NORAPS prediction. Kocin et al. (1984) attribute model deficiencies in MASS to a poor initial data base at jet stream level where several critical wind obsevations were missing.

The 06 GMT 29 March 1984 NORAPS forecast (Fig. 3.13a) continues the linear decrease in the central sea-level pressure to 978 mb. However, a marked departure in the track occurs (Fig. 3.1) as the storm is predicted to decelerate and move southeast. The southeast movement may be a delayed response in NORAPS to some mesoscale forcing which formed a mesoscale low center south of the major low at 21 GMT 28 March 1984 (Fig. 3.12). The model cannot adequately resolve the mesoscale forcing mechanism and therefore, decelerates the major low center and steers it southeast. A separate integration of NORAPS in which the convective component of the precipitation is eliminated has a more rapid movement of the low center to the northeast at the corresponding time. Strong latent heat release in a localized area may tend to decelerate the storm. The 500 mb NORAPS forecast (Fig. 3.13b) depicts a closed 5400 m low just to the west of the surface low. The 300 mb predicted wind field (not shown) continues to position the jet streak along the Gulf Coast, although it has probably translated east of the trough axis based on the severe weather outbreak in the Carolinas. The incorrect prediction of the translation of this jet streak may have also contributed to the erroneous surface low deceleration and movement to the east-southeast.

In the 12 GMT 29 March 1984 NORAPS forecast (Fig. 3.14a), the low center of 974 mb verifies well with respect to the NORAPS analyzed intensity of 973 mb. However, the forecast position is 360 n mi southwest of the analyzed position. The NMC surface analysis at this time depicts a 966 mb surface low center off the eastern coast of Maryland, which correlates well with the NORAPS analyzed position, but is 7 mb lower in pressure. The circulation of the storm is quite extensive and covers the entire eastern half of the U. S. and western Atlantic. The low-level thickness pattern (Fig. 3.14b) indicates warm advection extends around the low center and into the northwest quadrant. The system is becoming nearly vertically stacked in both the forecast and analysis, which indicates it has reached maximum intensity and has converted most of the available potential energy to kinetic energy. Although the 300 mb analysis (not shown) has a 70 m/s jet streak east of Georgia, a 60 m/s jet streak remains quasi-stationary over the northern Gulf of Mexico in the prediction.

A single 36 h Limited Fine Mesh (LFM) forecast valid at 12 GMT 29 March 1984 is available for comparison with the NORAPS model. A 974 mb low center is predicted by the LFM model to be in central Virginia, which is somewhat better than the NORAPS 36 h predicted location in southern North Carolina (Fig. 3.14a). The LFM forecast intensity of the low center (974 mb) was the same as the NORAPS forecast. This is 8 mb too high according to the NMC analysis but only 1 mb too high according to the NORAPS analysis. The LFM 500 mb forecast trough verified extremely well with a predicted 5300 m closed low center, whereas a 5280 m center was analyzed. The accumulated 6 h precipitation chart has large "bullseye" values in excess of two inches. Both NORAPS (see Fig. 5.14) and LFM models overpredict precipitation for this storm.

NOGAPS is a global model of relatively coarse resolution (2.4° lat by 3.0° long) that is designed primarily for longer-range weather prediction over the open ocean. This model is not able to resolve the mesoscale detail which the regional models can achieve. The NOGAPS 36 h forecast valid at 12 GMT 29 March 1984 had a 976 mb surface low center over western Virginia, whereas the analyzed position was some 500 n mi farther east. The intensity of the predicted low was 10 mb too high compared to the NMC analysis and 3 mb too high compared to the NORAPS analysis. It is difficult to determine whether numerical truncation or physical errors accounted for the slower predicted movement of the cyclone in NOGAPS.

D. SUMMARY

The intensity of the storm is predicted quite well by the NORAPS model as verified by the NORAPS analyses. The track of the low is also predicted fairly well for the first 24 hours although a large position error is evident at 36 hours. A sharp difference exists in the low center intensities at 12 GMT 29 March 1984 between the NORAPS and NMC analyses, which most likely can be attributed to the smoothing in the NORAPS objective analysis scheme and the coarse resolution of 268 km in the surface analysis. It is difficult to isolate whether the poor track prediction during the last 12 h was a result of NORAPS incorrectly responding to some mesoscale forcing mechanism occurring to the southwest of the major low (as in the MASS model) or whether it overresponded to convection occurring in the vicinity of the low. The organization of the multiple low centers into a consolidated center by 12 GMT 29 March 1984 suggests orographic forcing was responsible for a large portion of the mesoscale detail while the the storm was in the vicinity of the Appalachians.

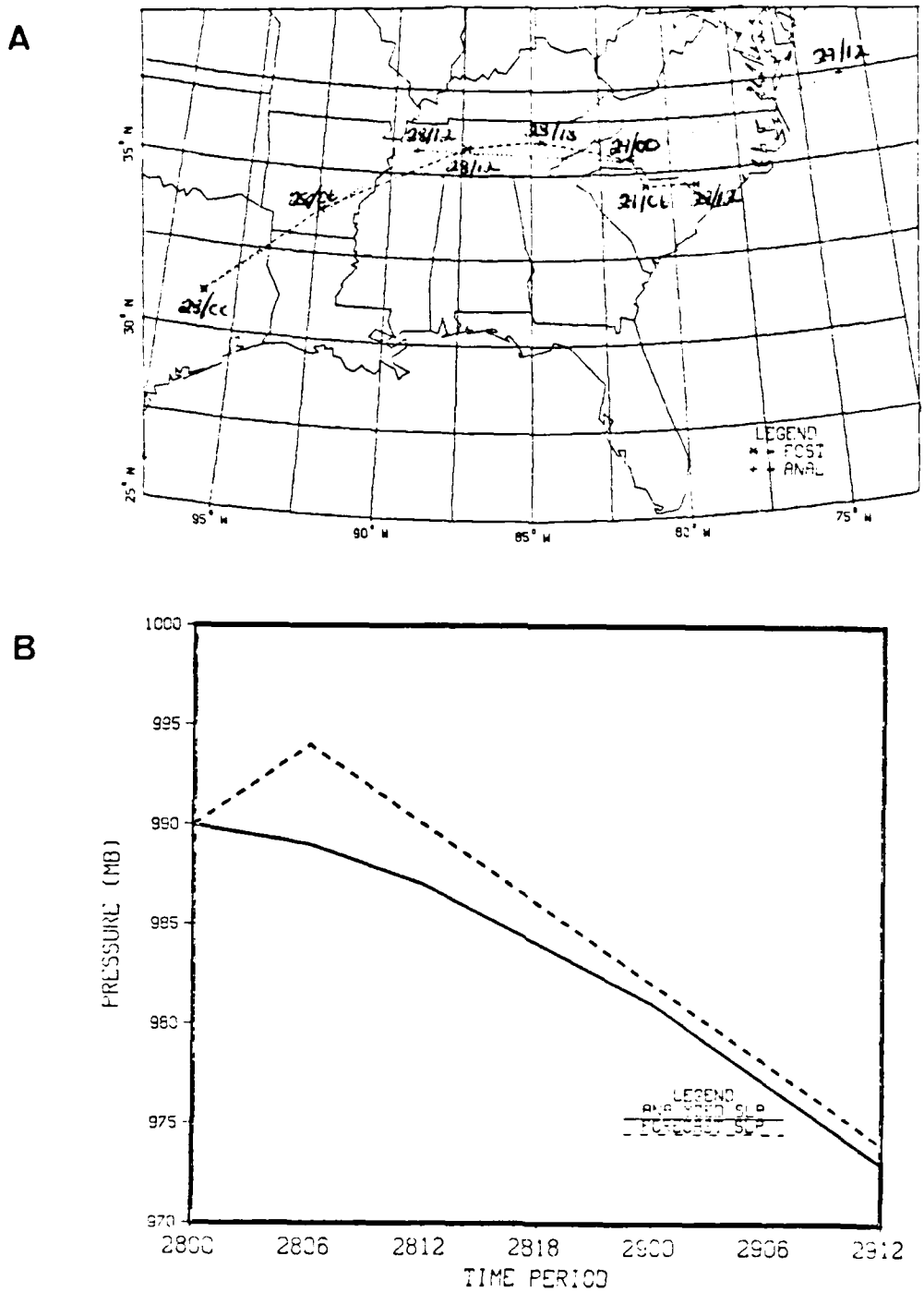

Fig. 3.1 (A) NORAPS analyzed (dotted) and forecast (dashed) surface low track for 28-29 March 1984. (B) NORAPS analyzed (solid) and forecast (dashed) sea-level pressure (mb) for low center above. Times are specified by date (first two digits) and hours (second two digits) in Greenwich Mean Time.

A

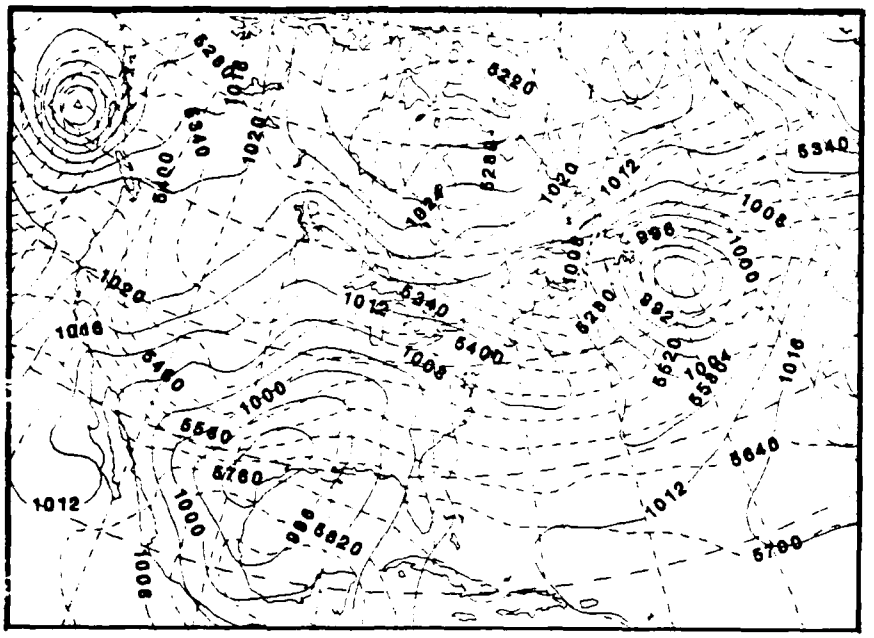

B

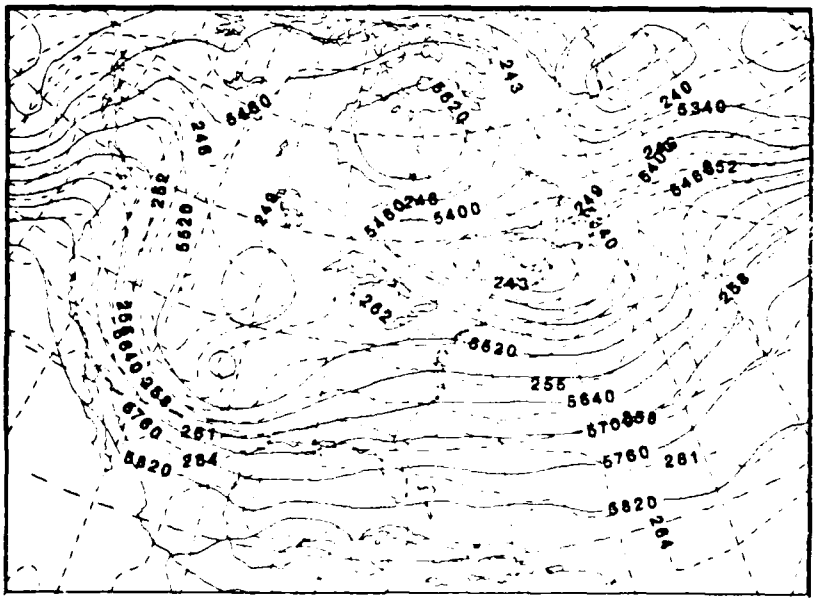

Fig. 3.2 (A) NORAPS surface analysis at 00 GMT 28 March 1984, sea-level pressure in mb and 1000-500 mb thickness (dashed) in gpm. (B) Corresponding 500 mb analysis with heights (solid) in gpm and isotherms (dashed) in degrees Celsius.

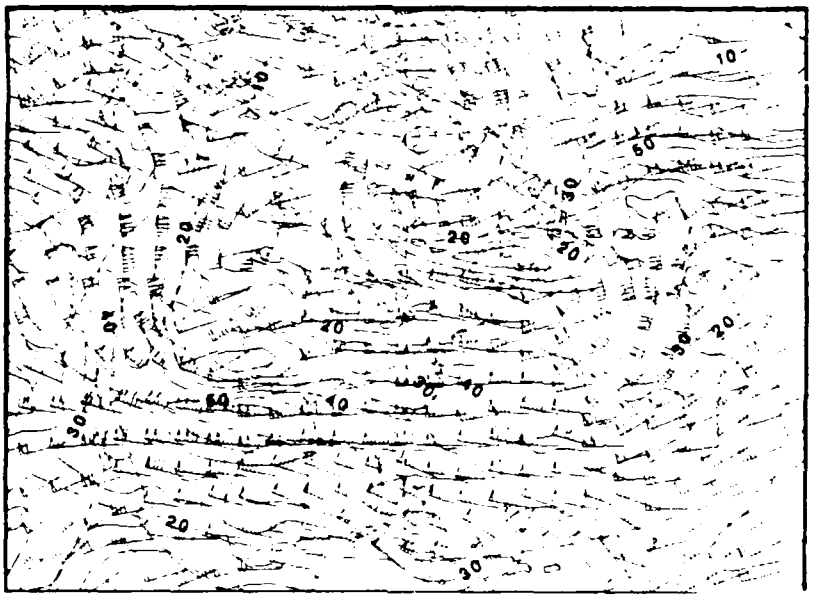

Fig. 3.3 NORAPS 300 mb wind/isotach analysis at 00 GMT 28 March 1984. Contour interval is 10 m/s. Pennant represents 50 m/s wind, full line is 10 m/s and half line is 5 m/s.

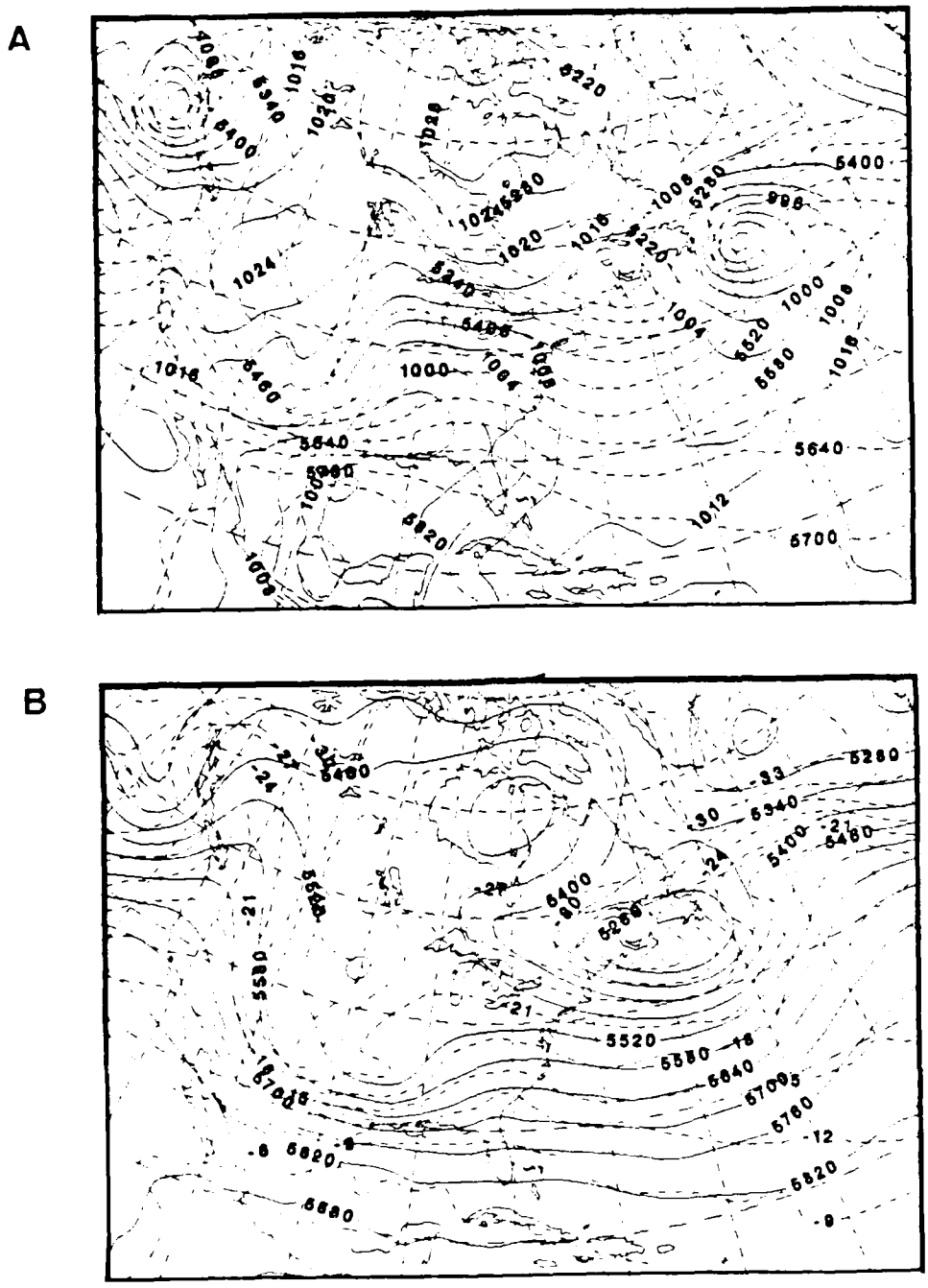

Fig. 3.4 As in Fig. 3.2, except for 06 GMT 28 March 1984 forecast fields.

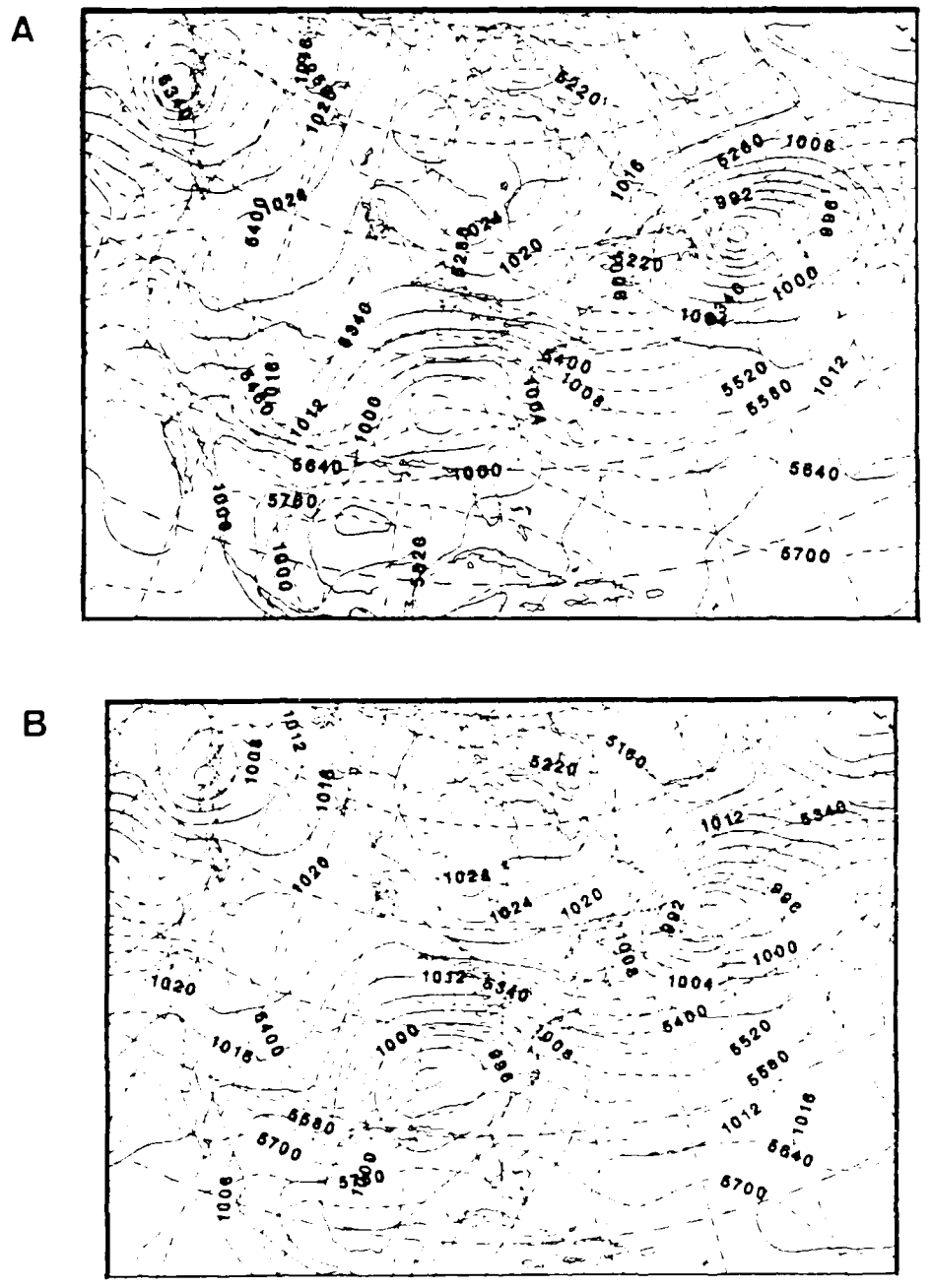

Fig. 3.5 NORAPS (A) surface forecast and (B) surface analysis at 12 GMT 28 March 1984 with isobars (solid) in mb and 1000-500 mb thickness (dashed) in gpm. Contour interval is 4 mb for isobars and 60 gpm for thickness.

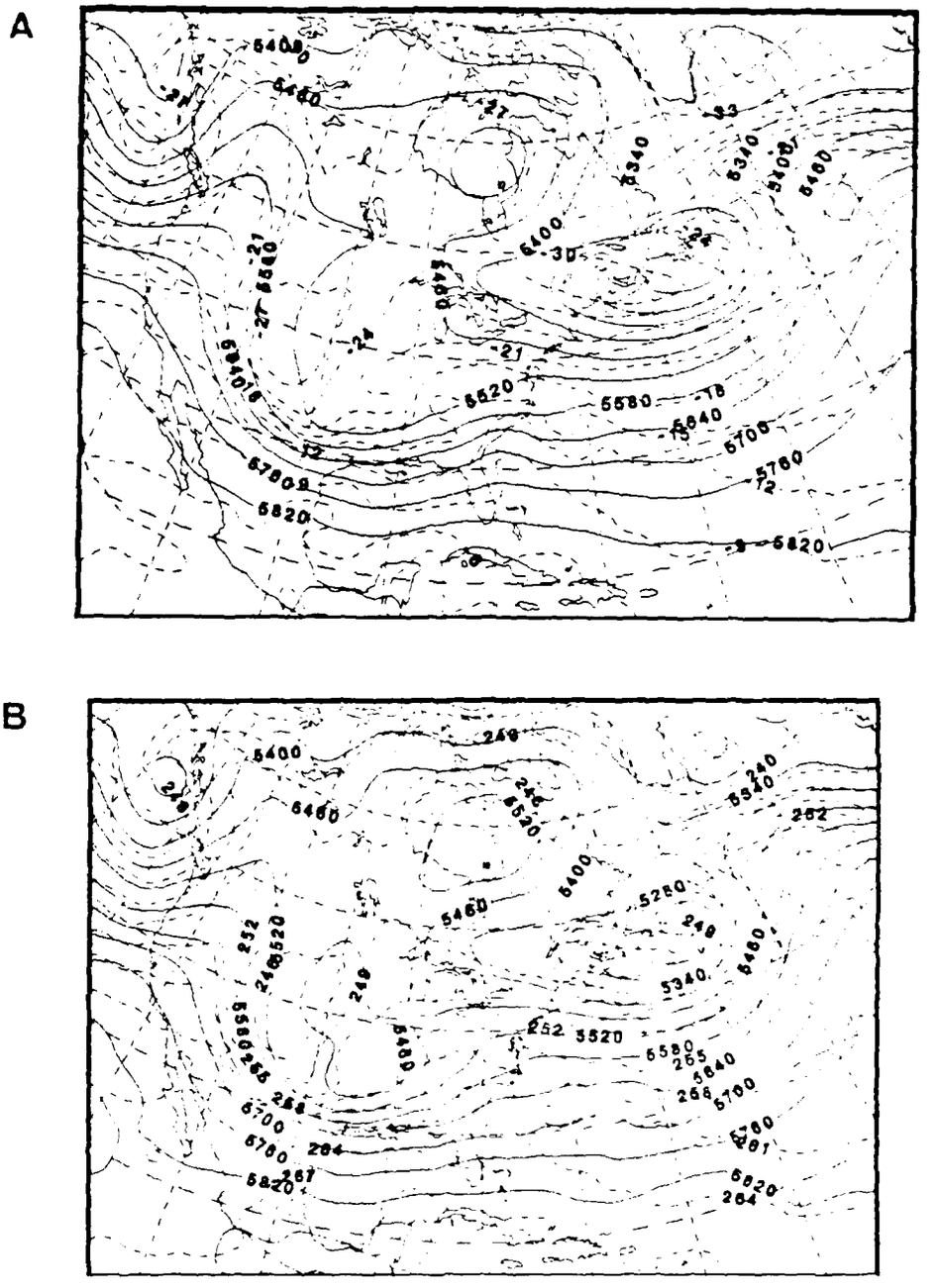

Fig. 3.6 NORAPS 500 mb (A) forecast at 12 GMT 28 March 1984 with heights (solid) in gpm, and isotherms (dashed) in degrees Celsius. (B) As in (A) except for analysis and isotherms in degrees Kelvin.

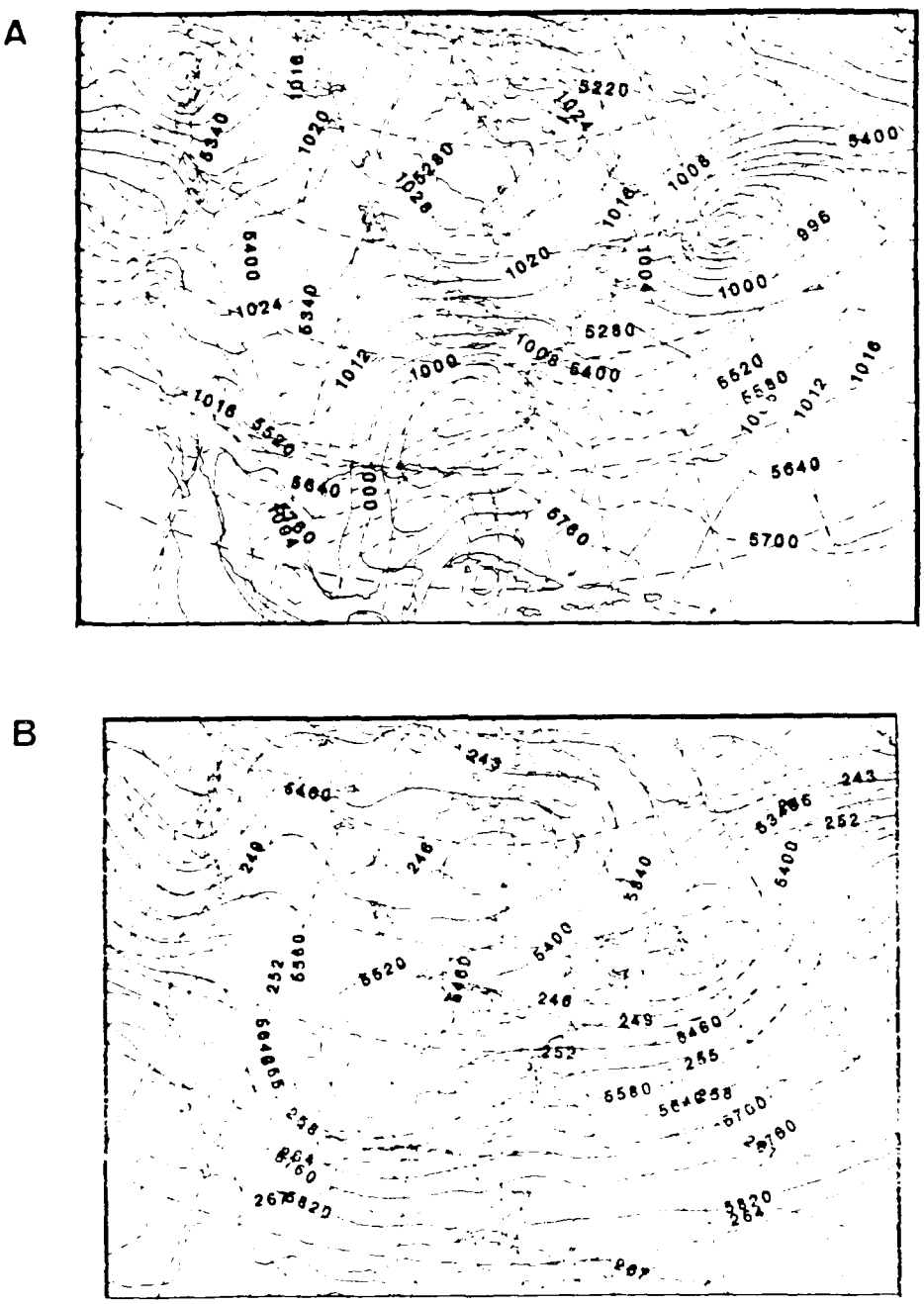

Fig. 3.7 As in Fig. 3.2, except for 18 GMT 28 March 1984 forecast fields.

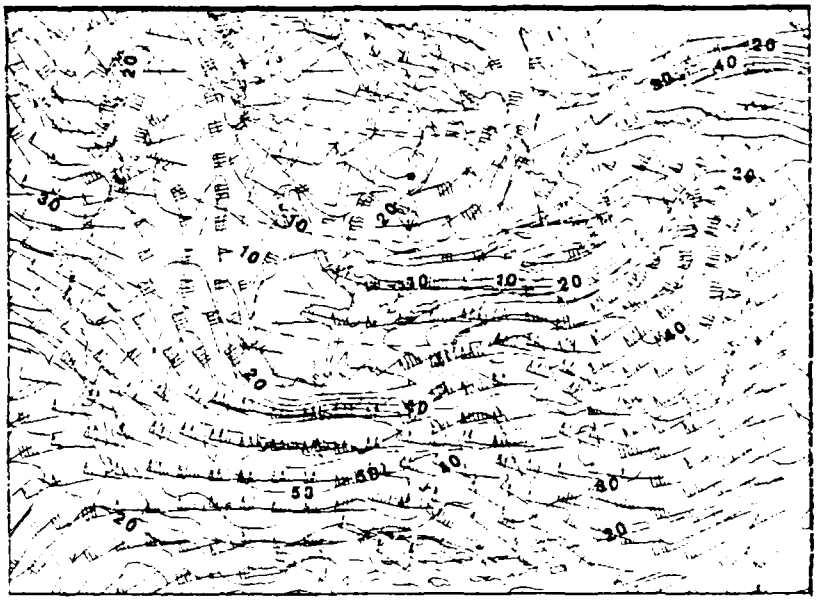

Fig. 3.8 As in Fig. 3.3, except for 18 GMT 28 March 1984 forecast.

A

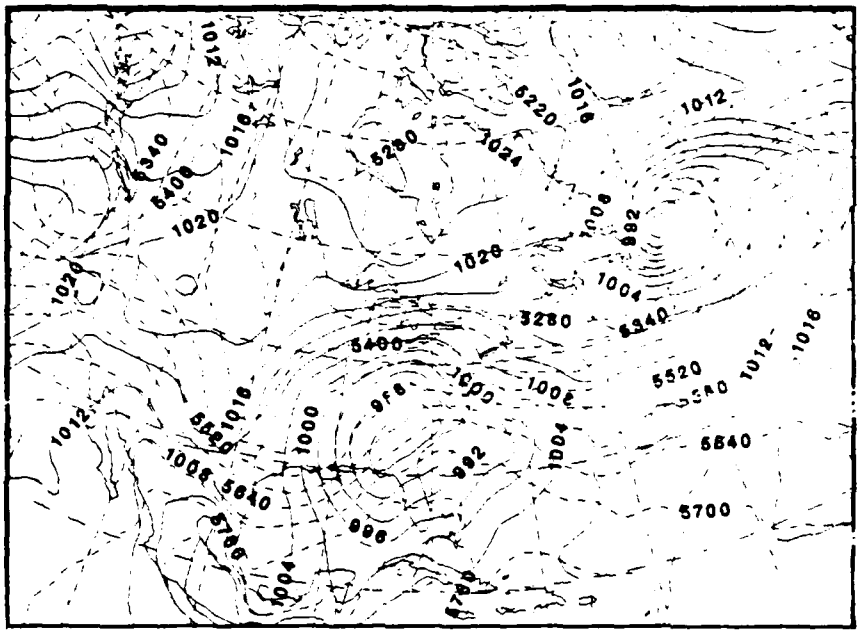

B

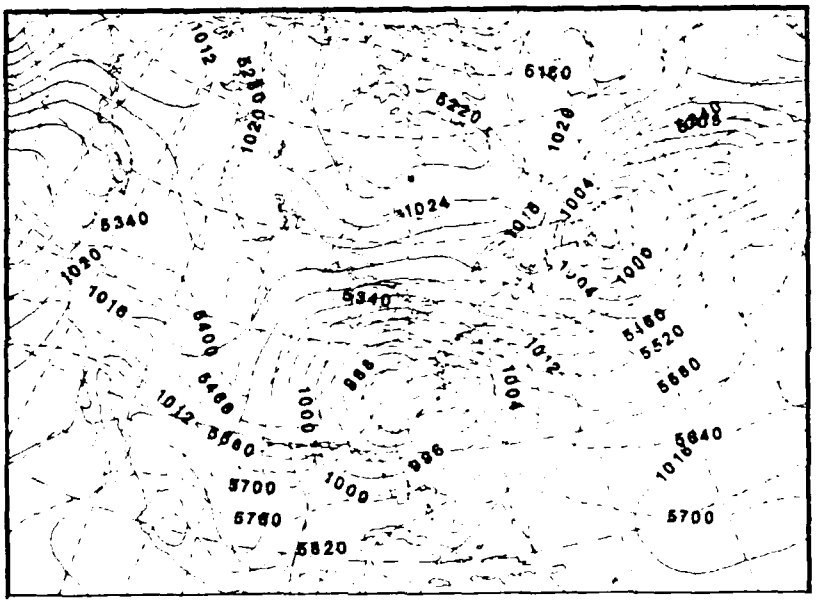

Fig. 3.9 As in Fig. 3.5, except for 00 GMT 29 March 1984.

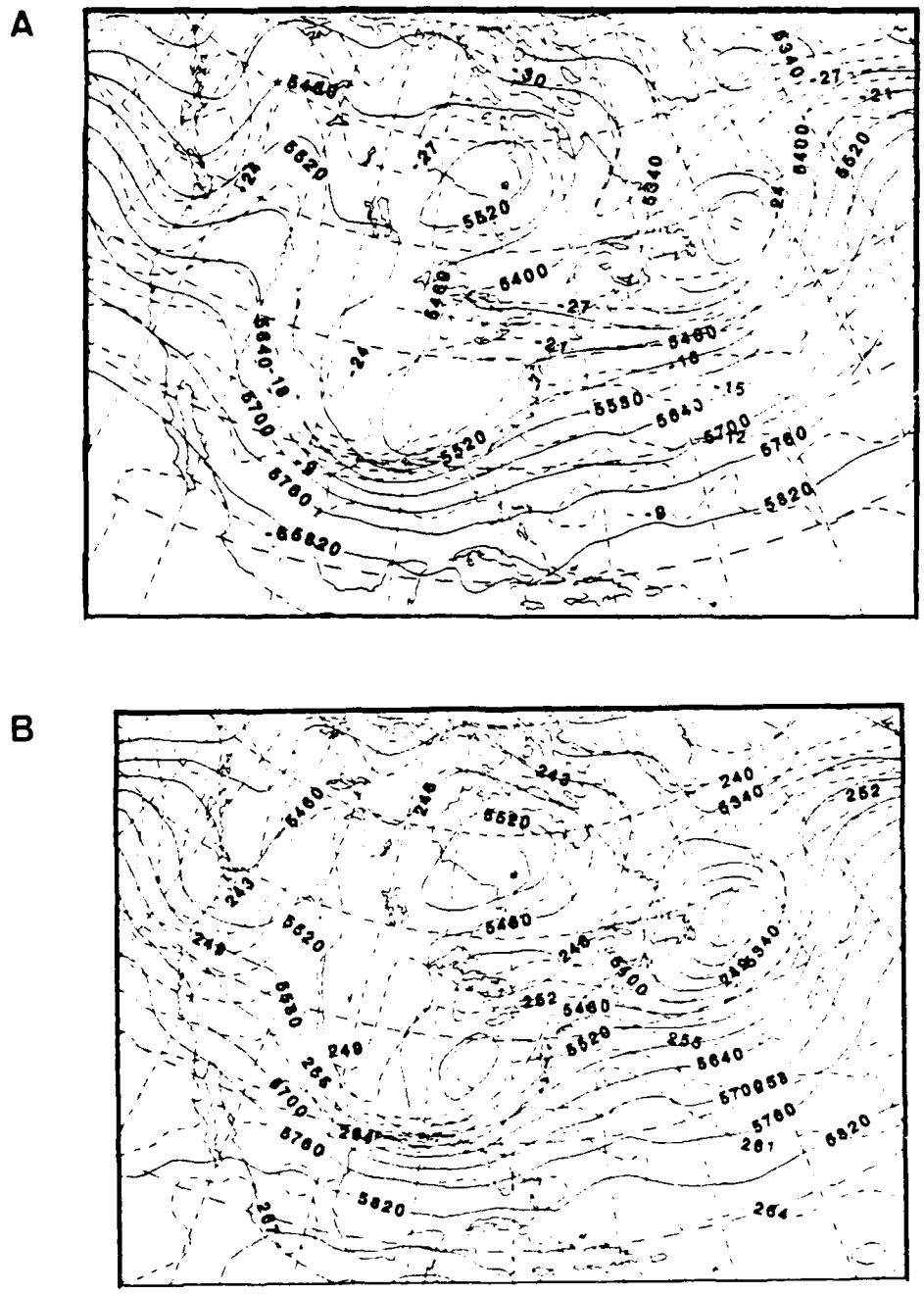

Fig. 3.10 As in Fig. 3.6, except for 00 GMT 29 March 1984.

A

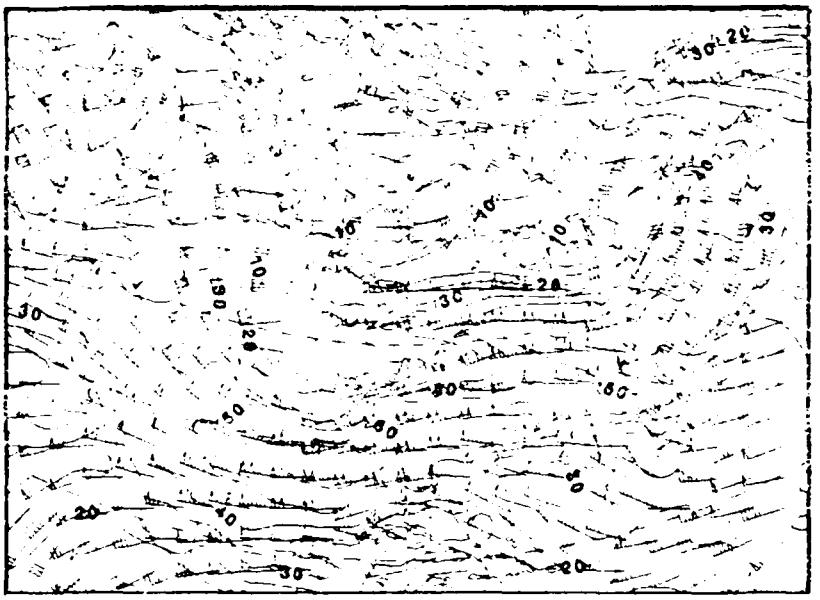

B

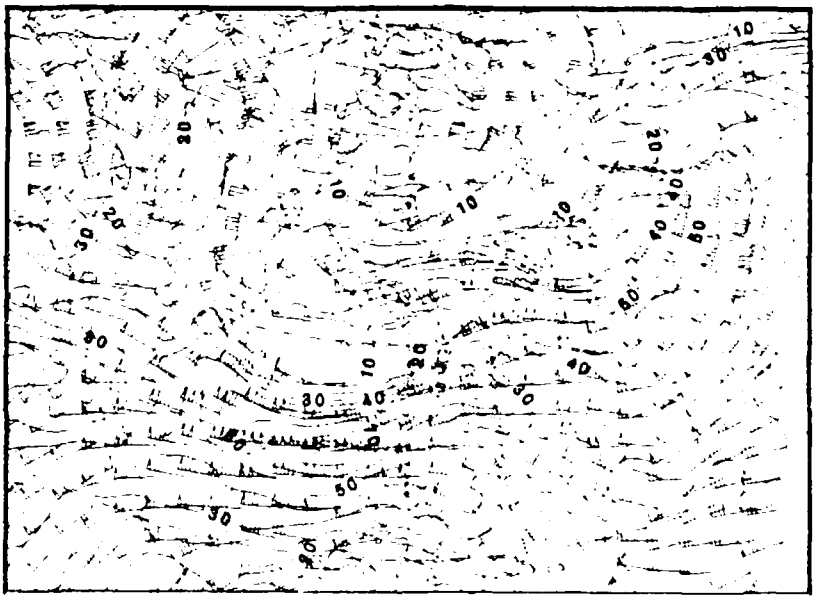

Fig. 3.11 NORAPS (A) forecast and (B) analysis of 300 mb wind/isotachs (m/s) at 00 GMT 29 March 1984.

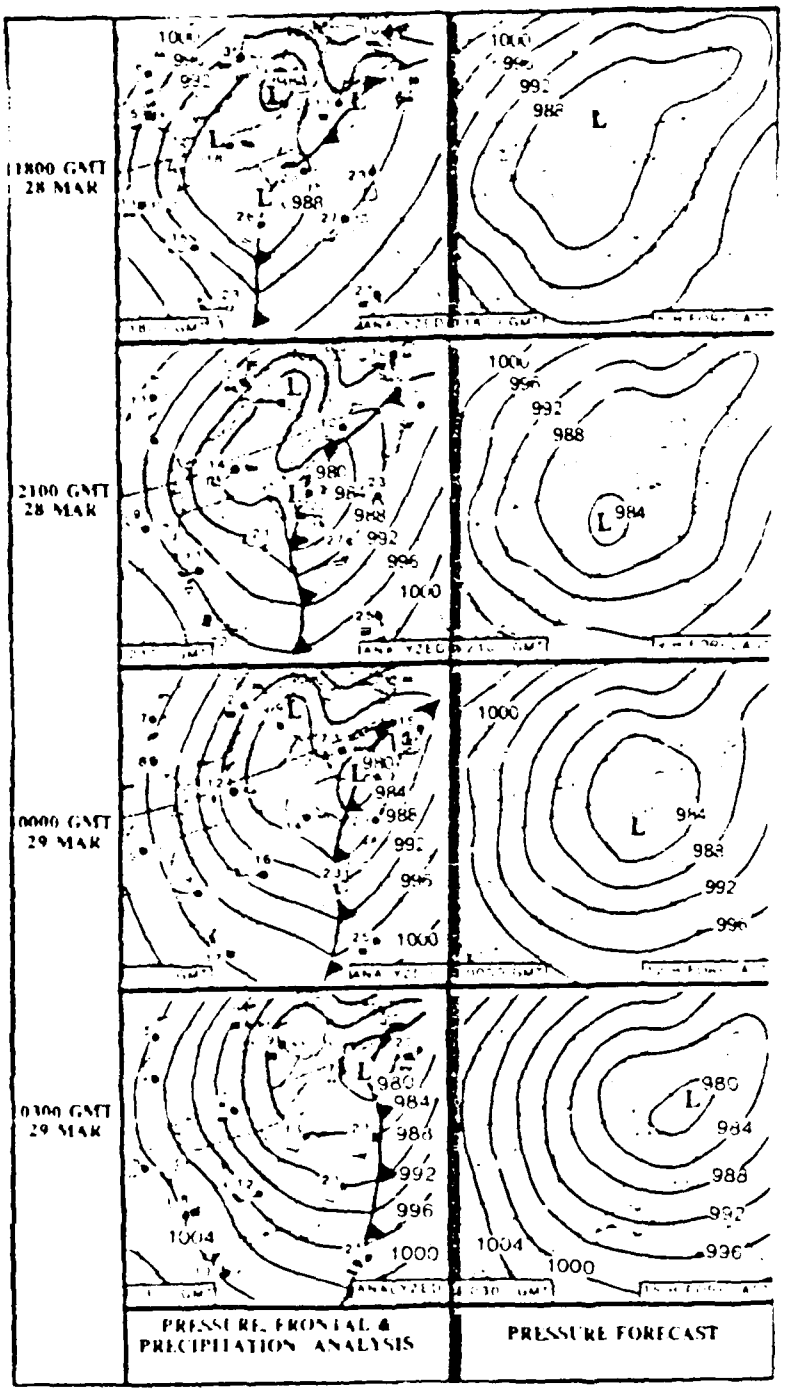

Fig. 3.12 Mesoscale Atmospheric Simulation System forecasts (right column) and verifying analyses (left column) for period 18 GMT 28 March to 03 GMT 29 March 1984. Contour interval of isobars (solid) is 4 mb, (Kocin et al., 1984).

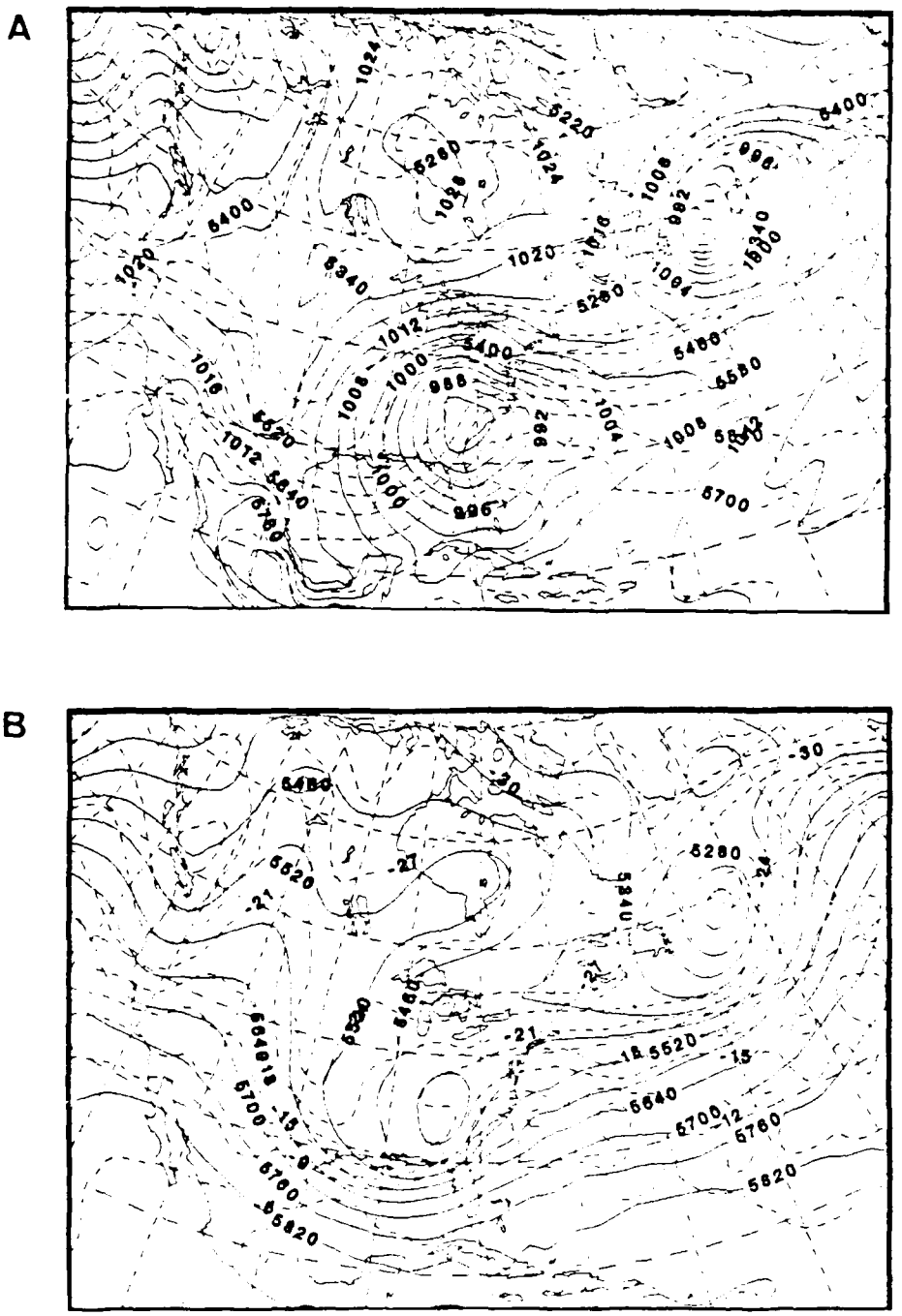

Fig. 3.13 As in Fig. 3.2, except for 06 GMT 29 March 1984 forecast.

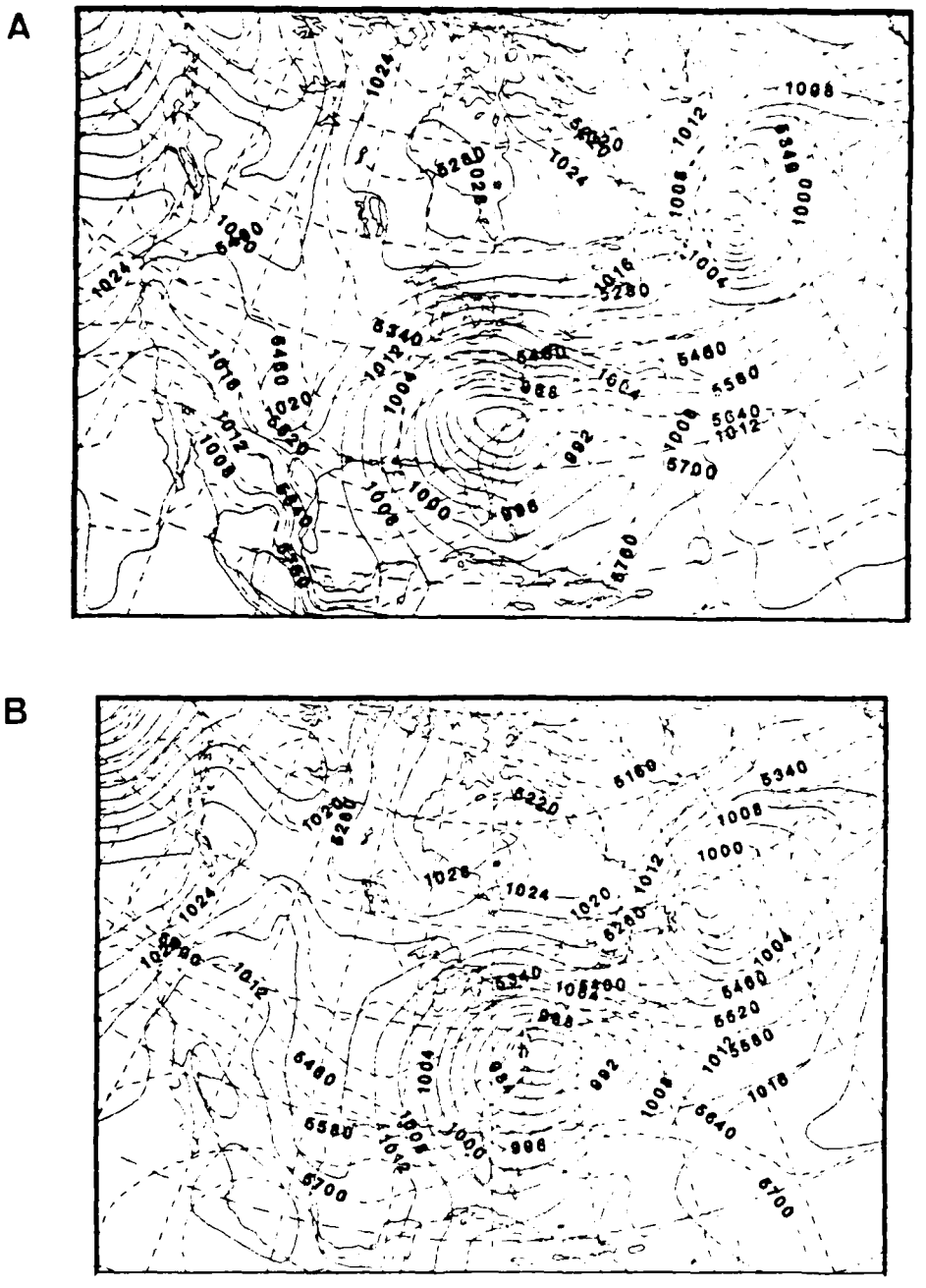

Fig. 3.14 As in Fig. 3.5, except for 12 GMT 29 March 1984.

IV. MASS AND VORTICITY BUDGET RESULTS

A. MASS BUDGET

The mass budget is performed using the finite difference form of the continuity equation in pressure coordinates. The values of vertical velocity, commonly referred to as omega, are computed kinematically and interpolated to the budget volume. Horizontal winds are likewise interpolated to the budget volume with normal and tangential wind components being computed for budget calculations. A method developed by O'Brien (1970) is used to adjust the horizontal and vertical winds to achieve mass balance. In this method, the total horizontal flux for a particular radius ring of the budget volume is computed using the line integral method. These horizontal fluxes are summed in the vertical to arrive at a vertically-integrated horizontal mass flux for each radius ring. The vertically-integrated horizontal flux is adjusted to balance the net vertical mass flux between the top (100 mb) and an arbitrary chosen bottom level of 1000 mb. In the forecast case, the model-predicted values of omega are used at the upper and lower boundaries, while omega is set equal to zero at the boundaries in the analysis case.

An adjusted divergence and normal wind are then calculated at 36 points around the budget center at each level. Based on these two adjustments, an adjusted vertical velocity is computed at interior levels. For the NORAPS forecast fields, a constant correction factor is used to adjust the horizontal divergence at each level. For the analyses fields, a weighting function that linearly decreases with pressure is used to correct the divergence due to the larger error in the wind estimates with height.

Besides the above adjustments required for mass balance, there can be other sources of errors in the budget analyses. Serious truncation error can be introduced when using finite differences and interpolating from sigma levels in the model to pressure levels in the budgets. Also, errors can arise when interpolating from the Lambert conformal grid to the cylindrical budget volume.

B. MASS BUDGET RESULTS

The mass budget consists of a horizontal and vertical mass transport term. The horizontal mass transport term represents convergence or divergence within a particular layer (averaged over two levels) with no time averaging involved. The vertical mass transport is inferred from the vertical velocity field, which has been adjusted according to O'Brien's (1970) method discussed earlier. The vertical velocity fields are averaged over two time periods, however, no layer averaging is involved.

A comparison will be made of the NORAPS forecast horizontal and vertical transport fields with the analysis fields. The forecast fields are available every 6 h from 06 GMT 28 March until 12 GMT 29 March 1984. The analysis fields are available only at 12 h intervals from 00 GMT 28 March to 12 GMT 29 March 1984. Mass fluxes and vertical velocities in a vertical/time section for radius 4^{0} lat. will be emphasized because this radius most nearly represents the inner core of the cyclone where heating and moistening tend to be concentrated.

The analyzed horizontal mass transport (Fig. 4.1a) has a pattern of inward mass transport below 700 mb and mass outflow or divergence above 700 mb. The forecast horizontal transport (Fig. 4.1b) has a similar two-layer vertical structure. However, the level of non-divergence (LND), where inward and outward mass transport changes sign, occurs at 500 mb. The much lower LND in the analyzed case is

typical of most explosive maritime cyclones which have been found to have a shallow vertical structure (Sanders and Gyakum, 1980). This shallow convergent layer (Fig. 4.1a) in the analyzed case is much greater in magnitude than the upper-level outflow, which occurs over a deeper layer. The absence of vertical variations in the LND during the course of this storm is different from the explosive maritime cyclogenesis case studied by Calland (1983), in which the convergent layer was found to deepen as the storm developed. Possible explanations for this are the lack of a clearly defined explosive cyclogenesis phase, stronger frictional effects occur over land, and the better data coverage over land which provides a more accurate vertical structure of the atmosphere.

Much larger values are observed for the inward mass transport in the analyzed case near the last time period (Fig. 4.1a). This suggests that some mesoscale feature not captured within the 4^{o} radius budget volume during the earlier time periods has moved into the budget volume at this last time period. An oscillating trend in the forecast field is seen with maxima at 12 GMT 28 March and 06 GMT 29 March 1984. These maxima of inward horizontal transport occur about 6 h prior to the peak model precipitation periods of 18 GMT 28 March and 12 GMT 29 March 1984. This strong oscillation pattern does not occur at radii greater than 4^{o} lat.

The area-averaged kinematic vertical velocity for the analyses (Fig. 4.2a) indicates an absolute maximum near 700 mb for the 00-12 GMT 29 March 1984 time period. The forecast area-averaged omega field (Fig. 4.2b) displays an absolute maximum at 03 GMT 29 March 1984 and a secondary maximum from 09-21 GMT 28 March 1984 near 500 mb. The differences in the level of maximum omega are sensitive to the vertical profile of diabatic heating (Gyakum, 1983b). Strong

diabatic heating in the lower troposphere is believed to induce greater vertical velocities and thus increase the low-level convergence which is necessary for the deepening of the cyclone. In the forecast case (Fig. 4.2b), there is a slight bias towards more intense vertical velocities. The two distinct maxima of omega evident in the forecast case will have important implications for the model-predicted precipitation pattern to be discussed in the next chapter.

C. VORTICITY BUDGET

In the vorticity budget, the goal is to determine the relative magnitudes of the terms in the vorticity equation,

$$\overline{\delta\zeta_a}/\delta t = -1/A \oint \zeta_a(V_n - V_o)\, dl - \partial/\partial p\, (\overline{\omega\zeta_a}) - \overline{\zeta_a (\nabla \cdot V)} + k \cdot (\overline{\partial V/\partial p \times \nabla\omega}) + \overline{Fr} + \overline{R}, \quad (4.1)$$

where ζ_a is the absolute vorticity, A is the area of a particular surface within the budget volume, V_n is the normal wind component, V_o is the cyclone's normal velocity component, ω is the vertical velocity, Fr denotes friction, R is the residual and the overbar denotes an area-average of a term. The term on the left side of (4.1) is the quasi-Lagrangian tendency of vorticity. On the right side of (4.1), the first term is the horizontal transport (flux) of vorticity, while the second term is the vertical transport. The vorticity divergence term is the third term on the right side of (4.1) and is considered as a source or forcing term which generates positive vorticity. The fourth term on the right side is the tilting term and the fifth term is the friction or dissipation term. The residual is the last term on the right side of (4.1) and includes the sources and sinks not explicity resolved by the other terms

and the effects of computational errors. If all the sources and sinks contributing to vorticity changes have been properly accounted for and interpolation errors have not be introduced, the size of the residual should be relatively small. Interpolation and calculation errors are the major source of uncertainty in budget studies based on numerical model outputs. For the analyses, an uncertainty due to incomplete observations is also present.

The lateral transport of absolute vorticity can be partitioned into mean and eddy modes, which may be referred to as symmetric and asymmetric components. The mean mode represents the effects due to mean cyclone convergence and divergence, whereas the eddy mode represents the horizontal transport due to asymmetries in the cyclonic flow which lead to correlations between the wind field and the vorticity deviations. Jet streaks and short wave troughs are two mechanisms which contribute to the eddy mode component.

The vertical component of vorticity is computed from the horizontal wind field by using a finite difference form of relative vorticity in cylindrical coordinates and adding the appropriate value of the Coriolis parameter at the grid point. The NORAPS forecast and analyzed winds are greatly smoothed by passing a 25-point filter eight times for display purposes. This smoothing can also lead to accumulated errors in the budget calculations. The absolute vorticity budget results for the NORAPS forecast and analyses are presented by vertical/time sections for radius 4^{0} lat.

D. VORTICITY BUDGET RESULTS

The time tendency of absolute vorticity is evaluated using a forward time difference. Since this finite difference approximation yields a time tendency at the mid-point of the two time periods, the remainder of the terms are averaged over two time periods to present all the terms in

the budget at common times. For the forecast case, 15 GMT 28 March refers to the 12-18 GMT 28 March 1984 time period. The analyses times refer to the time period between 12 h synoptic times (00 and 12 GMT).

The time tendencies of the analyzed vorticity (Fig. 4.3a) feature a large positive value at 275 mb for the initial period, a weak tendency pattern at the middle period, and a slightly increasing pattern in the lower troposphere for the last time period. The early increase at the upper levels can be related to the intensifying jet streak moving into the western part of the budget volume (Fig. 3.2). The forecast time tendency of absolute vorticity (Fig. 4.3b) reveals the same general pattern as the analyzed case, although with slightly greater magnitudes. The negative time tendencies in the middle and upper levels during the 18 GMT 28 March time frame are difficult to explain as the storm circulation intensifies. Calland (1983) found a similar feature in a North Pacific case study and suggested this decrease was due to a subsynoptic scale system in the wind field during that period. After 18 GMT 28 March 1984, positive tendencies occur in both the model and analyzed troposphere as the increased inward horizontal mass transport (convergence) spins up the cyclone.

The lateral transport of vorticity (Fig. 4.4a) in the analyses depicts a strong inward transport of vorticity below 775 mb and a moderate inward transport in the upper levels of the troposphere. A relative minimum of inward transport is located at 600 mb. The transport of vorticity oscillates in the vertical between inward and outward values from 00-06 GMT 29 March 1984. The horizontal transport (Fig. 4.4b) for the forecast case verifies well in the lower troposphere as the same general structure is depicted, although somewhat weaker. However, an anomalous feature of outward vorticity transport occurs between 200 and 600 mb

from 09-21 GMT 28 March 1984 in the forecast case, which is not verified by the analyses. The reason for this is the large divergence contribution which overcompensates the advective contribution during this time interval. Rather, an inward transport of vorticity at upper levels persists through this period in the analyses.

The vertical transport of vorticity serves to vertically redistribute the vorticity brought into the budget volume by the lateral transport. In the analyses (Fig. 4.5a), low-level vorticity is exported aloft, resulting in weak vorticity increases in the middle troposphere. Above 350 mb, a large amount of vorticity is fluxed vertically into the budget volume associated with the strong winds at the jet stream level which produce large vertical gradients of vorticity. Another possible explanation for the extremely high values in the upper levels of the model is that a smaller pressure interval (50 mb) can introduce significant errors in conjunction with large wind speeds when the finite difference of the flux is performed. The forecast case (Fig. 4.5b) verifies quite well with a slightly higher level (600 mb) where the flux changes sign from upward to inward, while slightly weaker features are predicted above 600 mb.

The divergence term in the vorticity budget equation is often viewed as a forcing term which spins up the vortex through low-level convergence. A relatively deep layer of vorticity convergence (to 350 mb) is seen in the analyses (Fig. 4.6a) until 00 GMT 29 March 1984. This layer of vorticity convergence shrinks by 300 mb at 00 GMT 29 March 1984. This may indicate a separate, distinct smaller-scale and shallower low center not previously being followed has entered the budget volume and results in the dramatic increase in vorticity convergence below 700 mb. By contrast, the forecast case starts with a shallower convergence layer which deepens throughout the forecast period to

450 mb. The distinct maximum in vorticity convergence below 700 mb verifies well. A forecast maximum in upper-level divergence occurs at 21 GMT 28 March 1984, which is 9 h earlier than in the analyses.

The tilting term arises from the vertical velocity components generated when horizontally oriented vorticity elements are tilted to the vertical by a horizontally varying vertical motion field. Thus, the vertical shear tilts the horizontal vorticity elements into the vertical position. The tilting term (Fig. 4.7a) in the analyses has a weak negative contribution throughout the depth of the atmosphere. For the forecast case (Fig. 4.7b), the same general pattern of weak negative values verifies in the middle troposphere with weak positive contributions near the top and bottom of the model atmosphere. By contrast, Calland (1983) found the tilting term to be a source of vorticity in his case study.

Frictional dissipiation is assumed to occur only in the lowest layer of the model and is parameterized using a stability dependent scheme (Johnson and Downey, 1975). The diagnosed friction (Fig. 4.8a) plays a very minor role until 18 GMT 28 March 1984 when the circulation has become well organized and leads to frictional effects that oppose further increases in vorticity. This frictional dissipation is strong at the inner radii (less than 6^0 lat. radius), which suggests that friction is a major contributor to the vorticity budget only near the central region of high winds. In the forecast case, the frictional dissipation (Fig. 4.8b) verifies well with slightly greater values at the last time period.

The residual term contains accumulated errors resulting from the budget calculations and any sources or sinks of vorticity not explicitly computed. A positive (negative) residual in the vorticity budget indicates an apparent

vorticity source (sink) in which the observed increases (decreases) at a point are larger than is estimated by the computed terms. Sources can be due to such things as cumulus friction which serves to transfer low-level vorticity aloft. An incorrect representation of friction can lead to a sink of vorticity. Residuals for forecast fields should be nearly zero if the sources and sinks of vorticity have been properly accounted for in a finite difference representation. Inaccuracies in the vertical motion and horizontal wind analyses contribute to the physical errors in the residual, while spatial and temporal finite differencing and the interpolation to the budget volume are causes for computational error.

In the analyses, the residual (Fig. 4.9a) depicts large negative values through the depth of the atmosphere with the exception of a positive region between 350 and 700 mb after 18 GMT 28 March 1984. The residual (Fig. 4.9b) in the forecast is generally smaller than the analyses. The large negative residual at low levels indicates the NORAPS model parameterizes friction much stronger than the stability-dependent scheme used in the budget formulation. The large vorticity sink in the analyses (Fig. 4.9a) in the upper levels at 18 GMT 28 March 1984 is hardly evident in the forecast case.

The terms of the vorticity budget are vertically averaged over the 1000-500 mb layer to obtain a clearer understanding of the contribution of each term in the spin-up of the low-level vortex for this relatively shallow cyclone case. These results are shown for the analyses (Fig. 4.10) and the forecast (Fig. 4.11). The friction term is not shown as it plays a relatively minor role. The leading term is the vorticity divergence term for both the analyses and forecast. The lateral transport of vorticity is normally the second leading term, except at 18 GMT 28 March 1984 in

the analyses (Fig. 4.10) where the residual becomes as large as the leading term. The time tendency of vorticity and the residual generally rank as the third or fourth leading term in the budget. The small magnitude of the residual in comparison to the other terms indicates a favorable budget result. The vertical transport and tilting term are also generally much smaller in magnitude than the leading terms. Therefore, the vorticity divergence term serves as the major source of vorticity to the budget volume through strong low-level convergence.

E. SUMMARY

In summary, the mass budget findings reveal a shallow layer of low-level convergence beneath a deeper layer of upper-level divergence. The level of maximum vertical velocity appears fairly constant (700 mb) during the course of the storm. The lateral transport is the leading term in the vorticity budget. A linkage exists between the mass and vorticity budgets as a consequence of the vorticity divergence term. Low-level convergence acts to spin-up the low-level vortex as viewed from the time tendency term in the vorticity budget results. This increase in vorticity is aided by a favorable upper-level divergence pattern, which serves to export mass aloft and strengthens the secondary circulation (in-up-out) in the vertical plane. The eddy lateral transport provides a large inward transport of vorticity above 700 mb to offset the relatively minor contribution from the mean or divergent mode.

The vertical transport term serves to transport vorticity that has been "spun-up" at low levels into the middle troposphere. The tilting term acts as a vorticity sink, which is inconsistent with earlier budget findings (Calland, 1983). Friction only plays a significant role at the inner core as it offsets the low-level vorticity spin-up during the later stages of the storm. The diagnosed

residual from the vorticity budget is observed to be the balance of the lateral transport and time tendency terms.

The following chapter will discuss heat and moisture budget results. The cooperation between the mass and vorticity fields is an essential factor in organizing the heating and moistening in the storm environment. The heating and moistening effects can alter the vertical structure of the vertical velocity profile and produce feedback effects which change the mass and vorticity balance.

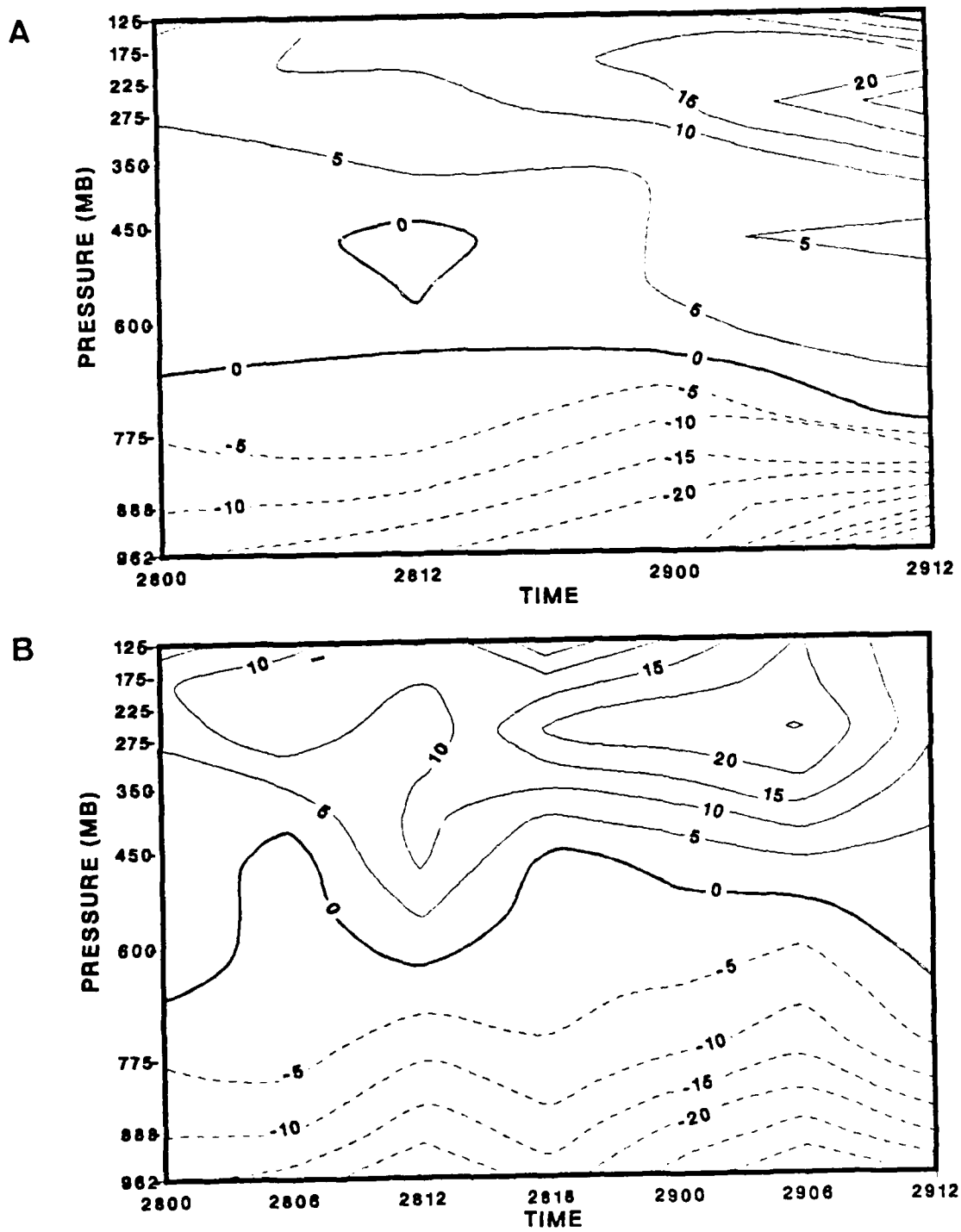

Fig. 4.1 Horizontal mass flux for radius 4° lat. in the (A) Analysis and (B) Forecast. Negative/positive values denote mass flux into/out of budget volume. Contours are 5 x 10**-11 g/s-100 mb.

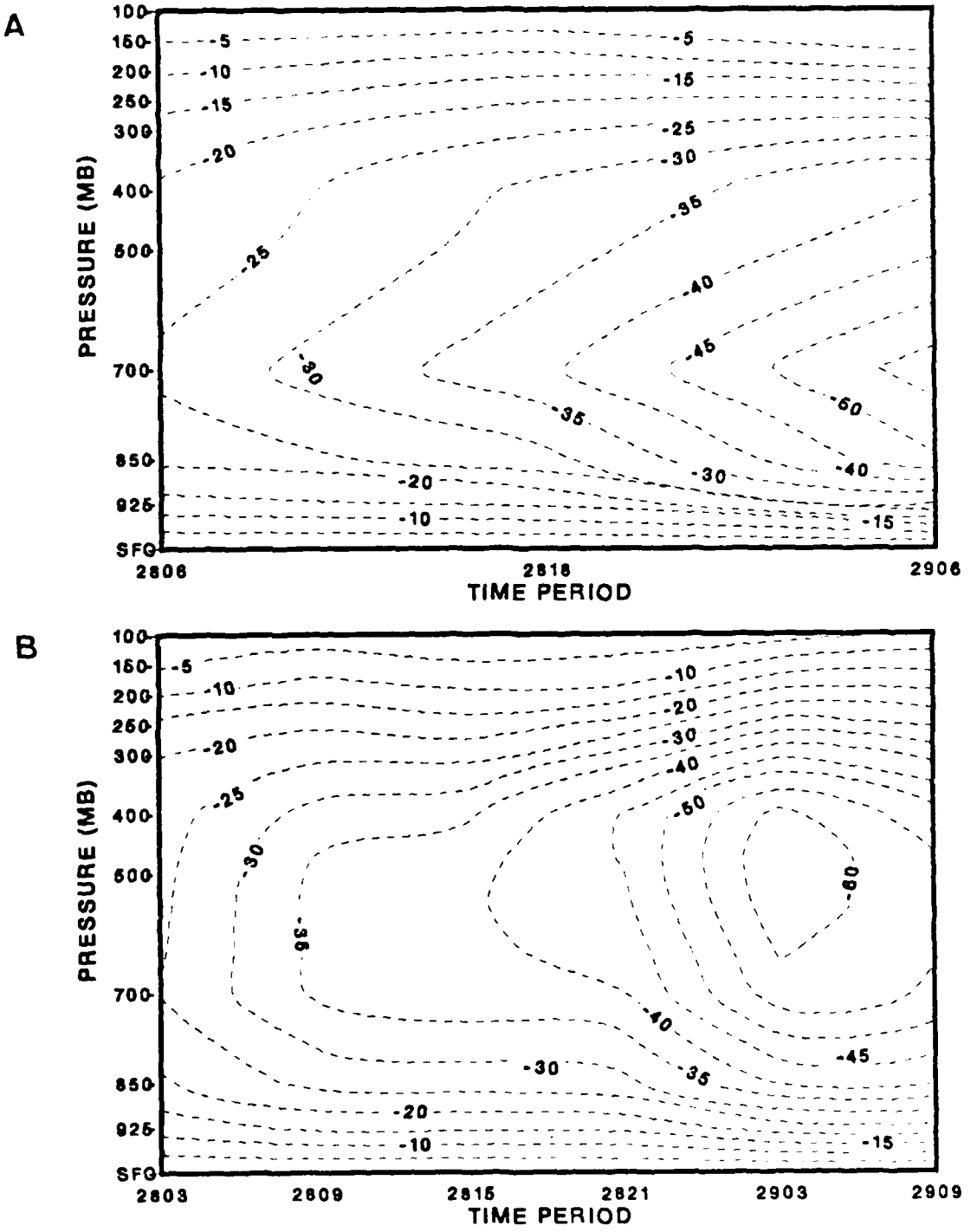

Fig. 4.2 Area-averaged vertical velocities in the (A) Analysis and (B) Forecast for radius 4. Negative values indicate upward vertical motion. Contours are 5 x 10**-4 mb/s.

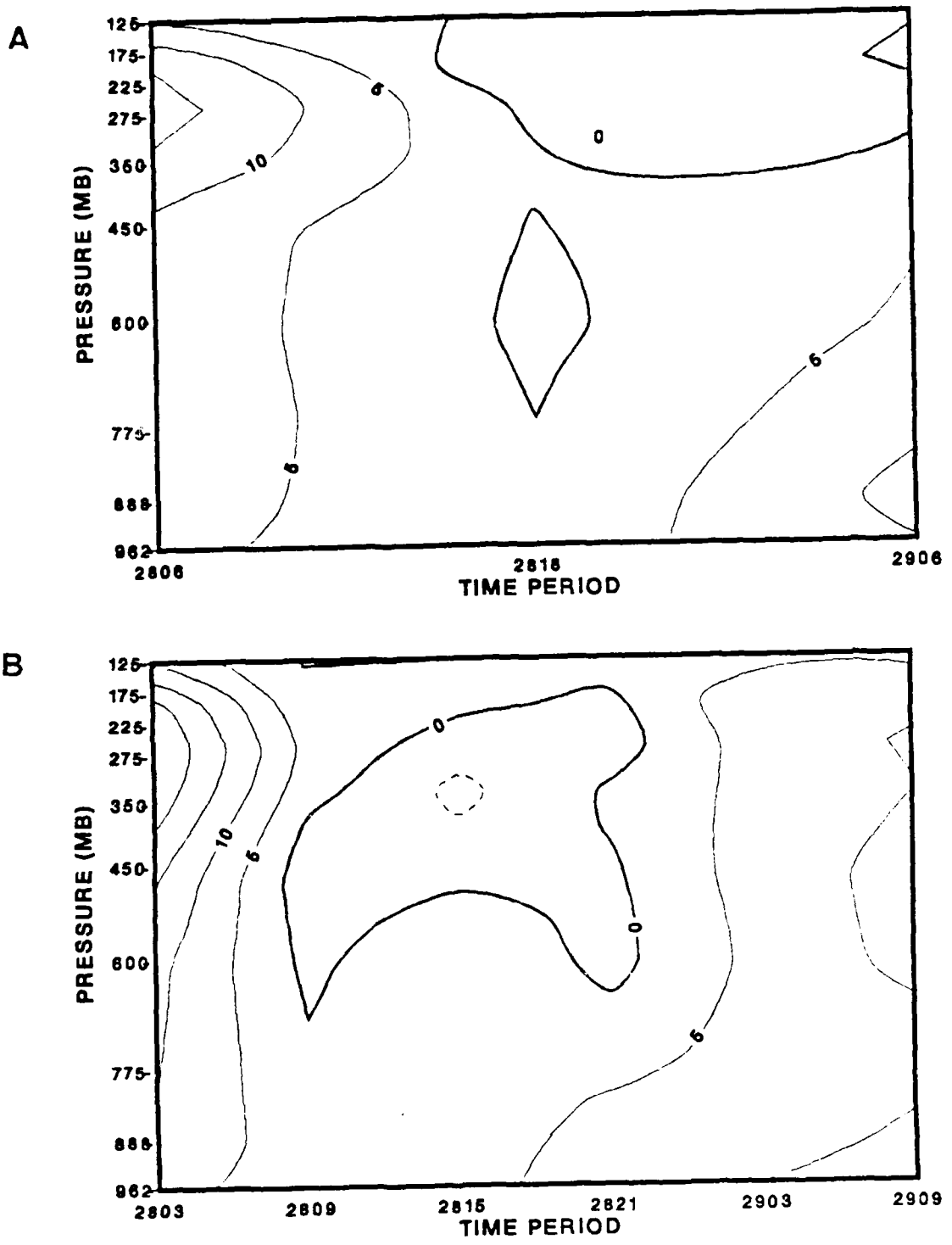

Fig. 4.3 Area-averaged time tendency of vorticity for radius 4 in the (A) Analysis and (B) Forecast. Solid/dashed contours indicated vorticity increases/decreases. Contours are 5 x 10**-10 s**-2.

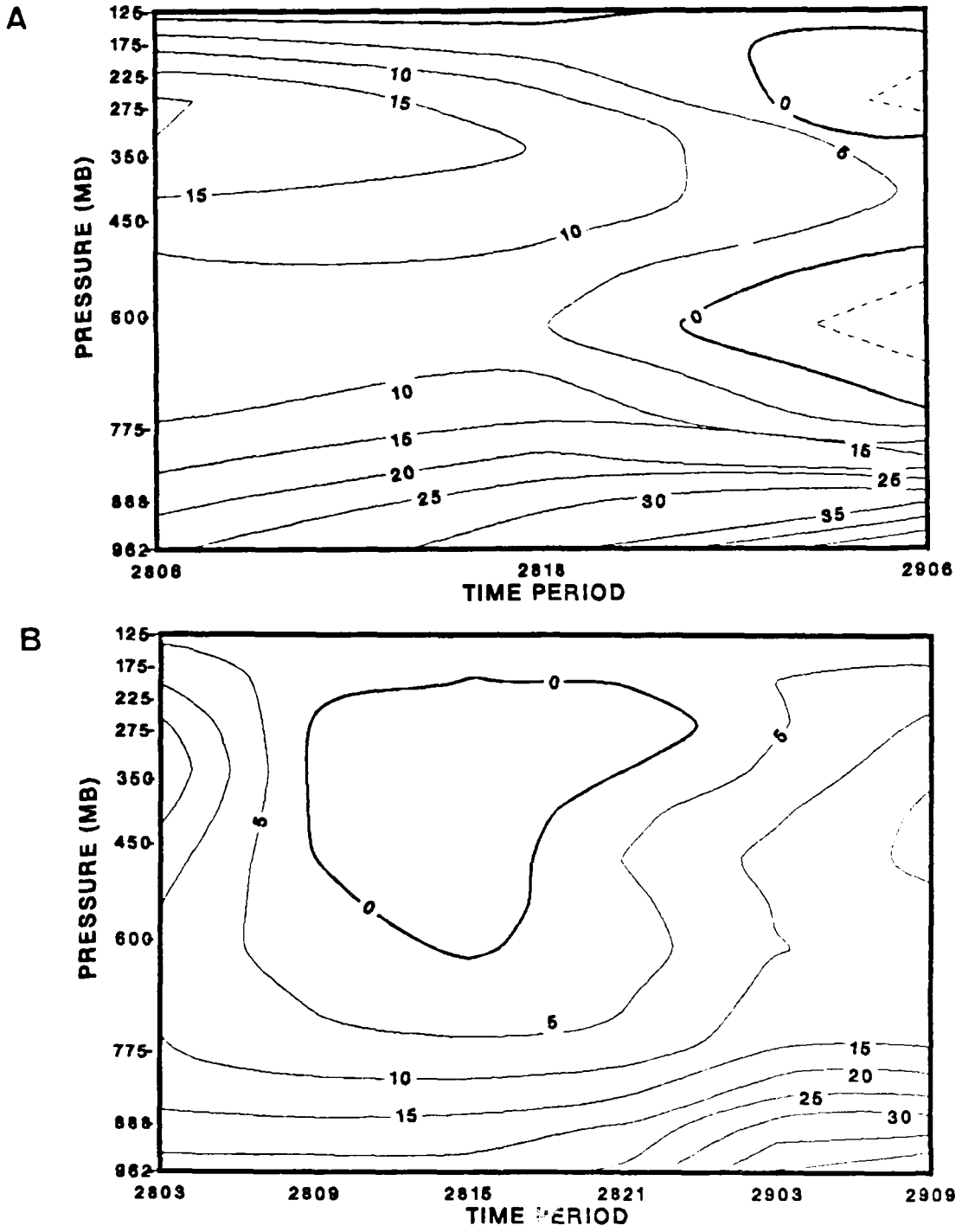

Fig. 4.4 As in Fig. 4.3, except for lateral transport of vorticity.

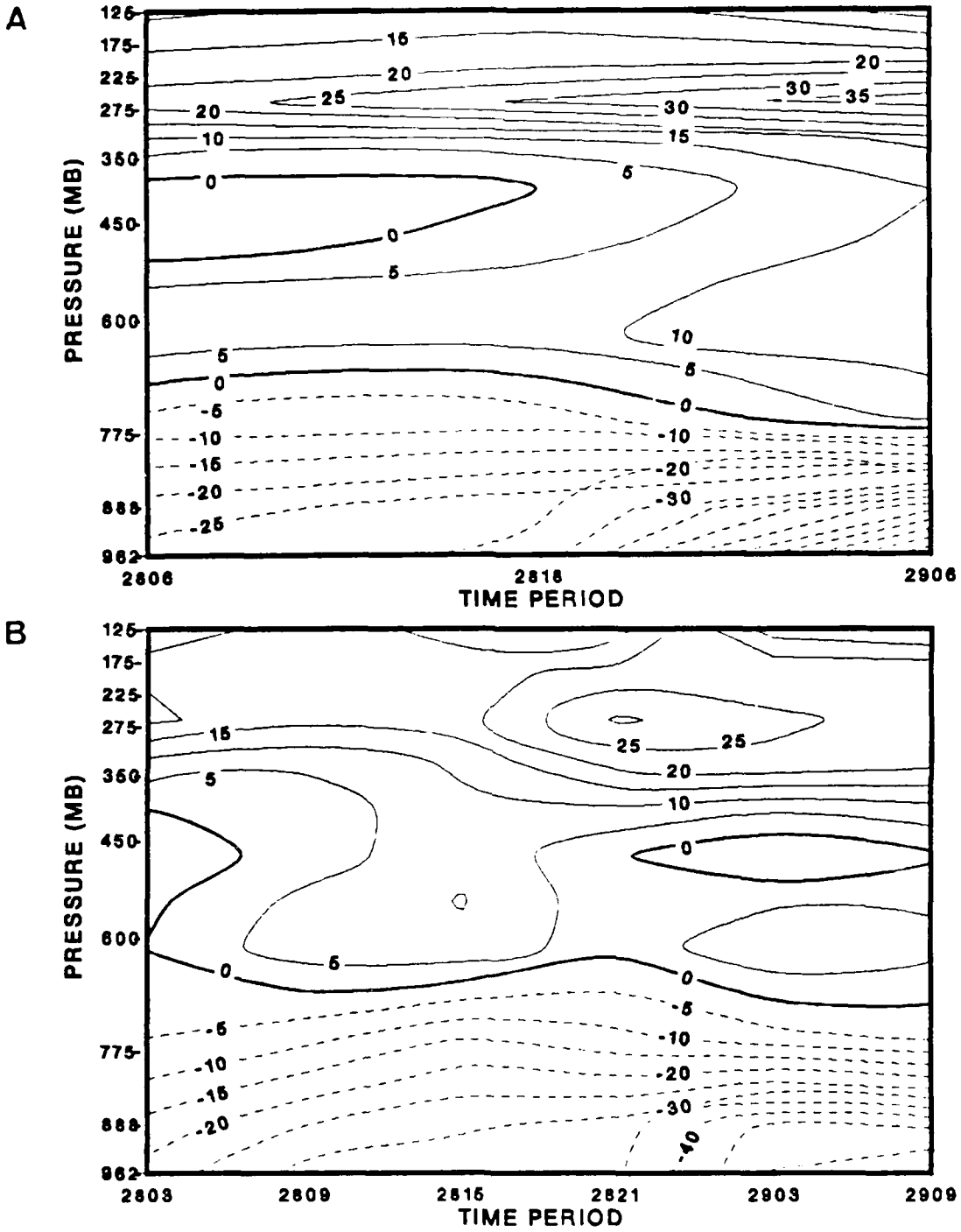

Fig. 4.5 As in Fig. 4.3, except for vertical transport of vorticity.

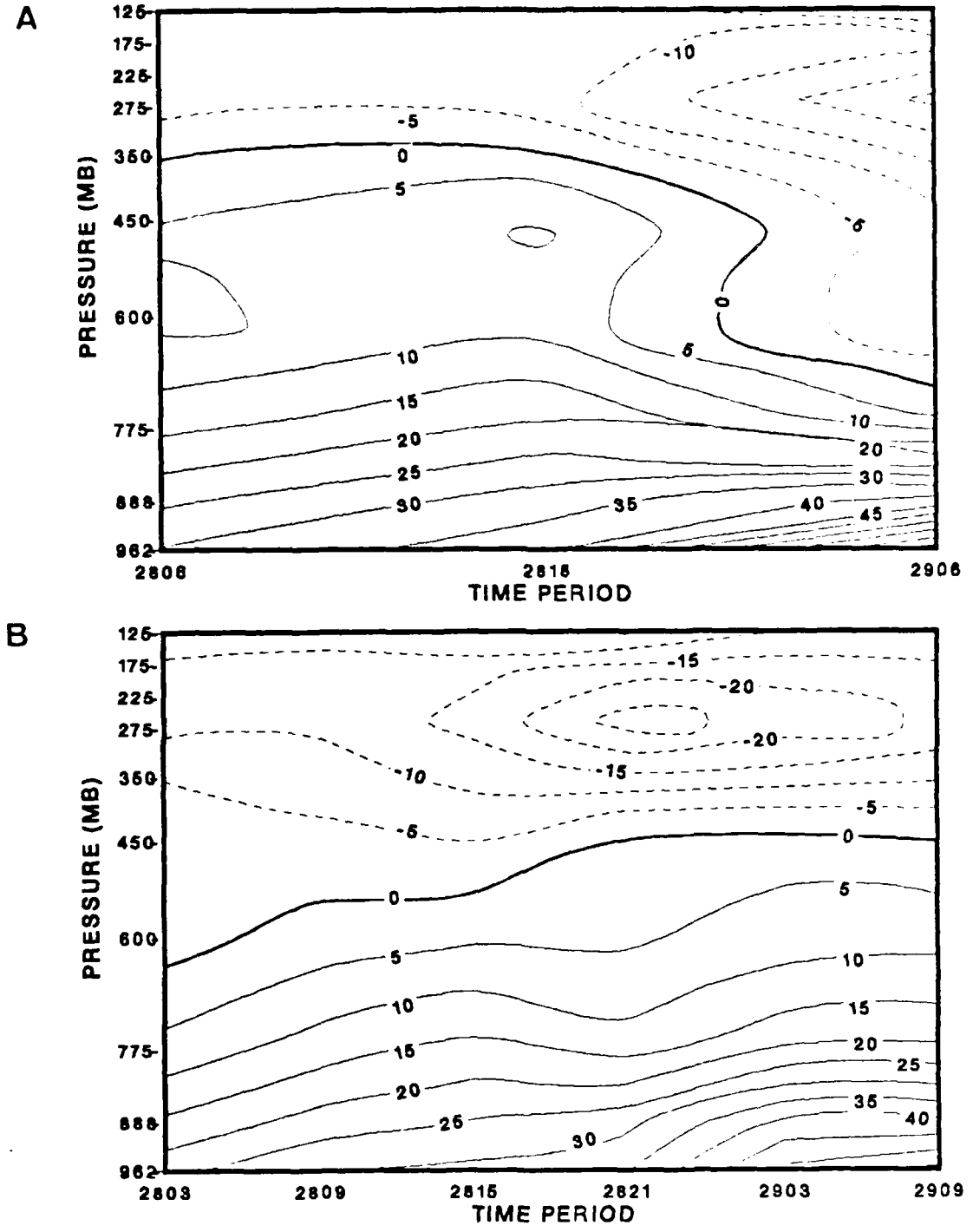

Fig. 4.6 As in Fig. 4.3, except for vorticity divergence term.

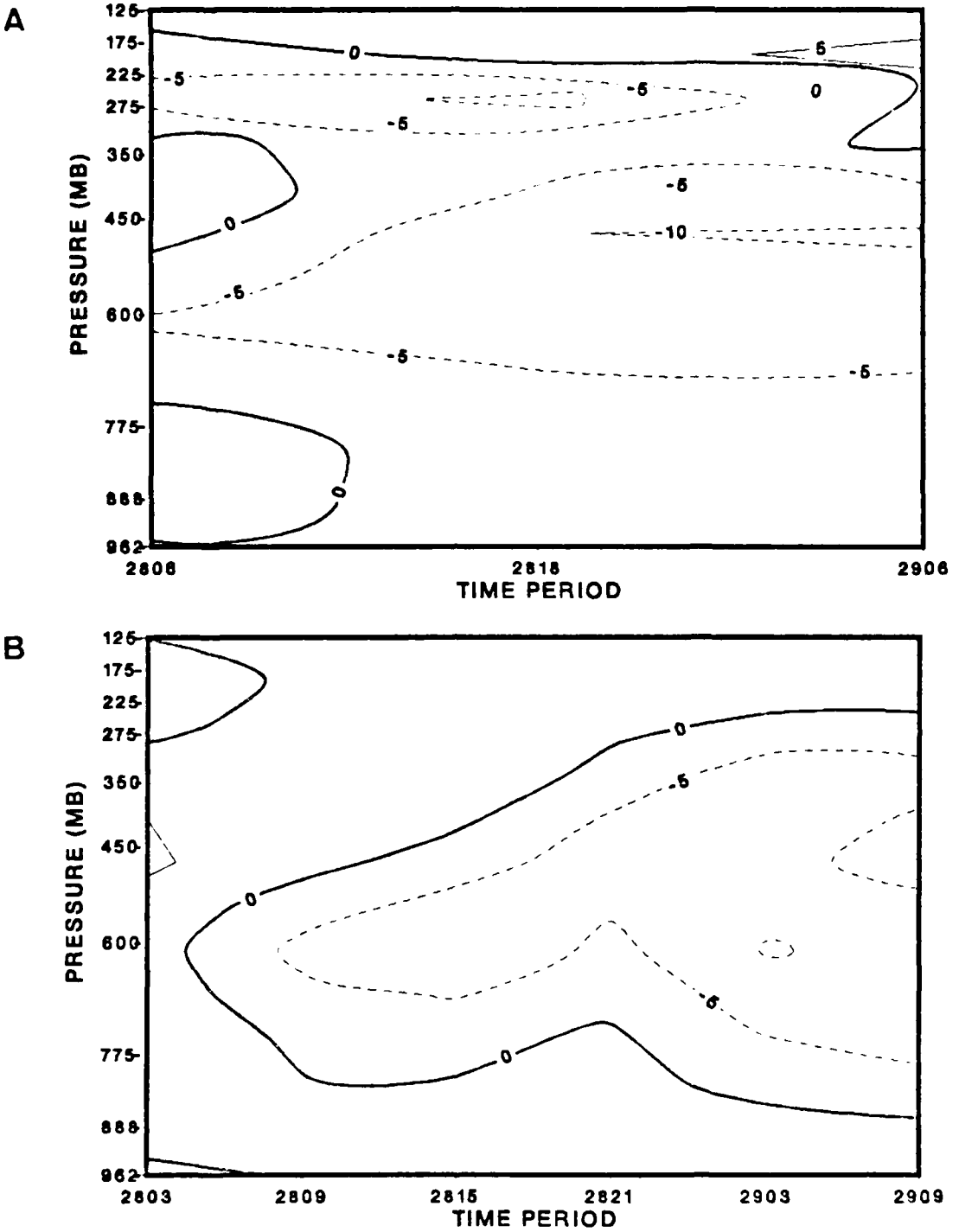

Fig. 4.7 As in Fig. 4.3, except for tilting term.

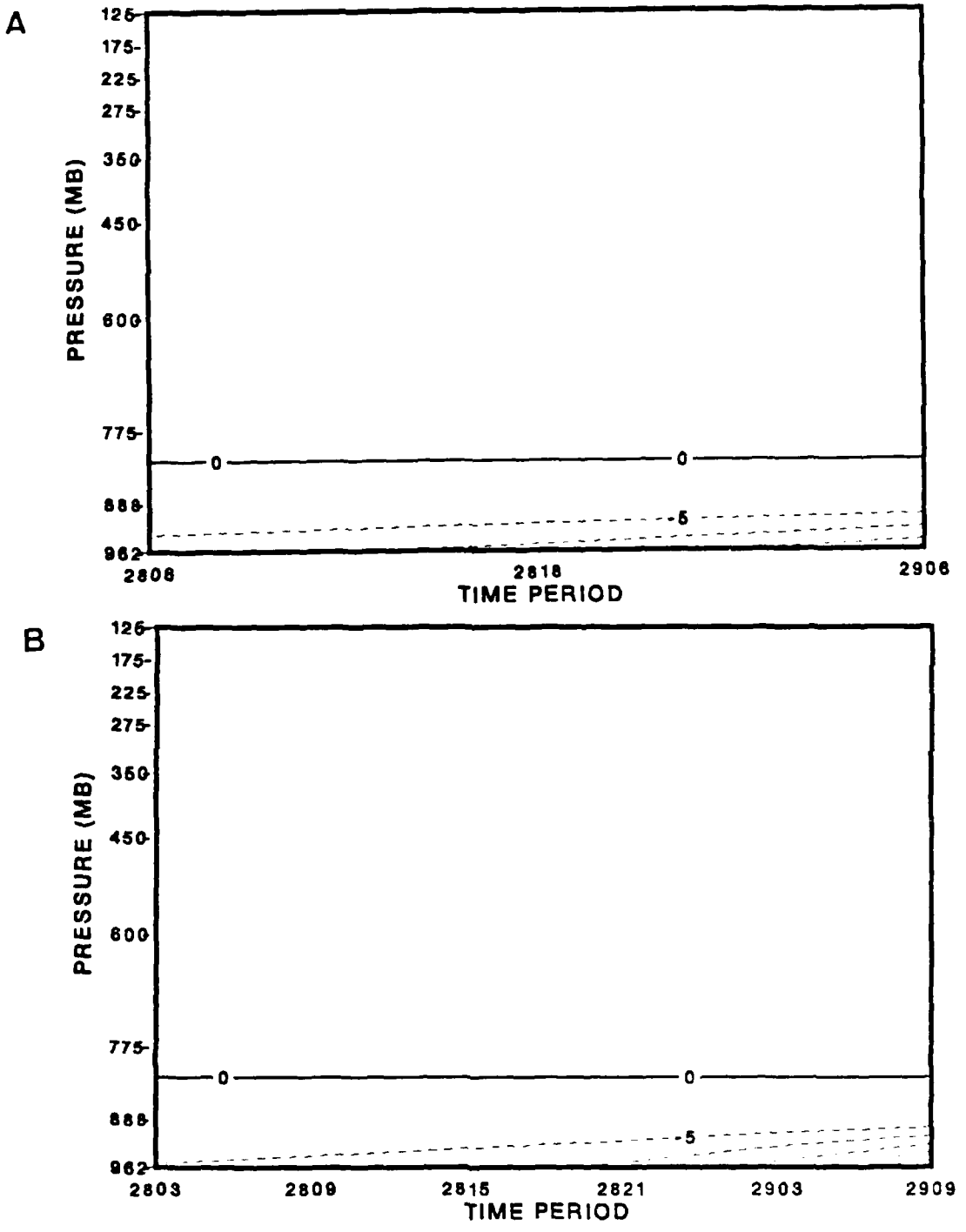

Fig. 4.8 As in Fig. 4.3, except for frictional dissipation.

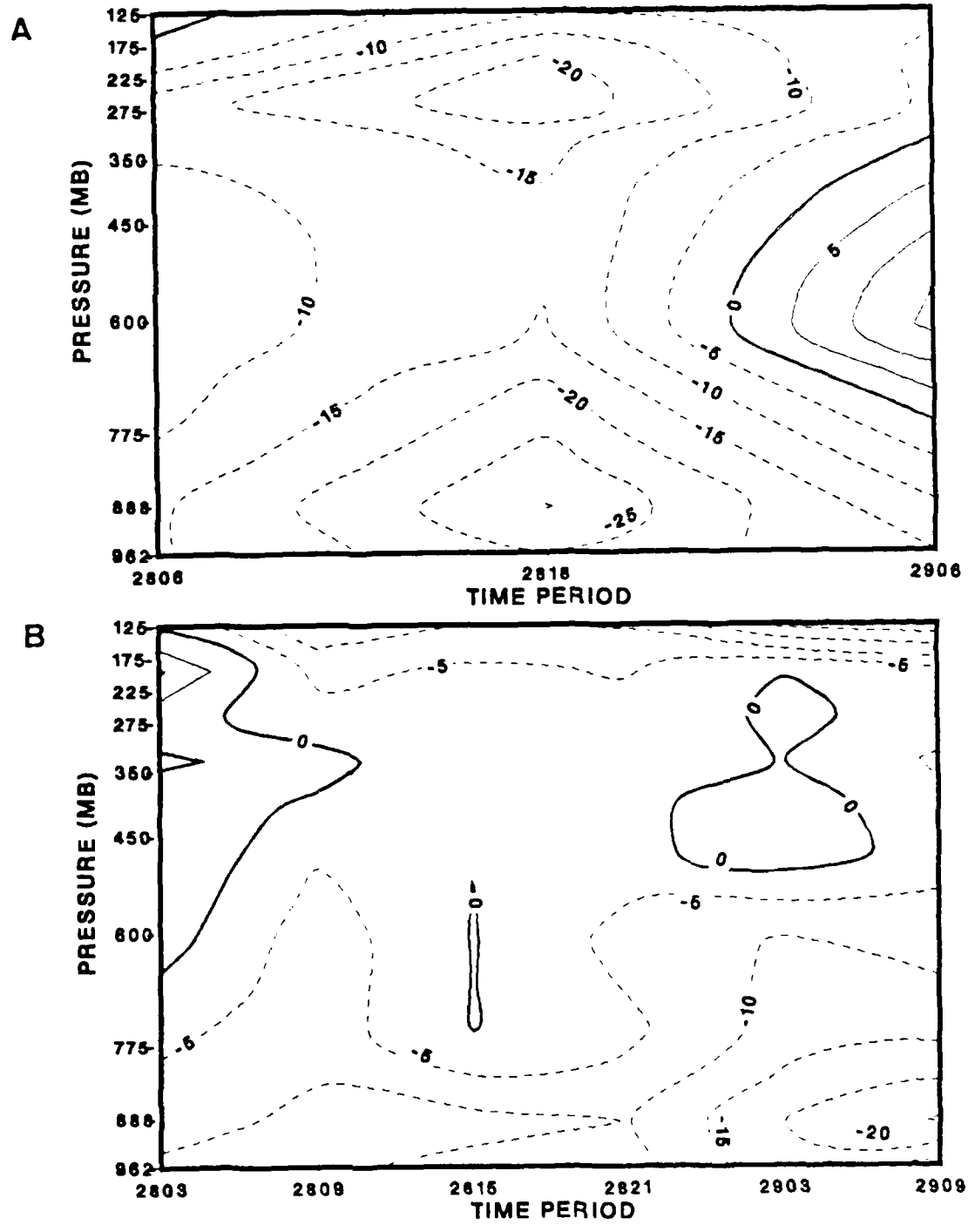

Fig. 4.9 As in Fig. 4.3, except for residual of vorticity budget.

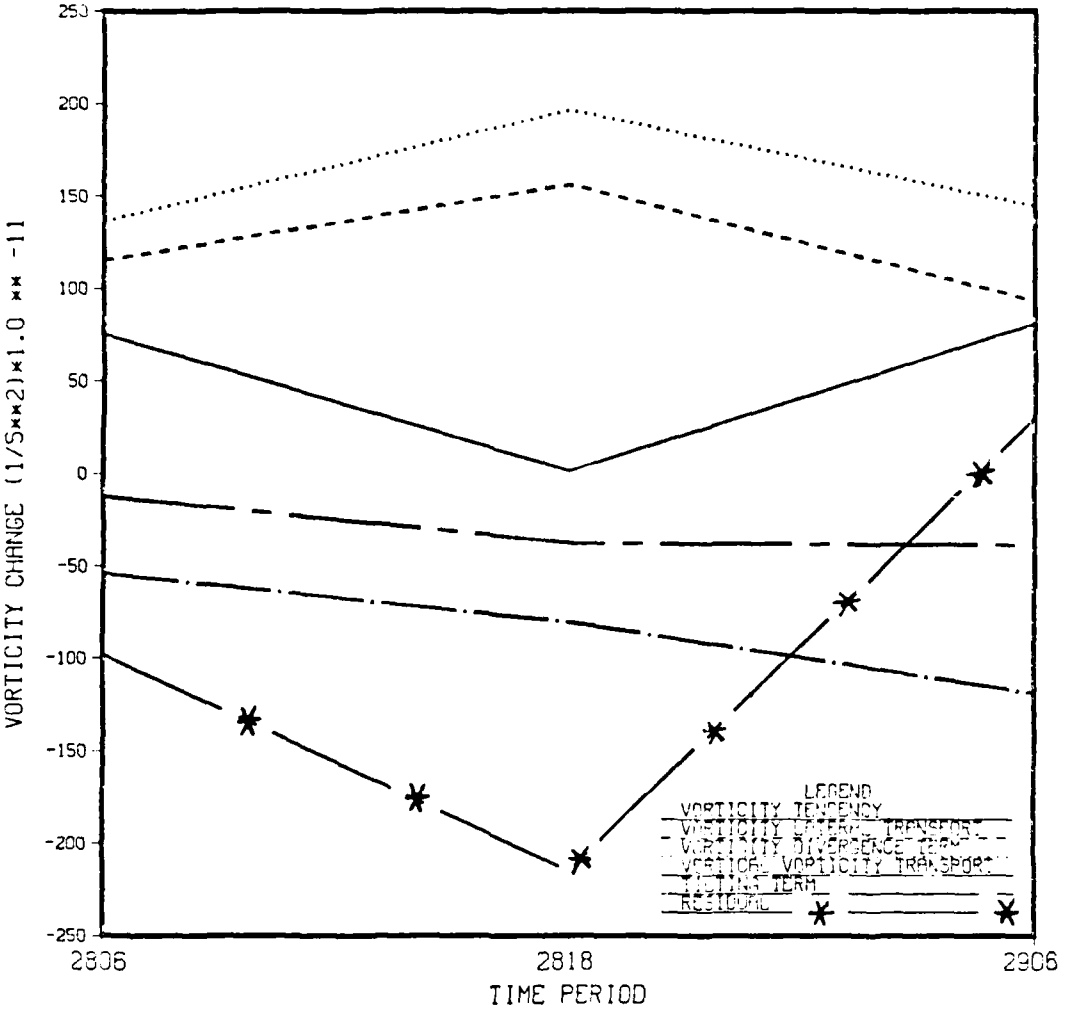

Fig. 4.10 Lower troposphere (1000-500 mb) average vorticity budget terms for analyses at radius 4: Lateral transport (dashed), time tendency (solid), vorticity divergence (dotted), vertical transport (chain-dotted), residual (chain-asterisk) and tilting term (chain-dashed). Units are 1 x 10**-11 s**-2.

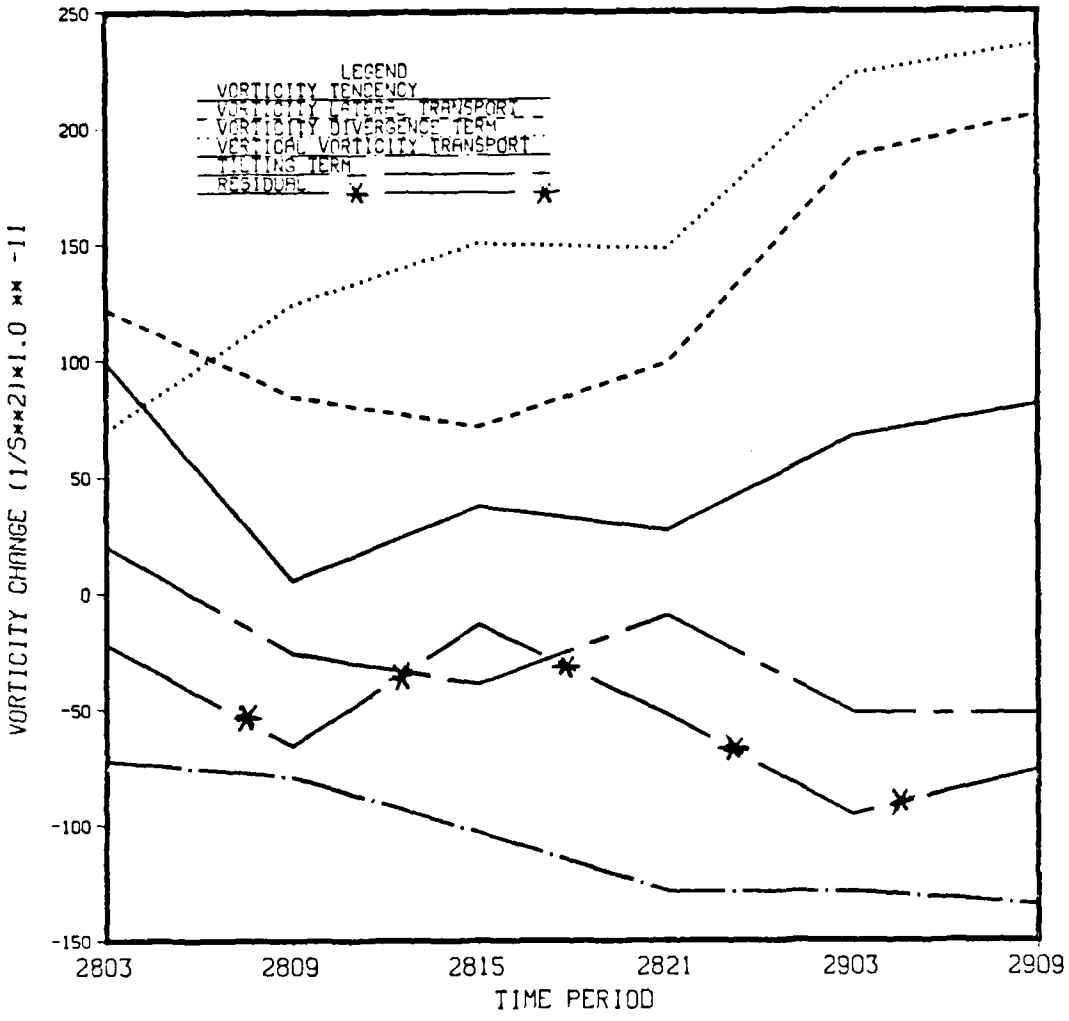

Fig. 4.11 As in Fig. 4.10, except for forecast fields.

V. HEAT AND MOISTURE BUDGET RESULTS

A. GENERAL

The objective of performing heat and moisture budgets using NORAPS data is to better understand the physical processes of diabatic heating and moistening in the evolution of explosive maritime cyclones. Specifically, we want to determine the leading terms of each equation and vertical distribution of heating and moistening in the troposphere. The diabatic heating and moistening rates are only available as a residual in the budgets based on the analysis fields. However, a direct comparison can be made between the rates diagnosed from the forecast fields in the budget formulation and the actual rates predicted in the model. In particular, a direct comparison can be made of the level and phase of the maximum heating and moistening rates.

The moisture budget is only performed for the forecast fields since a moisture analysis is not performed by NORAPS. The moisture source (residual) at model levels is vertically integrated for comparison with the area-averaged 6 hourly precipitation amounts from the model. The heat and moisture equations used for the budget calculations are presented at the beginning of their respective sections. Vertical/time sections for the various terms in each equation will be presented for radius 4^{0} lat. at the end of the chapter. The results at this radius represent the inner core of the cyclone where heating and moistening tend to be concentrated. Results are available out to radius 10^{0} lat. but not shown due to space limitations. After a comparison between the heating/moistening rates diagnosed from the budget calculations and the corresponding model-predicted rates, the column-integrated results are given.

B. HEAT BUDGET RESULTS

The area-averaged flux form of the thermodynamic equation is presented,

$$\overline{\delta T}/\delta t = -1/A \oint T(V_n - V_o)\, dl \qquad (5.1)$$
$$-\partial/\partial p\ (\overline{\omega T}) + \overline{\omega \alpha}/c_p + \overline{\dot{Q}} \quad ,$$

where T is the temperature, A is the area of a surface within the budget volume, V is the normal wind component, V_o is the cyclone's normal velocity component, ω is the vertical velocity, α is the specific volume, c_p is the specific heat at constant pressure and an overbar denotes an area-average of a term. The term of the left side of (5.1) is the quasi-Lagrangian temperature tendency. On the right-hand side (RHS) of (5.1), the first two terms are the horizontal and vertical heat fluxes. The third term on the RHS is the energy conversion term and the final term is the residual. The residual is a measure of the diabatic heating plus computational errors in the budget calculation. Using the flux form of the equation (as opposed to the advective form) reduces the computational errors and attaches greater physical significance to the diabatic heating term, which is not directly observed. A vertical average can be applied to each term of (5.1) to obtain column-averaged heating rates. This representation serves to highlight the important physical processes pertaining to heating or cooling during the growth of the storm. These results are presented at the end of this section.

The vertical time sections of each term in the thermodynamic equation is presented in the advective form of the equation to more easily interpret the physical processes. The energy conversion and the vertical advection terms are shown individually and then combined to form the adiabatic cooling term.

In the quasi-Lagrangian temperature tendency term (Fig. 5.1a), the analyzed case depicts a pattern of early-period cooling, mid-period warming, followed by late-period cooling below 600 mb. This pattern can be interpreted by viewing the cyclone track in Fig. 3.1a. The analyzed low center in eastern Texas is initially in an extremely warm environment. As the storm moves northeast into a colder environment, the cyclone experiences cooling. The cyclone subsequently tracks eastward and the self-amplification process (building of the downstream ridge) causes a warming at 18 GMT 28 March 1984 through the entire troposphere. At 06 GMT 29 March 1984, low-level cooling appears as the storm is nearing its mature stage and lower temperatures have filled most of the cyclone volume below 700 mb. The continued heating above 700 mb is a feature that will be discussed following the presentation of the moisture budget results. The temperature tendency (Fig. 5.1b) in the forecast case shows the same general pattern with the cooling at the last period extending to a higher level (350 mb). By comparison with the analyzed case, the magnitude of this term is slightly greater (2^{0}C/day) overall for the forecast case with sharp differences between 175 and 275 mb at 09 GMT 29 March 1984. Magnitudes of 12^{0}C/day are not considered physically realistic in this layer.

As the horizontal advection in the quasi-Lagrangian formulation has the advection effects due to cyclone velocity removed, this term isolates the purely developmental effects of horizontal temperature advection as the storm intensifies. This term is computed by subtracting the velocity convergence/divergence multiplied by temperature from the total horizontal temperature flux divergence. The horizontal temperature advection (Fig. 5.2a) in the analyses depicts unrealistically large magnitudes (20^{0}C/day) near 225 mb. If equal amounts of cold and warm advection occupied

the budget volume then small magnitudes of this term would be realized. Cold advection in the early periods is evident below 450 mb which rapidly shallows at 12 GMT 28 March 1984. This is consistent with the discussion in Chapter 3, wherein stronger cold advection is found in an area-averaged sense early in the storm, while the warm advection pattern is relatively weak. The horizontal advection (Fig. 5.2b) in the forecast case verifies well with the exception of higher values (30-35^{0}C/day) near 225 mb.

A disturbing factor is the unusually large values of horizontal temperature advection near 225 mb in both the forecast and analyzed fields. In general, one would expect to see weak warm advection aloft within the budget volume due to the westward tilt of a baroclinic system. Since the budget volume translates with the surface low center, warm advection aloft occurring to the east of the upper-level trough position would be a displaced to the west of the budget volume. Therefore, relatively weak upper-level horizontal temperature advection would be occurring within the budget volume. Such large values at this level are clearly in error. A possible explanation for the forecast case is that large errors can be introduced in the interpolation from sigma to pressure surfaces. However, since this problem likewise occurs in the analyses, a faulty interpolation scheme in a region of few observations can account for this problem. An alternate explanation is related to supersaturating the upper levels of the atmosphere which releases large amounts of latent heat, as will be discussed in more detail in the next section. However, this would only be true for the forecast case.

The vertical temperature advection (Fig. 5.3a) in the analyses has a maximum at 350 mb with a 40^{0}C/day rate at 06 GMT 29 March 1984. This maximum level in the forecast (Fig. 5.3b) verifies well, but a much higher value (65^{0}C/day) is

predicted. As the area-averaged levels of maximum omega (Fig. 3.2) are 700 and 500 mb for the analyses and forecast fields, clearly a large vertical temperature gradient causes the higher maximum level of vertical temperature advection. Large vertical gradients in temperature at 350 mb, where one would normally expect to find the tropopause for such a vigorous extratropical cyclone, would not be realistic.

The area-averaged temperature field (Fig. 5.4) indicates a decrease in temperature through the depth of the atmosphere (to 100 mb), without showing a tropopause in both the forecast and analyzed cases. Individual grid points were examined to confirm these unrealistic vertical temperature structures. These unrealistic vertical temperature profiles introduce errors into the column-averaged heat budgets at upper levels. Vertical temperature profiles in the data should be closely checked to ensure physical consistency prior to undertaking budget computations.

The level where energy conversion (Fig. 5.5a) is a maximum (-55^{0}C/day) is between 350 to 400 mb. The forecast case (Fig. 5.5b) depicts a much different profile with an absolute maximum of -90^{0}C/day near 350 mb at 03 GMT 29 March 1984. A secondary maximum of -45^{0}C/day is found at 09 GMT 28 March 1984 at the same level. The general pattern of the vertical profiles for both the analyzed and forecast cases looks very similar to the vertical velocity profiles in Fig. 3.2, except the maxima are shifted upward due to the weighting factor of specific volume in the energy conversion term.

To more easily facilitate the determination of the residual by viewing the contribution of individual terms, the energy conversion and vertical temperature advection are grouped together. These two terms have a common factor of omega and are of opposite signs. The resulting term is known as the adiabatic cooling term, written as $\omega(\Gamma_d - \Gamma)$

where Γ_d is the dry adiabatic lapse rate and Γ is the environmental lapse rate or vertical temperature gradient. $\Gamma_d - \Gamma$ is always constrained to be greater than zero in the model atmsophere (due to the dry convective adjustment scheme). As the mean vertical motion is upward in the region of the cyclone, i.e, ω is less than zero, this term is negative and opposes heating. This term can also be viewed as modulating the effects of latent heating during cyclone development. The adiabatic cooling profile (Fig. 5.6a) in the analyses depict the strongest cooling tendency (-25^{0}C/day) at 850 mb during the last time period. In the forecast case (Fig. 5.6b), a noticeable difference is seen above 350 mb with strong cooling rates of 25 to 35^{0}C/day which are 10 to 15^{0}C/day greater than the analyses. The 25^{0}C/day cooling rate at 03 GMT 29 March 1984 is 300 mb above the maximum in the analysis.

The surface sensible heat flux (Fig. 5.7) is archived for the forecast, but is not available for verification purposes since it is not directly observable. A definite diurnal trend is seen in the surface sensible heat flux pattern because most of the storm volume is over land. This term contributes to the warming of the column below 775 mb. In a column and area-averaged sense, its overall contribution is very small. A maximum heating rate of 10^{0}C/day occurs from 15-21 GMT 28 March 1984 (daylight hours) below 850 mb. However, its effect is significant over localized regions since this upward flux of heat can destabilize lapse rates and initiate convection and be an important contributor during a particular phase of storm development.

The residual term is computed as the balance of the other calculated terms, and thus includes diabatic heating and computational errors. Since such physical processes as latent heating and radiational cooling cannot be directly measured, they must be inferred as a residual in the

computation. The radiational cooling term is generally acknowledged to be small in relation to the latent heating. The residual in the budget based on analyses (Fig. 5.8a) depicts the level of maximum heating at 550 mb. The absolute maximum in heating (20^{0}C/day) occurs at 06 GMT 29 March 1984. This heating rate is in close agreement with the results of Liou and Elsberry (1985), who used European Center for Medium Range Weather Forecasting (ECMWF) analyses for a western North Pacific Ocean case study and found a 25^{0}C/day heating rate at 600 mb. By comparison with the residual in the forecast case (Fig. 5.8b), the level of maximum heating verifies well (500-550 mb) and a secondary maximum is predicted between 225 and 350 mb which is not realistic. Large-scale precipitation and middle-level convection occurring within the extratropical cyclone would produce a lower level of maximum heating as opposed to a tropical cyclone where deep convection would cause greater diabatic heating aloft. Two separate maxima in heating occur at 09 GMT 28 March (15^{0}C/day) and 03 GMT 29 March 1984 (20^{0}C/day). Another difference from the analyses fields is the cooling occurring below 850 mb at 03 GMT 29 March 1984, which is probably due to evaporational cooling.

The vertical profile of the heating rates (Fig. 5.9) predicted by the model is available for comparison with the budget diagnosed residual from the forecast fields. This heating rate is the average of two instantaneous values each 6 h during the integration and is not the accumulated 6 h total which would be more comparable to the values derived diagnostically. The instantaneous values (^{0}C/time step) have been converted to a daily rate (^{0}C/day). These heating rates include net condensational heating plus short and long-wave radiational effects. The surface sensible heat flux is an output field of the NORAPS model but is not included in the model heating rate since it is not

distributed over a constant depth in the model prediction as is assumed in the diagnostic model (lowest 200 mb). The level of maximum heating is 450 mb (Fig. 5.9a) which is higher than the level of 550 mb diagnosed in the analyses and forecast from the budget residual calculation. Two distinct maxima appear in the model-predicted vertical heating profile: a 30^{0}C/day center at 15 GMT 28 March and a 35^{0}C/day center at 03 GMT 29 March 1984. Although the presence of a double maximum pattern agrees with the diagnosed residual from the analyzed fields, the magnitudes of the model-predicted heating rates are about 100 and 50% greater, respectively. Values at individual grid points are on the order of 200-400^{0}C/day in localized regions of the storm.

The model-predicted rates are also approximately double those diagnosed for the forecast fields. This difference can be easily shown by subtracting the model heating rates from those diagnosed in the budget for the forecast fields (Fig. 5.9b). This figure gives us an estimate of calculation errors in the budget. Ideally, we would desire to have very small differences to verify the accuracy of the budget. The consistent profile of errors reveals an overestimation of heating by the model from 275 to 775 mb and excessive cooling predicted by the model in the lowest layers. The errors above 275 mb are a result of the spuriously large values of horizontal temperature advection in the budget calculation.

The column and area-averaged heat budget results are presented for the analyses (Fig. 5.10) and forecast (Fig. 5.11). The leading term (in a cooling sense) is the adiabatic cooling term, which is strongly modulated by the vertical velocity field. The diabatic heating term (residual plus errors) is the next largest term and is on the order of 10 to 12^{0}C/day during the last half of the storm. The primary role of diabatic heating is to offset adiabatic

cooling and promote heating within the budget volume which can contribute to storm intensification. The horizontal temperature advection is smaller than the residual during the early stage of the storm but becomes comparable to the residual during the last half of the storm. The quasi-Lagrangian temperature tendency contributes only weakly to heating or cooling the budget volume during the course of the storm.

The near-zero heating rates in the model at the beginning of the forecast period are not realistic because of the extensive convection observed along the Gulf Coast. The difference between the area and column-averaged budget residual and model-predicted heating rates at radius 4^{o} lat. (Fig. 5.12) is only 1 to 2^{o}C/day from 03 GMT 28 March to 03 GMT 29 March 1984. The quasi-Lagrangian temperature tendency can introduce errors due to the rapid deceleration of the storm during the last 12 h of the model storm. Although not previously discussed, the column and area-averaged residual for radius 6^{o} lat. is 8.5^{o}C/day during the intensification of the storm, which agrees well with Bosse's (1984) results for the same radius during an explosive stage of cyclogenesis in the western North Pacific Ocean. Thus, we are provided with additional evidence that this storm has many similarities to an explosive maritime cyclogenesis case.

C. MOISTURE BUDGET

An important topic to be discussed before presenting moisture budget results is how the initial moisture field is specified in the NORAPS model. The moisture analysis is obtained by using the 12 h NORAPS forecast specific humidity field. The NORAPS forecast fields of moisture content are output in terms of vapor pressure. The vapor pressure is internally converted into specific humidity within the budget program.

As with the other budgets, various sources of errors can arise. The interpolation from the NORAPS grid to the budget volume is with a bi-cubic spline interpolation scheme. For very small values of vapor pressure, particularly above 500 mb, small negative values of vapor pressure can be introduced. Another problem can arise in the vertical moisture flux calculation. A harmonic-mean scheme is used in NORAPS to interpolate the moisture field (at odd levels in the model) to the even levels where vertical velocity is specified. This scheme has the effect of biasing the smaller values downward, which can cause erroneously large moisture divergence/convergence in the vertical. Thus, the vertical flux convergence of moisture that is computed in the budget model by using a linear vertical interpolation scheme can also introduce errors.

A leapfrog (centered differencing) scheme is currently used for the moisture prediction equation. The original version of NORAPS used a forward-in-time and space (upwind or one-sided difference) scheme, which has larger truncation errors and tends to damp the smaller-scale features in time. The change to this new scheme resulted in some complications. One problem was the omission of a time filter to smooth the large computational modes that cause oscillations in a centered-differencing scheme. The resulting problem for the budget is that large errors can occur in the quasi-Lagrangian moisture tendency (either too small or too large).

The terms of the area-averaged moisture budget equation are given in (5.2),

$$\overline{\delta q/\delta t} = -\,1/A \oint q(V_n - V_o)\, dl \qquad (5.2)$$
$$-\partial/\partial p\ (\overline{\omega q}) + \overline{E} - \overline{P} \quad ,$$

where q is the specific humidity, A is the area of a particular surface within the budget volume, V_n is the normal wind component, V_o is the cyclone's normal velocity component, ω is the vertical velocity, E is evaporation , P is precipitation and an overbar denotes the area-average of a term. The quasi-Lagrangian moisture tendency is the term on the left side, whereas the horizontal and vertical moisture fluxes are the first two terms on the right side of (5.2), respectively. The last term on the right side is the residual or moisture sink term. This term includes the combined effects of condensation, evaporation and moisture fluxes from the surface. As these terms are not directly observable, they must be computed as a residual. The convention for this residual is negative (positive) if precipitation (evaporation) is occurring. The quasi-Lagrangian moisture tendency differs from the moisture sink term in that specific humidity is a measure of the amount of water vapor (relative humidity) in the air, whereas the moisture sink is a measure of the liquid water being condensed within the budget volume (assuming precipitation exceeds evaporation). When condensation occurs within a region, the phase change results in a decrease in the amount of water vapor. In practice, while precipitation is measured at regular intervals (over land) by the standard observing network, surface moisture fluxes and evaporation are not directly measured but must be inferred from approximations.

The primary objective in performing the moisture budget is to determine the agreement with the heat budget with respect to the level and phase of maximum heating and moistening. As in the other budgets, the moisture budget for radius 4^0 lat. will be discussed. Since a moisture analysis is not performed by NORAPS, a comparison of the diagnosed budget results in the forecast case cannot be made with the analyzed case. A comparison is made between the

moisture source term diagnosed from the budget and the moistening rate computed directly in the model. The moistening rate, as in the model-predicted heating rate, is the average of two instantaneous values each 6 h during the integration.

D. MOISTURE BUDGET RESULTS

The quasi-Lagrangian moisture tendency (Fig. 5.13a) in the forecast reveals an oscillating trend in phase with the precipitation cycle (Fig. 5.14). Relatively strong moistening occurs prior to 09 GMT 28 March 1984, and is followed by a weak period of moisture decrease within the budget volume from 09-18 GMT 28 March 1984. This period of moisture decrease correlates with the precipitation "burst" during the 12-18 GMT 28 March 1984. A strong increase in the moisture tendency centered at 775 mb occurs from 18 GMT 28 March to 06 GMT 29 March 1984 prior to the precipitation "burst" between 06 and 12 GMT 29 March 1984 (Fig. 5.14). A decrease in the moisture tendency occurs from 06 to 09 GMT 29 March 1984 which correlates with the moisture loss from the atmosphere during the heavy precipitation period.

The horizontal moisture flux (Fig. 5.15a) derived from the forecast fields has a layer of moisture convergence (surface to 500 mb) beneath a shallower and much weaker layer of moisture divergence from 275 to 500 mb. Fuelberg et al. (1986) observed a much deeper layer (up to 350 mb) of moisture convergence in a severe thunderstorm environment. They used a dense observation rawindsonde network in a stationary budget study over a relatively short time period with 3 h observations. The horizontal moisture flux is composed of an advective and convergence/divergence term. The convergence/divergence term accounts for 75% of the total moisture flux in this study, which is similar to the results of Fuelberg et al. (1986). The reason for the weaker moisture convergence aloft in this study is attributed to the shallower horizontal convergence layer as shown in the mass budget for this case.

The vertical moisture flux term represents the redistribution of moisture in the vertical. Horizontal moisture flux convergence at the lower levels must experience a corresponding vertical flux divergence from continuity considerations. The vertical moisture flux (Fig. 5.15b) based on the forecast fields shows the pattern of low-level moisture divergence below 775 mb and moisture convergence from 775 to 275 mb. However, an alternating and unrealistic pattern is noted in the vertical profile of the vertical moisture flux after 21 GMT 28 March 1984. The individual grid points were examined in the neighborhood of the storm to determine which variable contributed to this unrealistic profile. The 400 mb specific humidity field at 06 GMT 29 March 1984 (Table 1) is displayed for the region surrounding the storm. Unrealistic values in excess of 10 g/kg are seen in the fourth and fifth rows of this field. Small negative values are also noted in this field which may be due to the bi-cubic horizontal interpolation with such large moisture gradients. An oscillatory trend in the vertical specific humidity profile (not shown) is evident between 850 and 400 mb at 06 GMT 29 March 1984, which is directly responsible for the vertical flux profile (Fig. 5.15b).

The question naturally arises as to the cause of such unrealistic specific humidity values. Checks (by Dr. C.-S. Liou) of the NORAPS program revealed two sources of error. First, an incorrect specification of the moistening rate occurred during the switch to a centered-differencing scheme. The heating rate was likewise in error since only one-half the appropriate rate was used in the heat prediction equation. The moistening rate appropriate for the one-sided differencing scheme was used in the centered-differencing scheme, and therefore was too low by a factor of two. Since the (negative) moistening rate is only one-half of the true precipitation rate, moisture is

continuously carried over into each successive time step, which leads to a supersaturation. Second, the omission of a time filter in the moisture prediction equation using the leapfrog scheme could result in erroneous specific humidity values if left unsmoothed.

The "over-moistening" has a direct effect on the precipitation predicted by the model. The model precipitation field (without area-averaging) has a maximum value exceeding 10 cm/6 h at 12 GMT 29 March 1984 (Fig. 5.14). Maxima in precipitation during the 36 h forecast period occur at 18 GMT 28 March and 12 GMT 29 March 1984. A nearly linear increase in precipitation for this storm would be more consistent with available observations (over land). A review of NWS daily weather summary sheets for 28 and 29 March 1984 showed the largest observed rainfall rates (north of the warm front) to be on the order of 5 cm/day. Area-averaged precipitation for radius 4^{0} lat. from the NORAPS model ranges between 2 and 4 cm/day until the last time period when the rate increases to 6 cm/day.

The residual in the moisture budget includes the condensation, evaporation and the surface moisture fluxes. A negative value indicates more condensation would be occurring than evaporation, while a positive value indicates more evaporation would be occurring than condensation. Since no liquid water is retained in the model atmosphere, a positive residual at upper levels indicates an unrealistic result. The vertical cross section of the residual (Fig. 5.16a) in the budget based on forecast fields reveals a large moisture sink in the middle troposphere throughout the entire period due to condensation exceeding evaporation. The maximum levels of moistening occur at 600 and 350 mb. An exception is an anomalous positive region near 400 mb at 03 GMT 29 March 1984 that is associated with the spurious vertical flux profile discussed above. The small residuals above 275

mb are an artifact of the negligible amount of moisture in this region. An absolute maximum in moistening occurs at 09 GMT 29 March 1984, which is slightly contaminted by the problem discussed with the profile of the vertical moisture flux. This strong moisture sink (precipitation) agrees favorably with the large precipitation rates predicted by the model at this time. Another maximum in moistening occurs at 15 GMT 28 March 1984 which correlates well with the precipitation maximum at 18 GMT 28 March 1984 (Fig. 5.14).

The archived moistening rate in the forecast model (Fig. 5.16b) has a different structure with much greater rates than diagnosed from the moisture budget. Distinctive maxima are located near 450 mb at 15 GMT 28 March and at 03 GMT 29 March 1984. These moistening rates necessarily correspond in level and phase to the heating rates (Fig. 5.9). These archived rates are approximately double those diagnosed in the budget calculation. This is a result of the incorrect specification of the moistening rate when switching to a centered-difference scheme, which introduces a factor of two difference. The column-integrated moisture budget results for the diagnosed residual (moisture source), the model-predicted moistening rate and the area-averaged precipitation rates are presented in Fig. 5.17. As the moistening rate predicted by the model contains the accumulated effects of condensation, evaporation and surface moisture fluxes of the time average of two instantaneous values each 6 h apart, it differs from the model precipitation which is an accumulated 6 h total. In fact, the two would be exactly equal if an accumulated 6-h archived moistening rate was used and there were no computation errors in the budget. However, the diagnosed moisture source from the budget is systematically less than the model-predicted precipitation and moistening rates. Since this error is systematic, this provides

further evidence of a model problem if the budget calculations have been performed properly. This difference between the curves (Fig. 5.17) can be traced to the application of only one-half the moistening rate in the centered-differencing scheme for the moisture prediction equation. This error in the model leads to an overprediction of the moistening and precipitation rates.

E. SUMMARY

The moisture budget results show the pattern of horizontal moisture flux convergence in the surface layers which is modulated by the vertical velocity field. The moisture is then transported into the upper troposphere through the vertical moisture flux, cools moist adiabatically until it reaches saturation and then condenses and falls as precipitation. The phase change from water vapor to liquid releases heat at a certain level in the troposphere which is an essential ingredient to the energetics of the cyclone.

The major factor for many of the errors in the vertical distribution of heating and moistening is believed to be linked to the incorrect specification of the heating and moistening rate which leads to an "over-moistening" of the model atmosphere. The harmonic-mean scheme used in calculating the vertical moisture fluxes for the moisture prediction may also account for some of the variance in the vertical moisture flux during the last two time periods (Fig. 5.15b).

The moisture budget results reveal a discrepancy between the diagnosed and the archived precipitation results. The precipitation fields, the vertical moisture flux and the model-predicted moistening rates provide evidence of a systematic error in the NORAPS model. A distinct oscillating pattern is found in the model precipitation field. This oscillatory trend is likely linked to the area-averaged vertical motion field in the model forecast (Fig. 3.2b) which also exhibits a double maximum in the field.

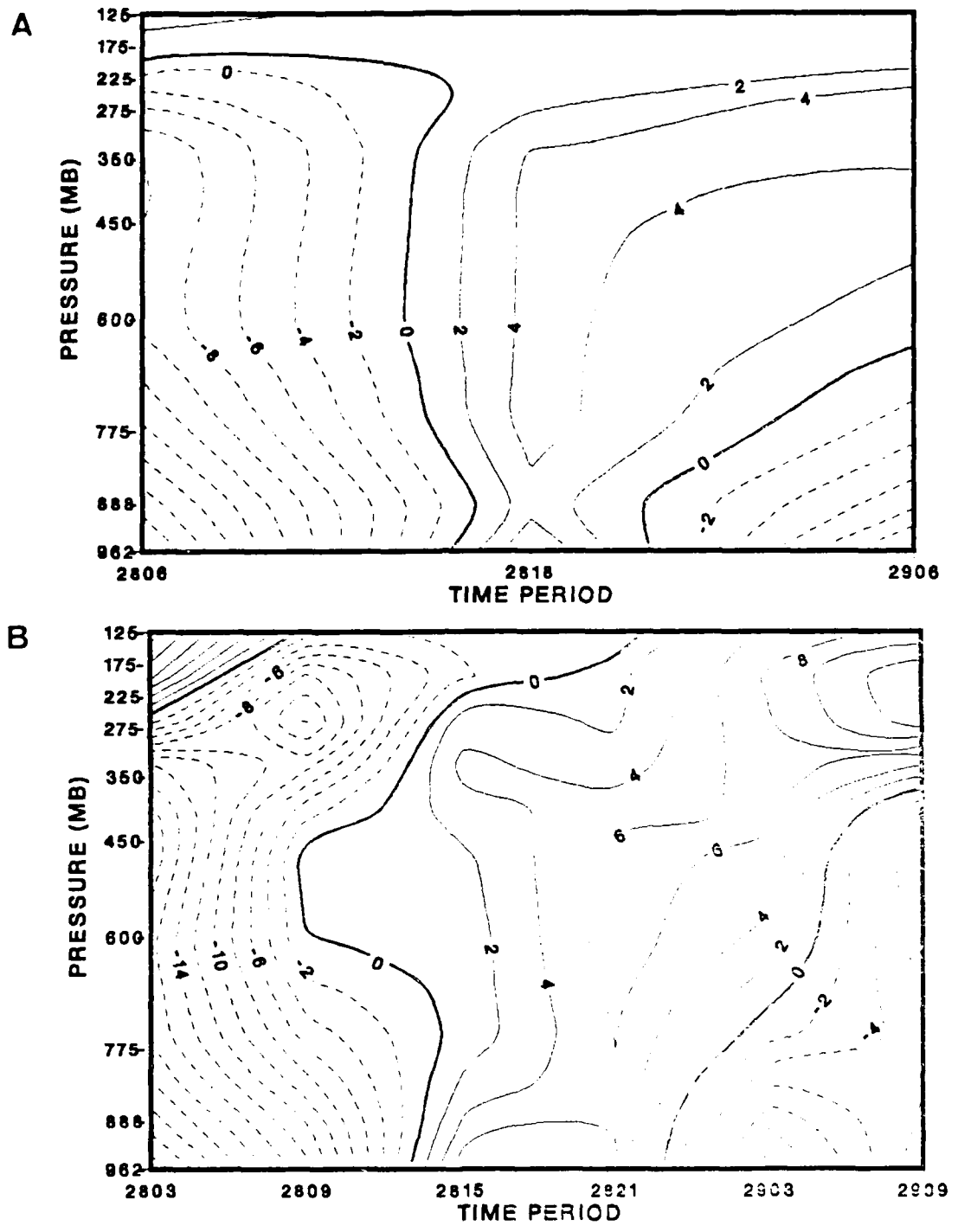

Fig. 5.1 Quasi-Lagrangian temperature tendency for radius 4 in the (A) Analysis and (B) Forecast. Positive/negative values indicate heating/cooling of budget volume. Contour intervals are 2°C/day.

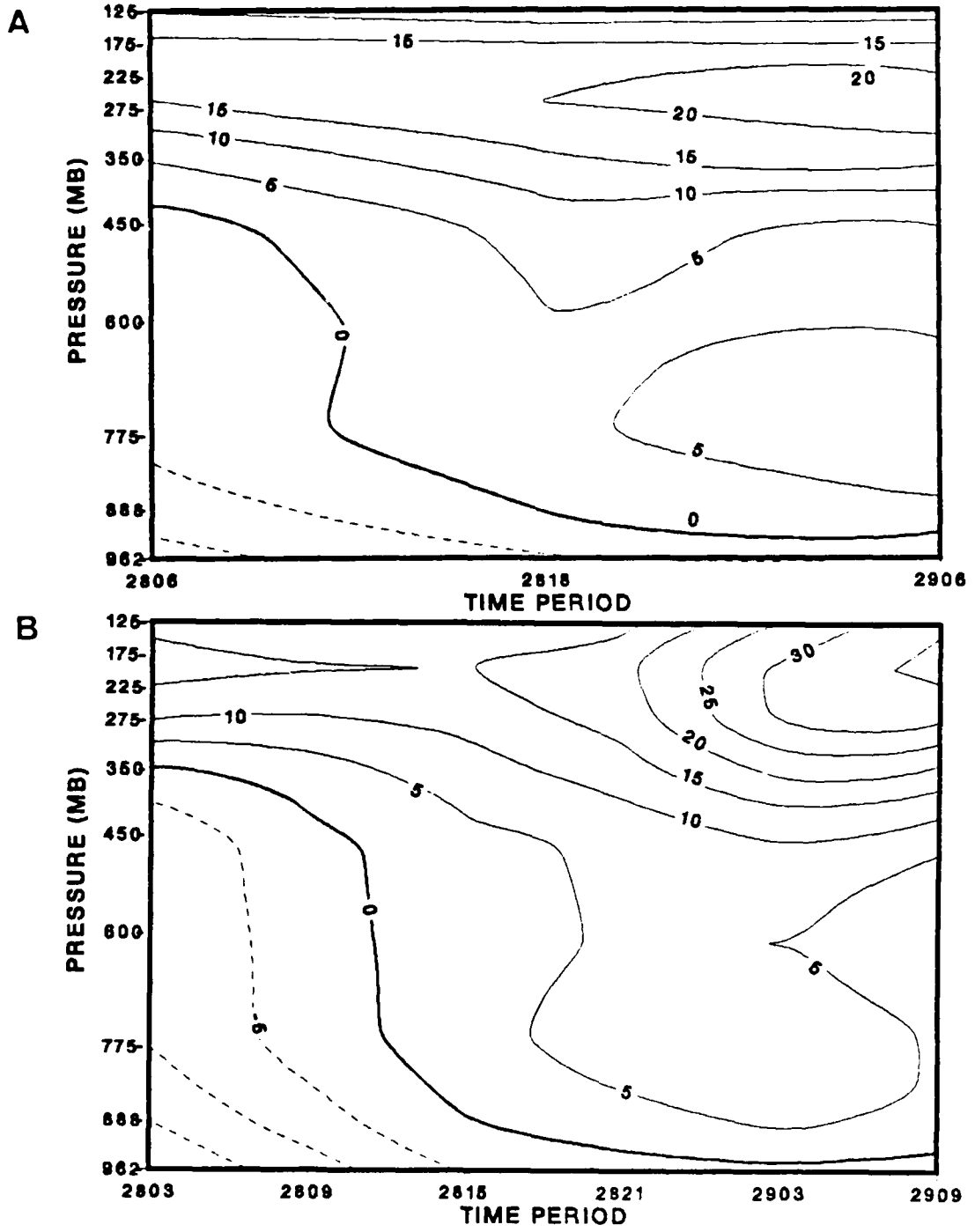

Fig. 5.2 Horizontal temperature advection in the (A) Analysis and (B) Forecast. Positive (negative) values indicate warm (cold) advection. Contour interval is 5°C/day.

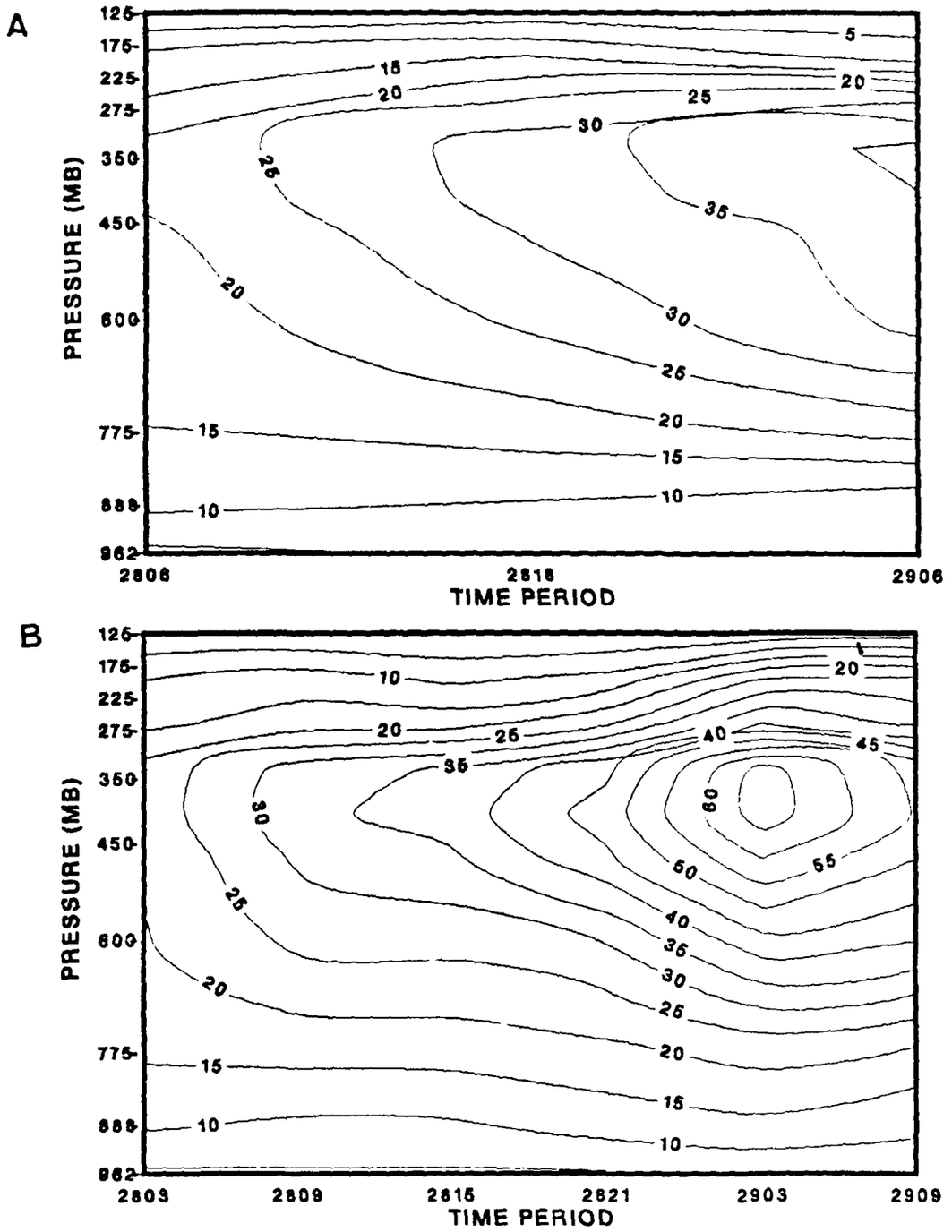

Fig. 5.3 As in Fig. 5.2, except for vertical temperature advection.

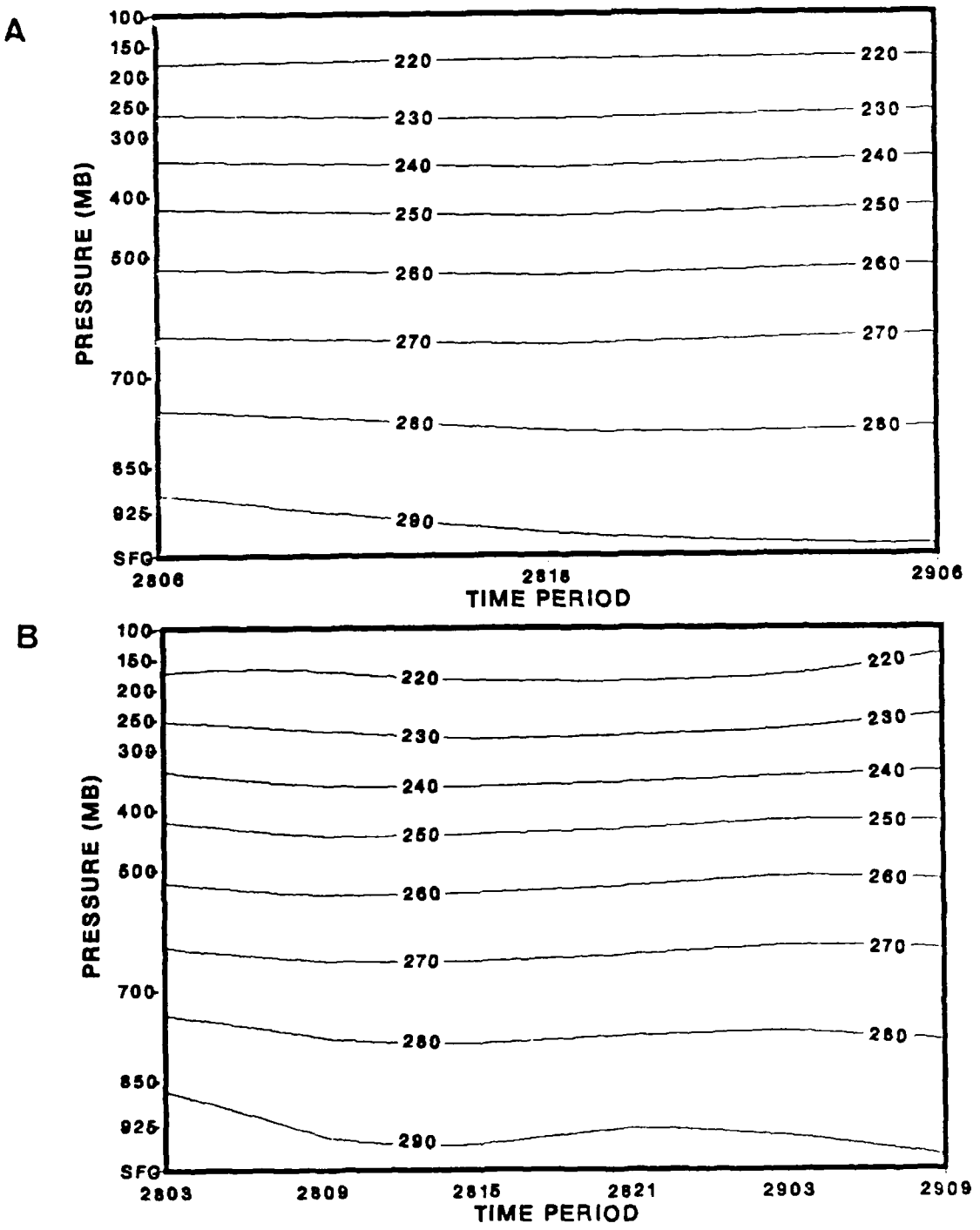

Fig. 5.4 Area-averaged temperature in the (A) Analysis and (B) Forecast for radius 4. Contour interval is 10°K.

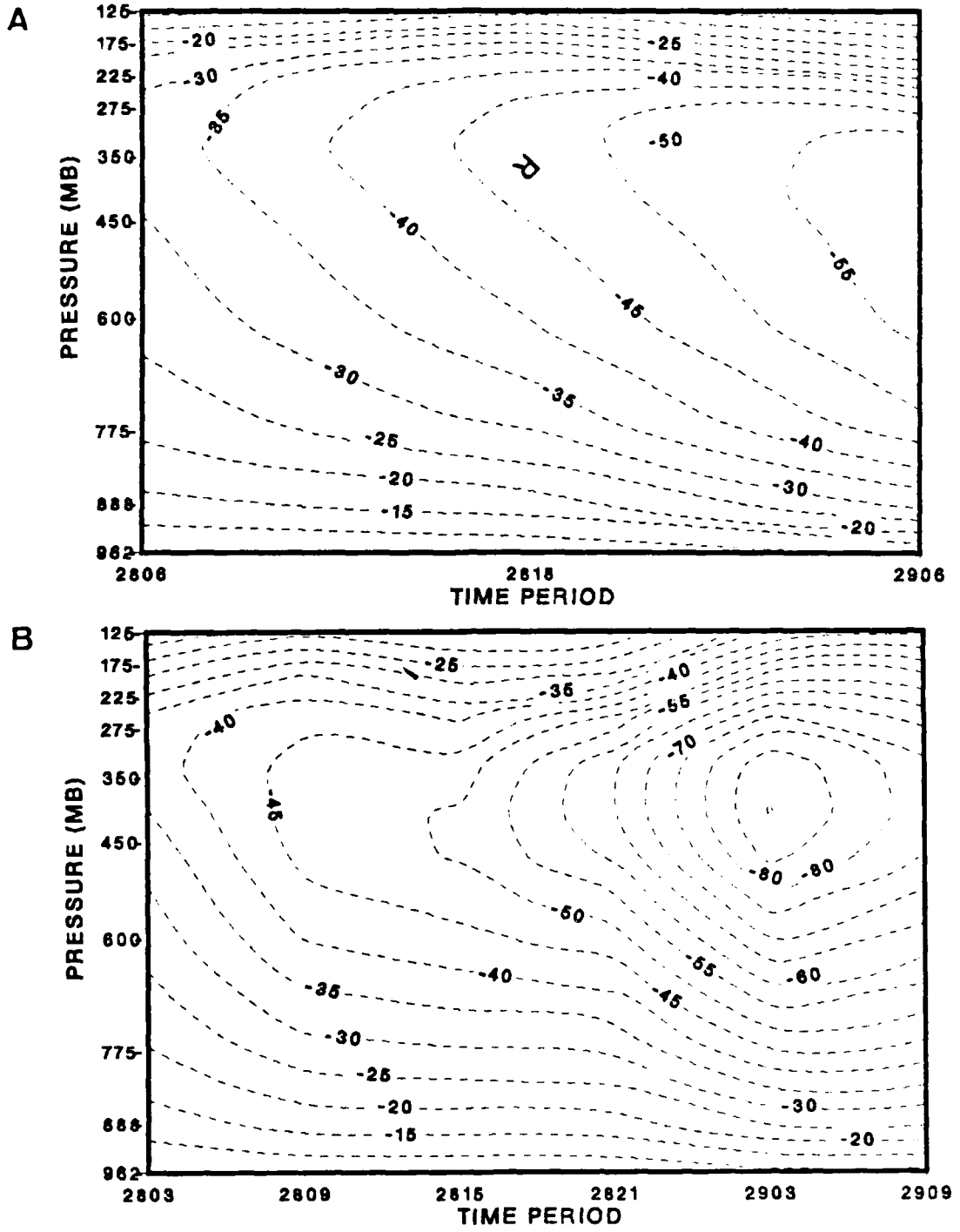

Fig. 5.5 As in Fig. 5.2, except for energy conversion $(\omega\alpha/c_p)$.

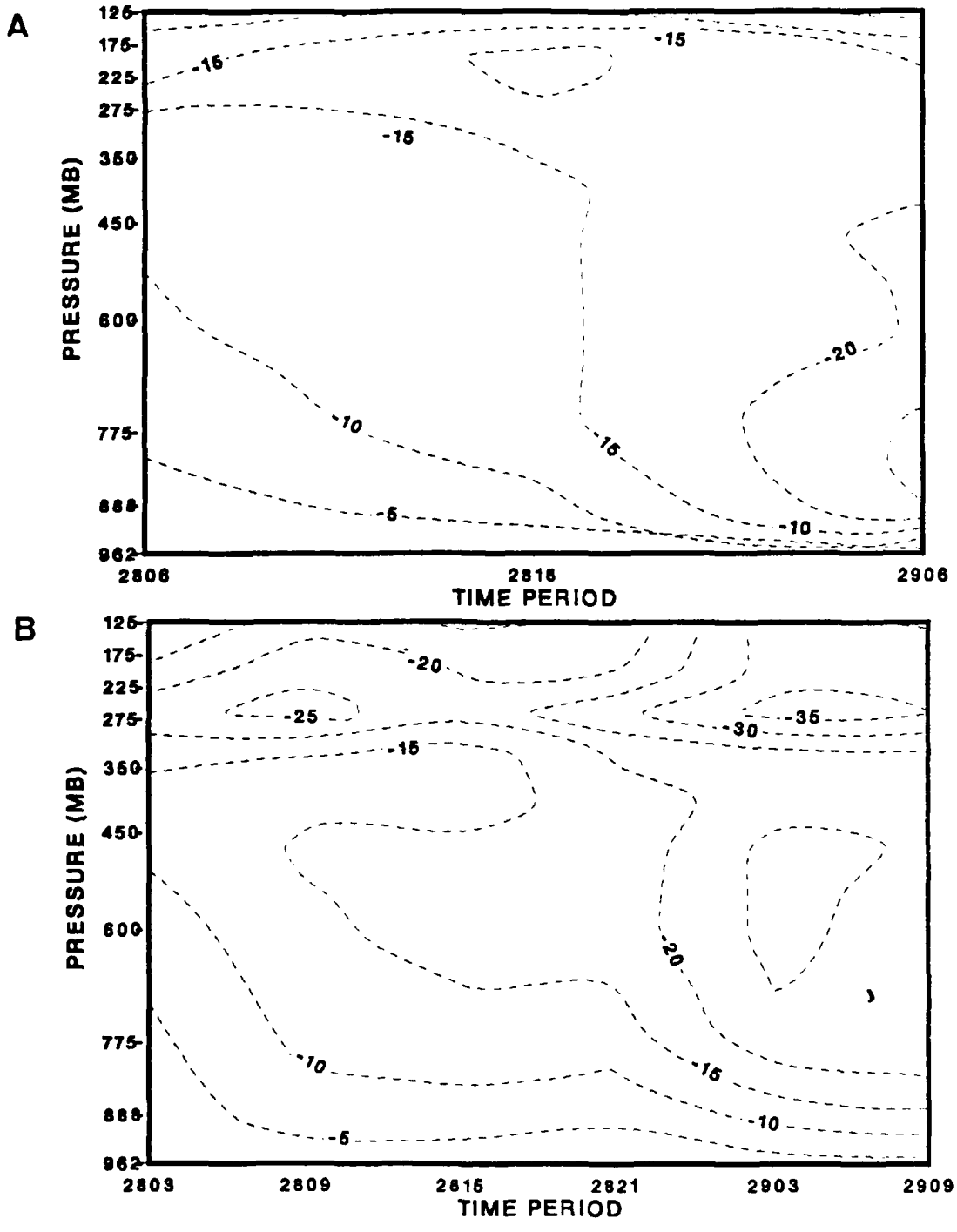

Fig. 5.6 As in Fig. 5.2, except for adiabatic cooling.

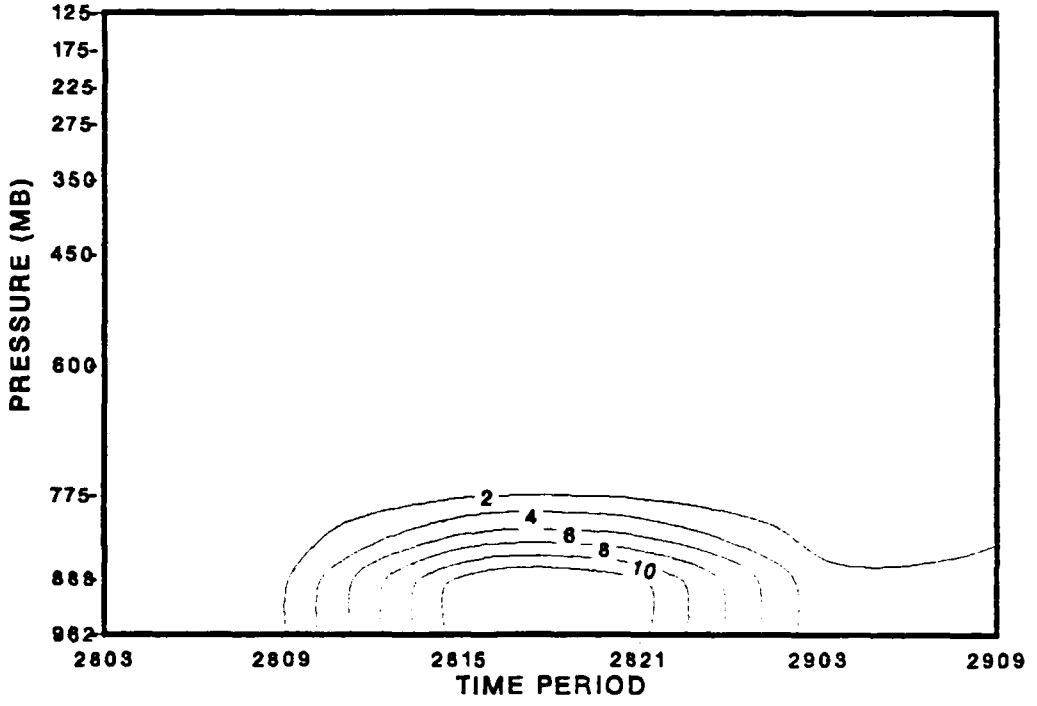

Fig. 5.7 Forecast surface sensible heat flux convergence within lowest 200 mb for radius 4 in ^{o}C/day.

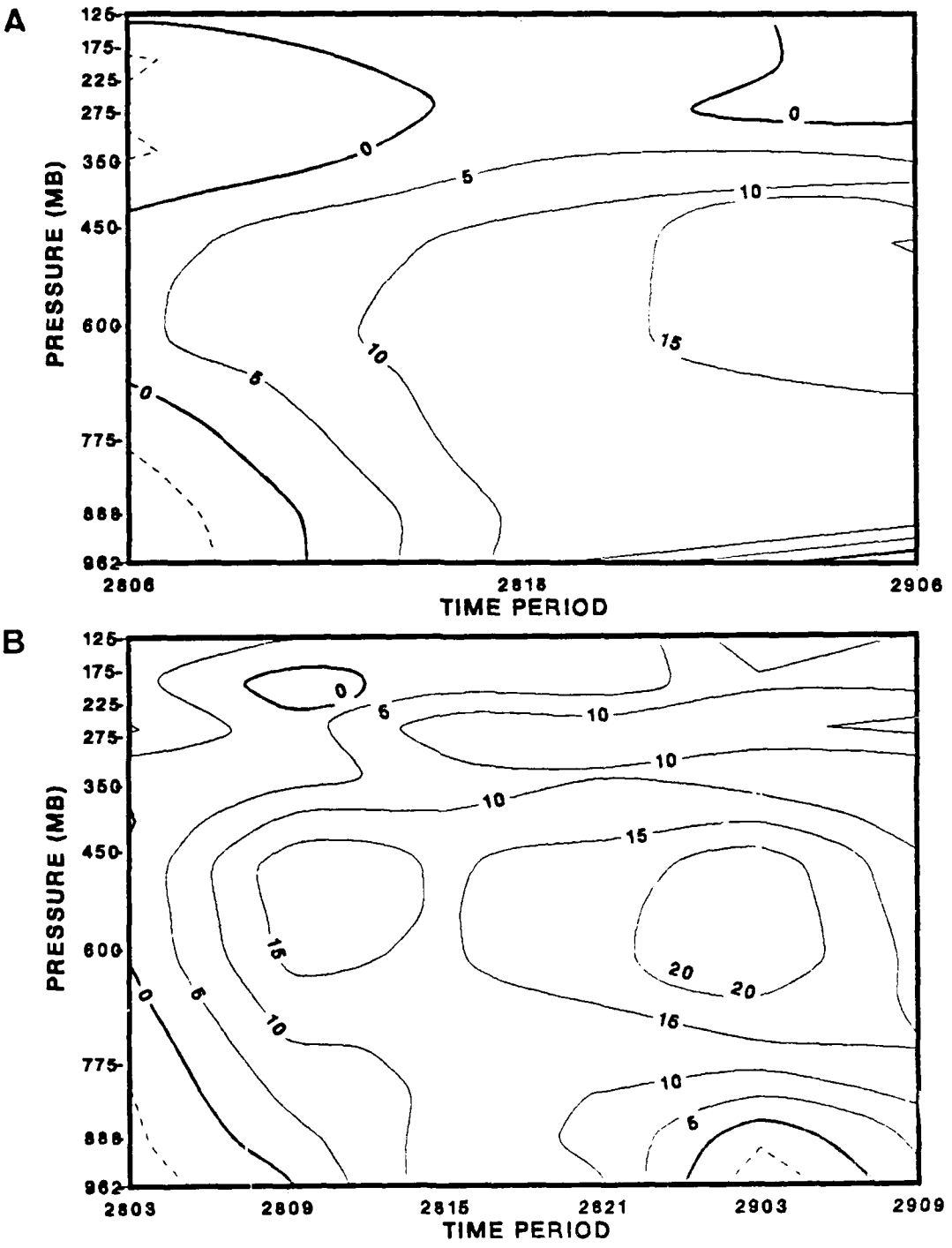

Fig. 5.8 Heat budget residual for the (A) Analysis and (B) Forecast for radius 4. Positive (negative) values indicate heating (cooling). Contour interval is 5°C/day.

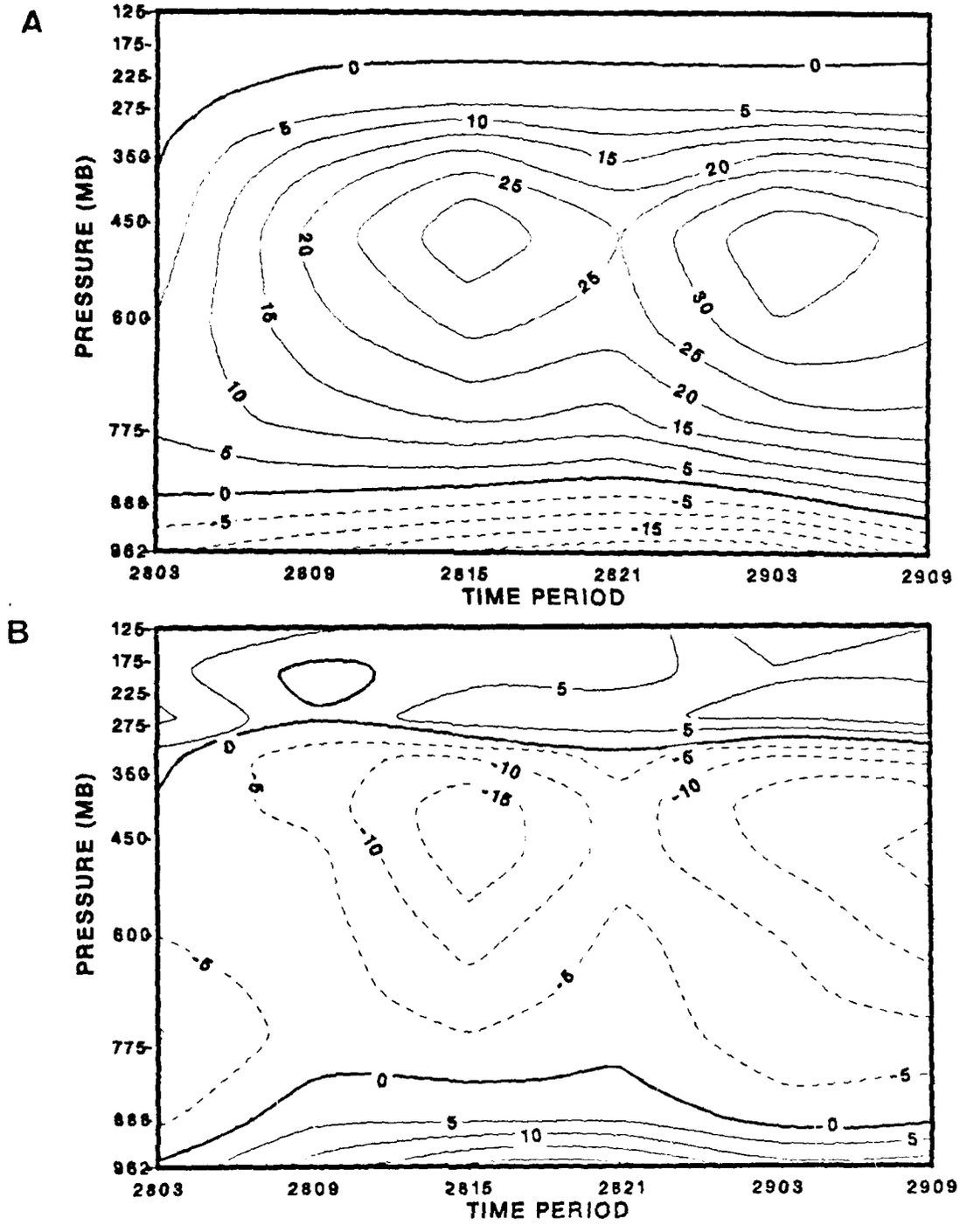

Fig. 5.9 (A) Model-predicted diabatic heating rate. (B) Difference of budget residual and model-predicted diabatic heating rate for radius 4. Contour interval is 5°C/day.

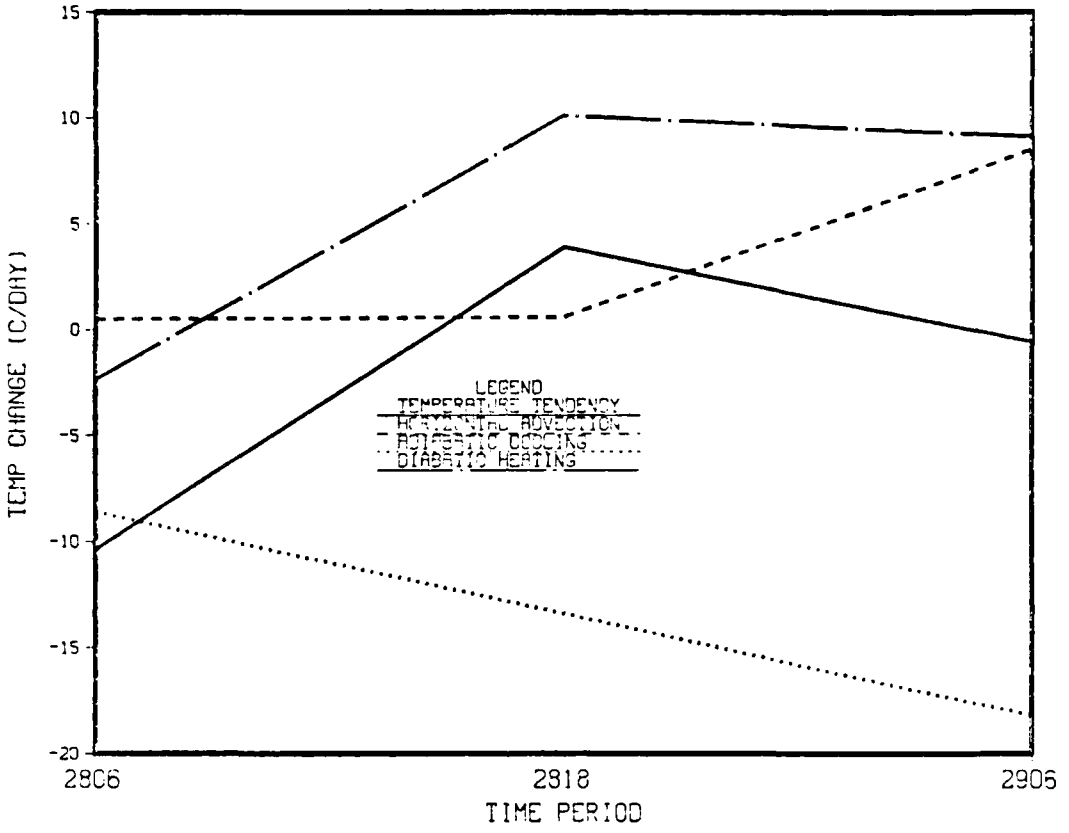

Fig. 5.10 Area and column-averaged heat budget terms at radius 4 based on analyzed fields. Solid line depicts temperature tendency term, dotted line is adiabatic cooling, dashed line is horizontal temperature advection and the chain-dotted line is the diabatic heating. Units of heating are °C/day and the time is given in day (first two digits) and hours (in Greenwich, second two digits).

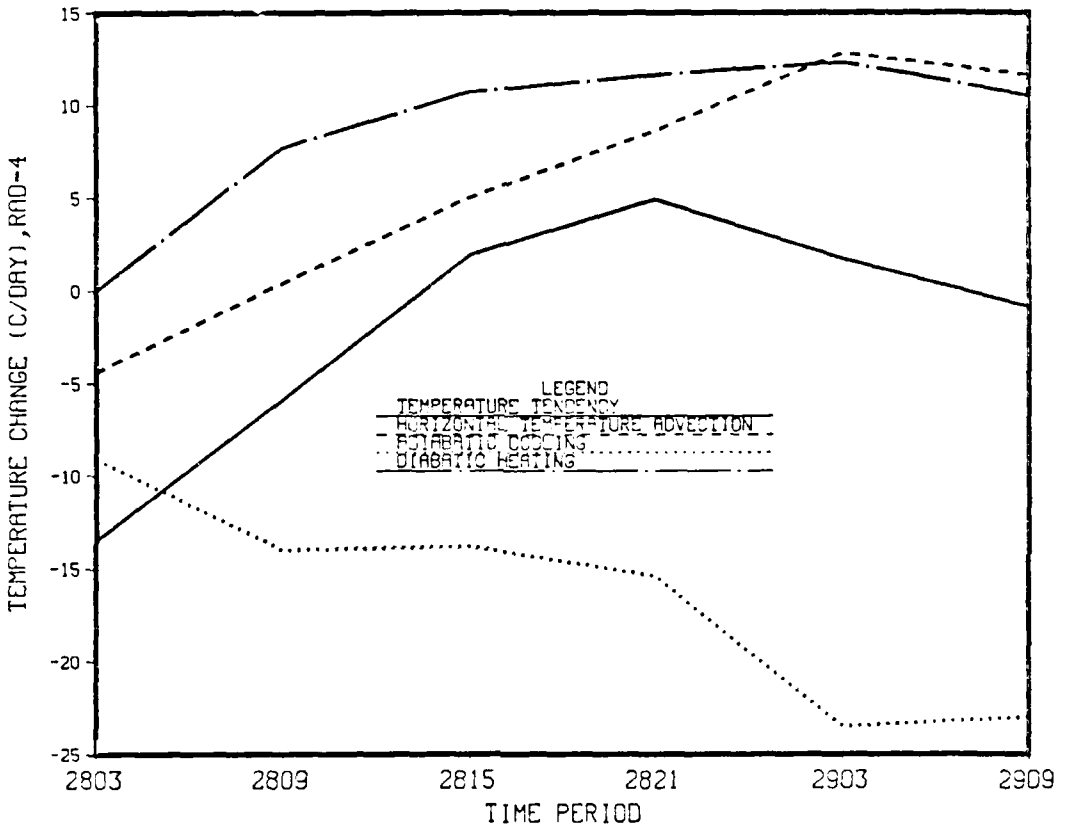

Fig. 5.11 As in Fig. 5.10, except for the forecasts.

AD-A174 494 HEAT AND MOISTURE BUDGETS OF AN EXTRATROPICAL CYCLONE BASED ON NAVY OPERA (U) NAVAL POSTGRADUATE SCHOOL MONTEREY CA R E RAU JUN 86 2/2

UNCLASSIFIED F/G 4/2 NL

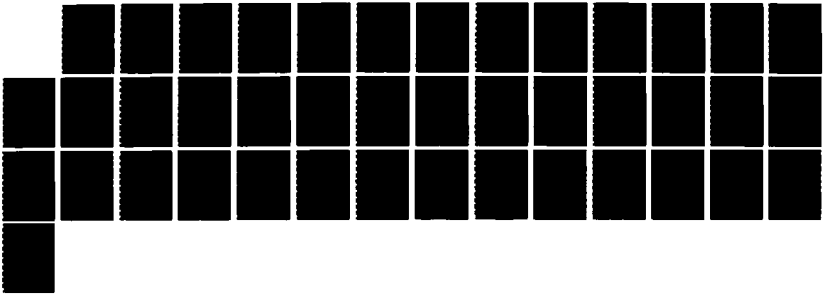

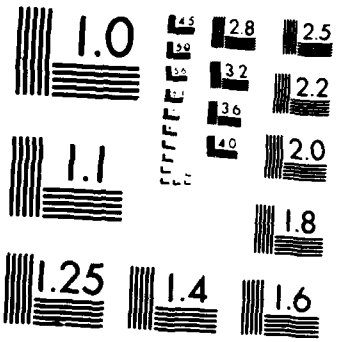

MICROCOPY RESOLUTION TEST CHART
NATIONAL BUREAU OF STANDARDS 1963-A

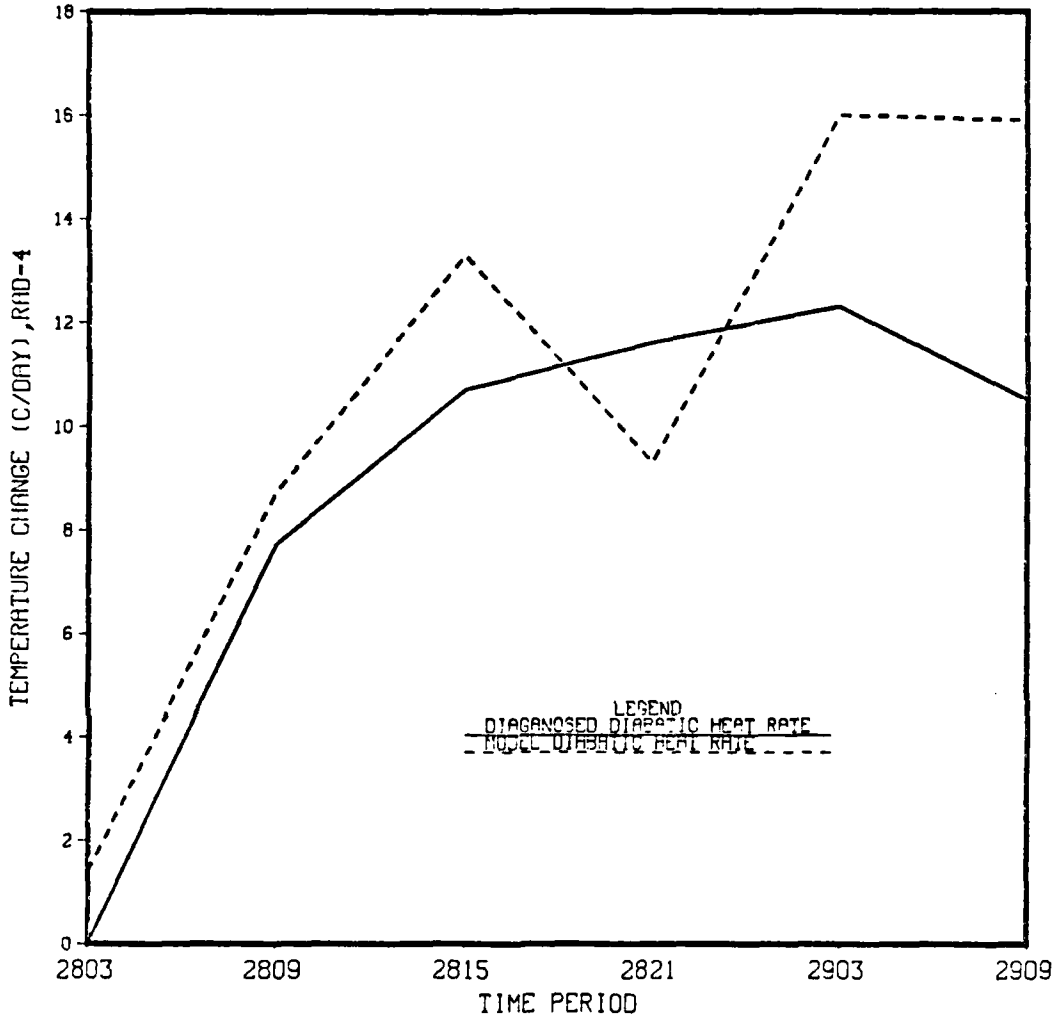

Fig. 5.12 Column-averaged heat budget residual (solid) and model-predicted diabatic heating rate (dashed) for radius 4. Units are ^{o}C/day.

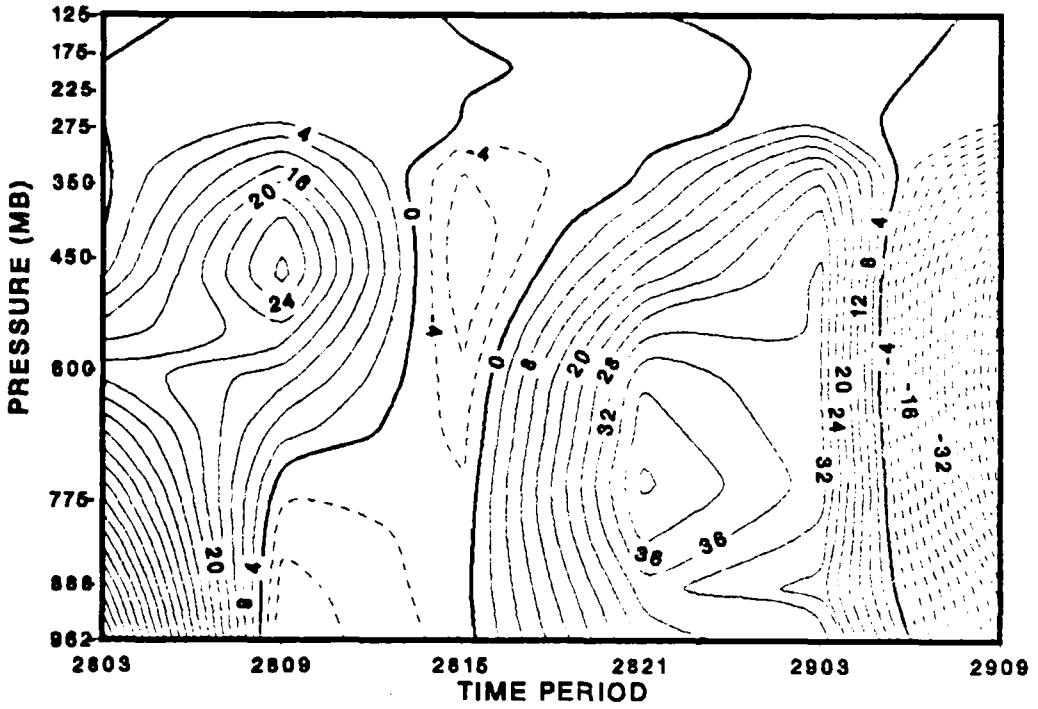

Fig. 5.13 Quasi-Lagrangian moisture tendency for radius 4 based on forecast fields. Positive (negative) values indicate moistening (drying). Contours are 4 x 10**-4 g/g/day.

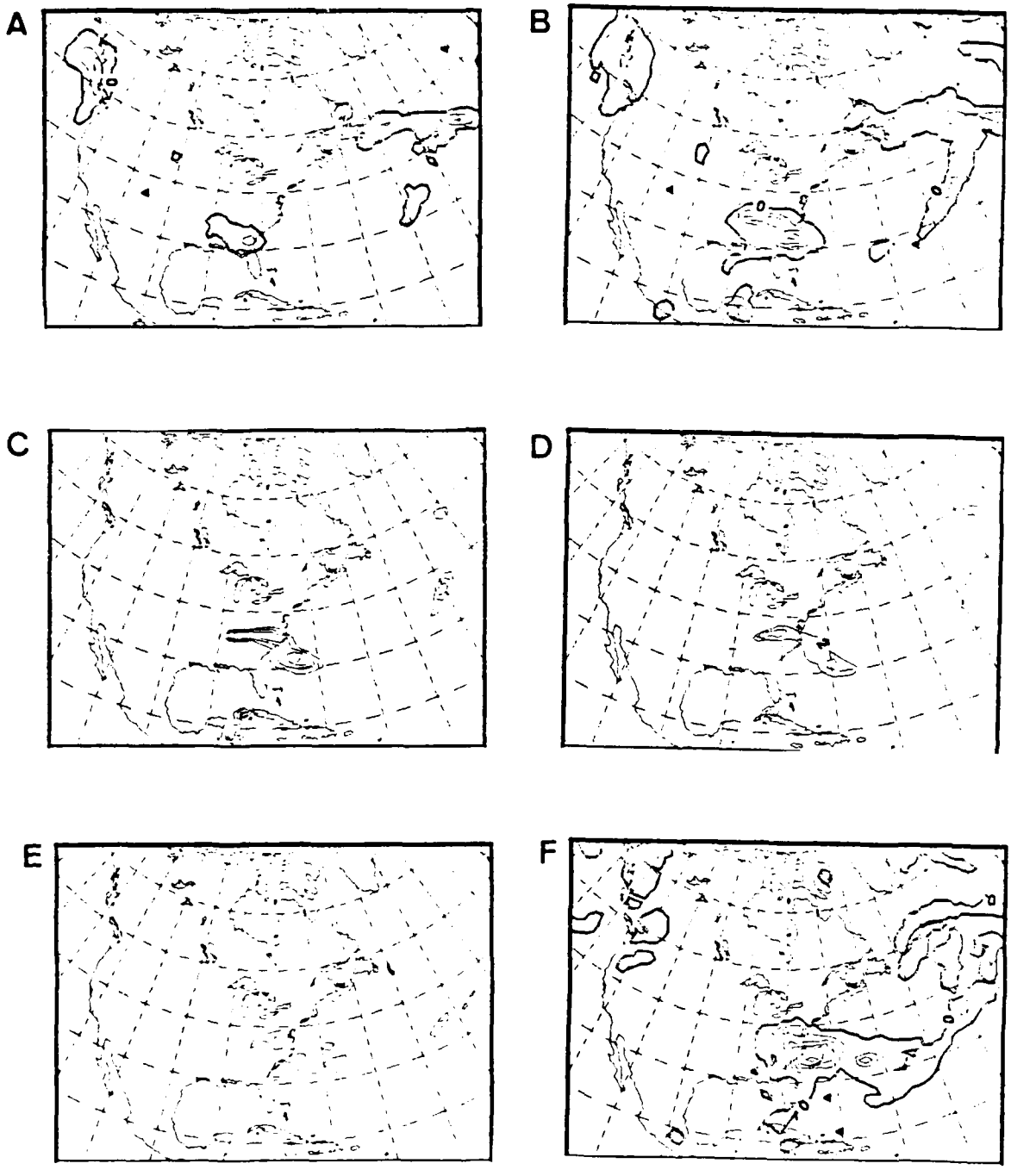

Fig. 5.14 NORAPS predicted precipitation (cm/6 h) for period ending (A) 06 GMT 28 March, (B) 12 GMT 28 March, (C) 18 GMT 28 March, (D) 00 GMT 29 March, (E) 06 GMT 29 March, and (F) 12 GMT 29 March 1984. Contour interval is 1.0 cm/6 h for (A) and 2.0 cm/6 h for the remainder.

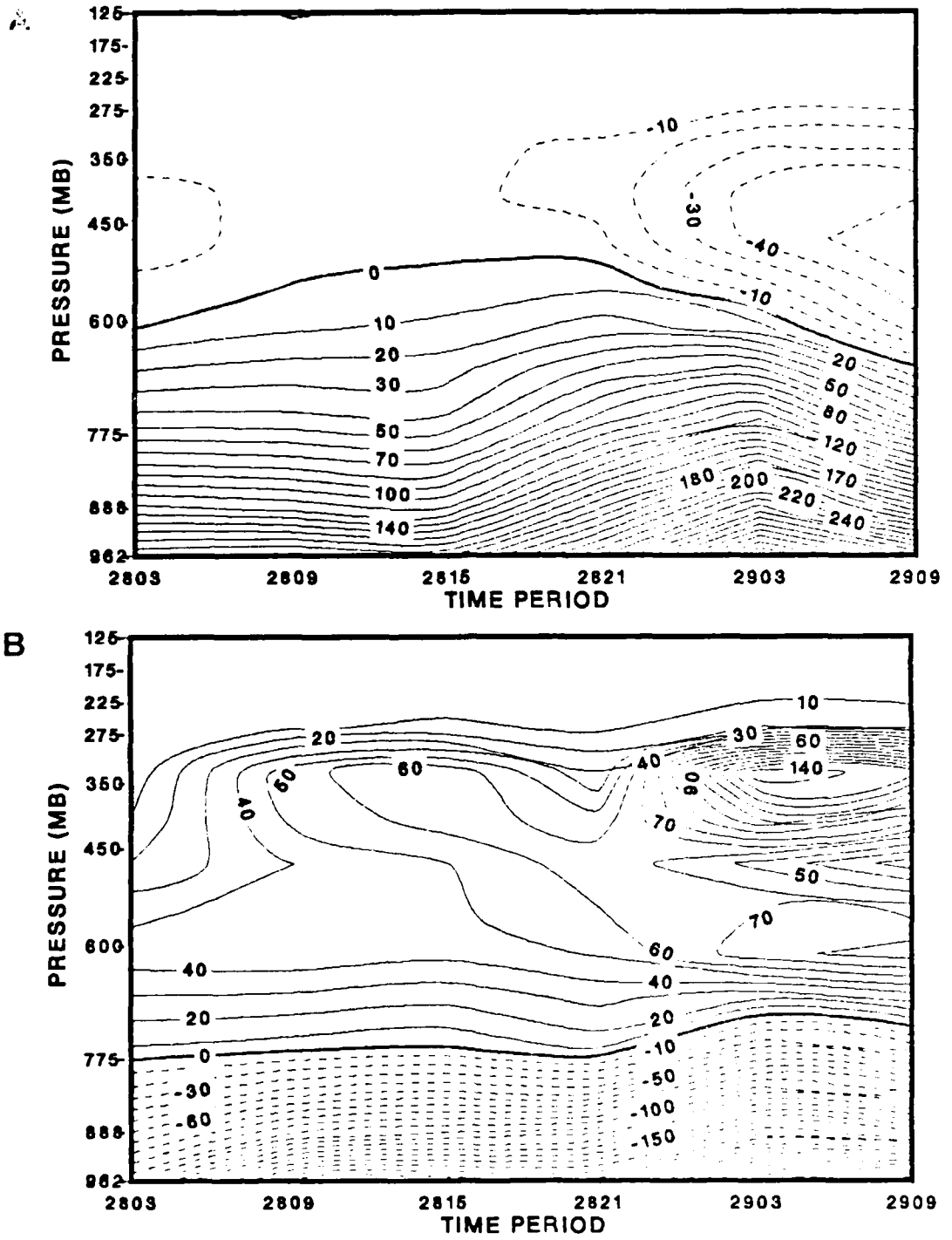

Fig. 5.15 (A) Horizontal and (B) vertical moisture flux for radius 4 based on forecast fields. Contours in 10 x 10**-4 g/g/day.

TABLE 1

NORAPS SPECIFIC HUMIDITY (G/KG) VALUES AT 400 MB FOR 06 GMT 29 MARCH 1984 (L MARKS POSITION OF THE LOW)

0.1	0.2	0.2	0.1	-0.1	-0.1	0.2	0.6	1.0	1.2
0.1	0.0	0.0	0.4	1.2	2.3	2.9	2.7	2.1	1.6
0.0	-0.3	-0.2	1.0	3.9	7.0	8.3	6.9	4.3	2.3
0.1	-0.5	-0.4	1.7	6.4	11.3	13.0	10.4	6.0	2.8
0.0	-0.5	-0.4	1.8	6.7	11.6	13.1	10.3	5.7	2.5
0.1	-0.2	-0.1	L 1.5	4.8	8.1	9.0	7.0	4.0	1.9
0.4	0.3	0.5	1.2	2.6	3.9	4.2	3.4	2.2	1.5
0.6	0.8	1.0	1.2	1.4	1.6	1.6	1.4	1.4	1.6
0.8	1.0	1.2	1.2	1.2	1.0	0.9	0.9	1.3	1.8
0.9	1.1	1.2	1.2	1.1	0.9	0.8	0.8	1.0	1.5
0.9	1.0	1.1	1.1	1.0	0.9	0.7	0.6	0.7	1.1

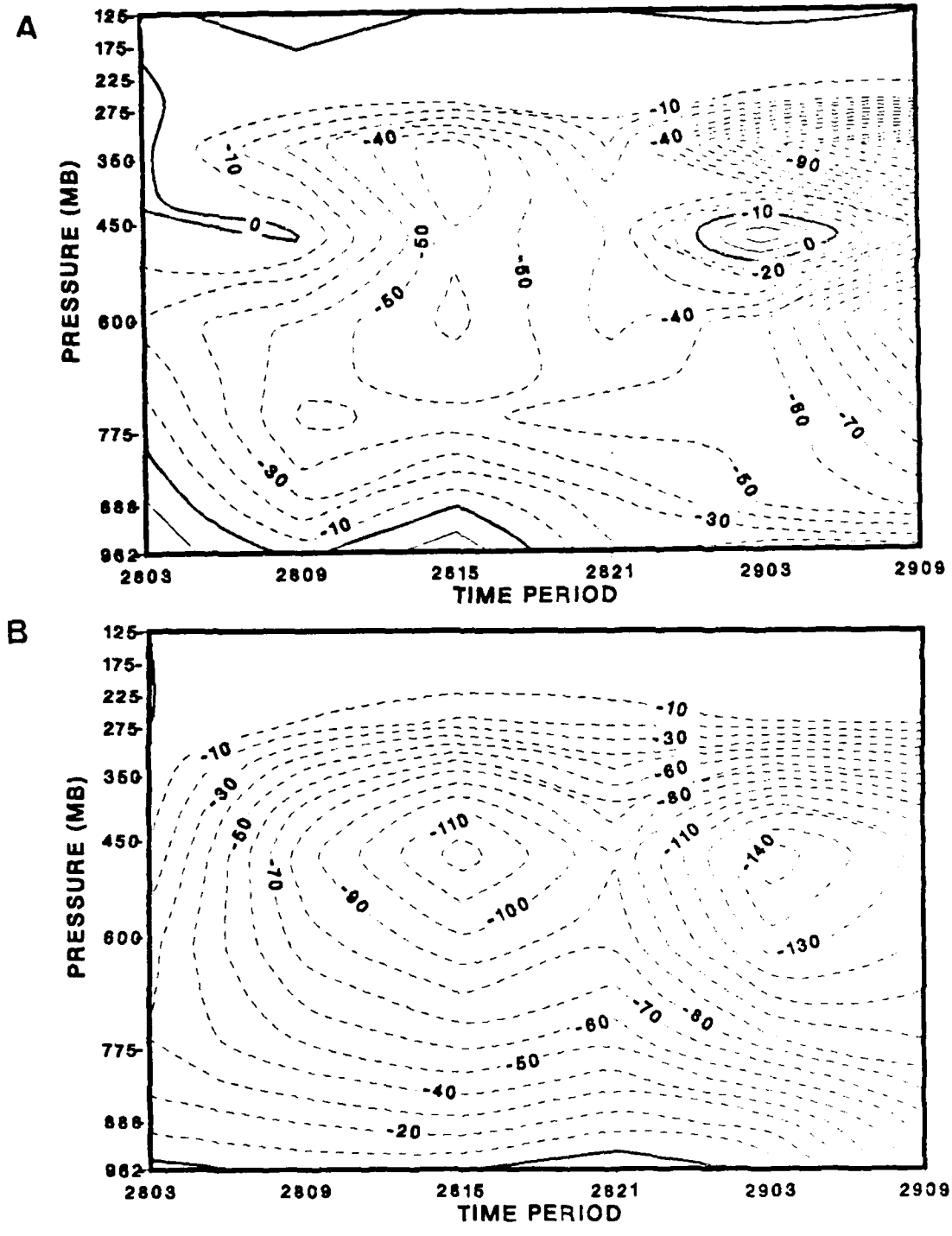

Fig. 5.16 (A) Residual for moisture budget and (B) Model-predicted moistening rate for radius 4. Contour interval is 10 x 10**-4 g/g/day.

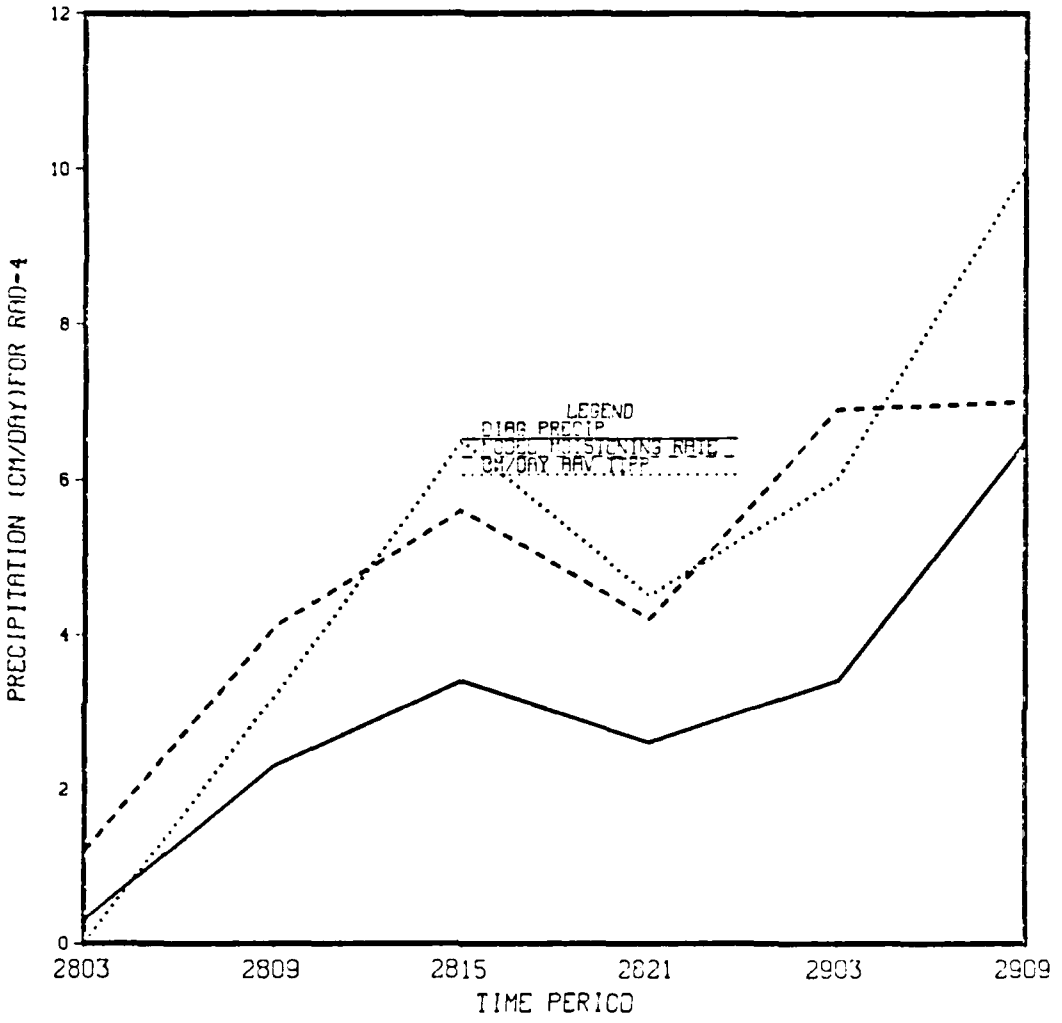

Fig. 5.17 Area-averaged, column-integrated moisture budget results for radius 4. Solid line represents the budget residual, dashed line is the model-predicted moistening rate and the dotted line is the model precipitation. Units are cm/day.

VI. CONCLUSIONS AND RECOMMENDATIONS

A. CONCLUSIONS

The physical processes in the development of the extra-tropical cyclone occur over a broad spectrum of space and time scales. This study has concentrated on the dynamic and thermodynamic forcing on the cyclone scale as it relates to storm intensification. The low-level mass convergence serves to spin up the low-level vortex as viewed in the vorticity budget results. Increased upward vertical motion results in stronger convergence, which serves to increase the horizontal moisture transport at the lower levels. This moisture is transported aloft as seen in the vertical moisture flux. The net increase in moisture within the column plus the cooling process (moist adiabatic) leads to precipitation, which greatly exceeds the quasi-Lagrangian moisture tendency. The release of latent heat contributes to a positive quasi-Lagrangian temperature tendency aloft (Fig. 5.1a), while cooling occurs in the lower troposphere in response to cold advection, evaporation and forced lifting of sub-cloud air by diabatic processes in the cloud.

In particular, special emphasis has been placed on heating and moistening which are essential components in the cyclone evolution. Results indicate the heating and moistening rates predicted by the model are 50 to 100% greater than the rates diagnosed from budget residual calculations. This difference is largely systematic and can be attributed to the incorrect specification of the moistening and heating rates within the NORAPS model. Consequently, the heat and moisture budgets suffer in terms of yielding physically inconsistent results at various times and levels. Revised heat and moisture budget results (based on corrections in predicting the heating and moistening rates) are presented

in Appendix C and constitute an important section of this study.

The release of latent heat caused by strong inward moisture transport in the lower troposphere into the storm's central core is believed to play a critical role in early intensification of the extratropical cyclone. The phase and shallow level of diabatic heating are key ingredients in modulating the sea-level pressure tendency. Previous investigations by Danard (1966), Gyakum (1983b) and Anthes et al. (1983) stress that diabatic heating only contributes to storm intensification during the later stages. This view is generally accepted since a sizeable precipitation field is rarely evident in the early stages of the storm. However, strong conditional instability is often observed upstream of surface troughs during the initial stages of baroclinic instability over ocean regions. As a consequence of the relatively warm ocean surface underlying the extremely cold air above the planetary boundary layer, near-neutral lapse rates with strong low-level moisture convergence cause the atmosphere to respond with cumulus convection. The latent heat released by the convection along with cumulus-induced subsidence play a major role in strongly heating the lower troposphere. Chang et al. (1982) suggest that the release of latent heat aids in the conversion of potential to kinetic energy by acting as a catalyst. Thus, the latent heating in a favored region of the developing storm (northwest quadrant) could accelerate the the baroclinic instability process.

There is a definite need to understand how diabatic heating alters the mass field around the storm, creating strong dynamic mesoscale features. Secondary ageostrophic circulations, forced by diabatic heating, have been suggested as one mechanism where the mass field is forced to respond. If diabatic heating is a major contributor to the

forcing of mesoscale features, which are believed to trigger explosive cyclogenesis events, a better definition of these events will need to be obtained through a higher resolution observational network.

B. RECOMMENDATIONS

The use of the higher spatial (horizontal and vertical) resolution NORAPS model is important in modeling the evolution of mesoscale features which affect the cyclone scale. These budget results, although seemingly contaminated by several sources of errors, do provide a baseline for future studies using the NORAPS model.

The following recommendations are made for future studies:

- Resolve problems with the NORAPS heating and moistening rates for a more accurate comparison of budget residuals with the model-predicted rates;
- Initiate a moisture analysis for NORAPS to better predict precipitation and other moistening processes within the storm environment.
- Use higher resolution (spatial and temporal) analyses to validate the thermal and moisture structure of explosive maritime cyclogenesis cases.

APPENDIX A

NAVY OPERATIONAL REGIONAL ATMOSPHERIC PREDICTION SYSTEM

(NORAPS)

1. MODEL CHARACTERISTICS

NORAPS, which includes an analysis and a regional forecast model, produces high spatial resolution (typically 80 km in the western Atlantic version), short term (36-48 hr) numerical forecasts over a limited domain. NORAPS was developed by Dr. Rich Hodur of the Naval Environmental Prediction Research Facility (NEPRF), who kindly provided the fields used in this research. The principle advantage of using NORAPS as opposed to a global or hemispheric model is the small spatial scale features that are resolved. This model has the additional asset of flexibility as the grid is globally relocatable, and the user may specify the dimensions and horizontal/vertical resolution. An additional feature is the "terrain enveloping" concept in which topography is calculated at a high horizontal resolution to incorporate the effects of the sub-grid scale features into the topographic field. A thorough discussion of NORAPS is provided by Hodur (1982 and 1984).

The four major components of NORAPS are the analysis, initialization, forecast and output. The analysis component consists of acquiring different types of data (radiosonde, pibal, aircraft, satellite, land and ship reports) and applying quality control checks to determine data validity. A single bad observation can have an adverse effect on the regional model if not removed prior to initialization. The next step in the analysis is to interpolate the observations to the grid. The data fields for the model are the u and v wind components, temperature, geopotential, specific

humidity, surface pressure, sea-surface temperature and terrain height. A regional update cycle is used where the 12 hour NORAPS forecast, which serves as the first guess and the latest observations are blended together. A sucessive corrections technique is then used for the NORAPS objective analysis to improve the first-guess fields of wind, temperature, and geopotential. An exponential weighting function takes into account the distance of the observation to the grid point and the number of observations surrounding a certain grid point. The analyses are performed at 1000, 925, 850, 700, 500, 400, 300, 250, 200, 150 and 100 mb.

The purpose of the initialization phase is to approximately balance the mass and wind fields and thus suppress the growth of large amplitude inertial-gravity waves which would contaminate the forecast fields. The static initialization procedure uses diagnostic constraints to relate the wind and mass fields. The nondivergent (rotational) wind component is obtained from the mass field through the balance equation, while the divergent (irrotational) component is computed from the omega equation.

The forecast component is the heart of the NORAPS model and this phase requires the majority of the computation time. The model uses the flux form of the primitive equations on a staggered grid scheme C (Arakawa, 1977). This grid scheme has excellent geostrophic adjustment properties and group velocity characteristics (Haltiner and Williams, 1980). The vertical coordinate is sigma, which orients all coordinate surfaces parallel to the terrain surface. Thus the vertical velocity is identically zero at the lower boundary, even in the vicinity of mountainous terrain. The vertical structure of the atmosphere is normally represented in 12 discrete layers, although as many as 19 layers may be specified. All prognostic variables (u, v, q and T) except vertical velocity are carried at the middle of each layer.

A split-explicit time integration scheme is used to permit larger time steps for the slower meteorological modes, while still being able to predict all the gravity modes. The size of the time step is governed by the computational stability criterion for the horizontal resolution selected. The momentum, thermodynamic and moisture equations are solved with conventional centered time (leapfrog) and space differencing scheme. Fourth-order advection is used for the predictions equation set to reduce errors in phase speed.

One-way influence boundary conditions are used to specify the time-dependent lateral boundary conditions on the finer mesh NORAPS model from the NOGAPS predictions. The one-way influence refers to the NOGAPS solution forcing the fine-mesh model, without the fine grid affecting the coarse grid solution. For timeliness required in operational use, these boundary conditions must be derived from an earlier forecast rather than utilizing the corresponding NOGAPS forecast from the same time. A method developed by Perkey and Kreitzberg (1976) is used to spatially interpolate the solutions near the boundary of the finer mesh. The NOGAPS time tendencies are blended with the NORAPS time tendencies over a distance of several grid points to dampen spurious reflections at the regional model boundary due to the change in grid spacing.

The output phase of NORAPS prepares the forecast data for interpolation to the standard pressure levels. The output fields can include winds, temperature, specific humidity, surface pressure, relative humidity, absolute vorticity, divergence, surface sensible and latent heat flux, terrain height and precipitation. The output domain can be either the entire grid or a subset of it. Three different projections (Mercator, Lambert conformal, or polar stereographic) are available to minimize distortion in the tropics, mid-latitudes or polar regions.

2. MODEL PHYSICS

The model physics contained in NORAPS constitute a crucial component in this experiment. The treatment of diabatic processes is important to simulate the effect of the surface fluxes across the air-sea interface on the atmosphere. NORAPS includes representations of the following physical processes:

(i) dry convective adjustment;
(ii) surface heat, momentum and moisture fluxes;
(iii) cumulus parameterization;
(iv) large-scale precipitation; and
(v) radiative transfer processes

1. Planetary Boundary Layer

The planetary boundary layer (PBL), which is defined as the lowest layer in the model atmosphere, is well mixed in temperature, momentum and moisture. Interactions occurring between the lower boundary and overlying atmospheric layer provide sources and sinks for momentum, heat and moisture. The effects of the PBL should be included in any numerical model to physically simulate maritime cyclogenesis on the time scales of more than a few hours as stated by Anthes et. al. (1983).

The NORAPS PBL parameterization follows Deardorff (1972). After the layer mean values of V, θ and q are known, a bulk Richardson number (Ri_b in A.1) is computed to determine the stability of the PBL,

$$Ri_b = gh(\theta_{v_m} - \theta_{v_s})/U_m^2 \quad , \qquad (A.1)$$

where g is the gravitational constant, h is the PBL height, θ_v is the virtual potential temperature, subscript s denotes surface values and subscript m denotes mean PBL values. For unstable conditions ($Ri_b<0$), i.e., strong winds, daytime

heating over land surfaces and strong mixing, a predictive equation for the PBL height (h) proposed by Stull (1976) is used. The rate of change of the PBL height is related to the surface sensible heat flux, mean PBL wind speed, the large-scale vertical motion and cloud-induced subsidence. For stable or neutral conditions ($Ri_b>0$), i.e., light winds, nighttime over land with weak mixing, a predictive equation for the PBL height after Nieuwstadt and Tennekes (1981) is used. Transfer (drag) coefficients for heat (C_θ) and friction (C_u) are computed from empirical formulas that include the stability dependence via the Ri_b. Surface fluxes of heat, moisture and momentum (A.2, A.3, and A.4) are computed using the bulk aerodynamic formulas, which assume the transfer coefficients are constant in time:

Sensible heat flux,

$$H_s = \rho c_p(\overline{w'\theta'}) = \rho c_p u_* c_\theta(\theta_s-\theta_m); \qquad (A.2)$$

Latent heat flux,

$$H_l = L_v(\overline{w'q'}) = \rho c_p u_* c_\theta(q_s-q_m); \text{ and} \qquad (A.3)$$

Surface stress,

$$\tau = \rho u_*^2 = \rho u_m^2 c_u^2 \ , \qquad (A.4)$$

where ρ is the density of air, u_* is the frictional velocity, θ is the potential temperature, L_v is the latent heat of vaporization, w is the vertical velocity, q is the specific humidity, c_p is the specific heat of dry air at constant pressure, subscript m denotes the mean PBL value and subscript s denotes the surface value. The PBL is constrained to extend through at least the bottom layer of the model (approximately 40 mb) to avoid extrapolation problems in determining mean PBL quantities.

Another feature of the NORAPS PBL is that seasonally dependent climatological values of albedo, sea ice, ground wetness and surface roughness are specified. A predictive equation for the ground temperature after Blackadar (1979) is used to model the lower boundary condition for the temperature over land. The sea-surface temperatures are assumed to be constant over the forecast period, which is valid for short-range forecasts.

2. Cumulus Parameterization

The NORAPS model uses a modified version of the Kuo (1965) cumulus parameterization scheme. This version links the convection to the PBL by requiring moisture convergence in the PBL. By constrast, the original Kuo version required net moisture convergence in the entire column before convection was initiated. The moisture convergence (A.5) is

$$M_t = 1/g \nabla \cdot (q_m \pi V_m)(1-\sigma_{pbl}) + \rho_s(\overline{w'q'})_s \quad , \qquad (A.5)$$

where the first term on the RHS is the vertically-integrated moisture *convergence* and the second term is the surface moisture flux. Convection is assumed to occur when $M_t > 4.0 \times 10^{-6}$ gm m^{-2} s^{-1} and the equivalent potential temperature decreases with height (conditionally unstable) from the PBL to the first model layer above the PBL. The final constraint is that deep convection cannot occur if the lifting condensation level (LCL) is above the PBL. This scheme partitions the moisture transport into two fractions: the first (bM_t) serves to moisten the environment to saturation conditions through the cloud layer, and the second ($(1-b)M_t$) condenses and falls instantaneously as rain. The factor b is expressed as the vertical average of one minus the relative humidity (RH), where $0 \leq RH \leq 1$. This factor serves to moisten the column when RH is low and condense moisture when the RH is high.

In addition to large-scale advection, temperature and moisture changes at any level are caused by convective clouds. It is assumed that the temperature of the cloud is warmer than the environment. Cloud production, which is the ratio of the water vapor available to the water vapor needed to form the cloud, is computed for each gridpoint. The fractional cloud area is used to adjust the layer mean temperatures and moistures to account for the presence of clouds.

3. Precipitation

Large-scale precipitation (non-convective) can occur when supersaturation is achieved at any level. The excess moisture is allowed to fall into the next layer and increase the moisture content of that layer, or continue to fall if that layer is already supersaturated. Precipitation occurs only when the air is saturated from the cloud to the ground. Convective precipitation occurs according to the modified Kuo cumulus convection scheme discussed in the previous section. The precipitation routines are only called every eight time steps for computational efficiency. The heating and moistening rates are then spread evenly over subsequent time steps until the next call to these routines.

4. Radiation

The incorporation of solar radiation into numerical models is essential for prediction of surface temperatures and the cooling rates at cloud tops that may deepen cloud layers. The radiation parameterization in NORAPS follows Katayama (1974) for short-wave radiation and Sasamori (1968) for long-wave radiation.

APPENDIX B

DATA ACQUISITION AND PROCESSING

1. DATA ACQUISITION

The NORAPS analyses and forecast fields for this budget study were obtained from Dr. Rich Hodur at the Naval Environmental Prediction and Research Facility (NEPRF). The data on 9-track tape were transferred to the mass storage device on the NPS IBM 3033. The unprocessed NORAPS data fields were on a 109 x 82 grid at 12 sigma levels. A horizontal grid spacing of 80 km is used. A slightly smaller window (103 x 76 with 11 pressure levels) was extracted to accomodate easier storage and access from the disk. The analysis base time for the model run is 00 GMT 28 March 1984. A 36-hour model forecast is produced with output fields generated every six hours to 12 GMT 29 March 1984. NORAPS analyses were available every 12 hours from 00 GMT 28 March until 12 GMT 29 March 1984.

The Lambert conformal projection used for the output fields is ideally suited for mid-latitudes since there is minimum distortion between the true parallels of 30° and 60°N. The Lambert conformal map is a bi-conic, secant type of projection which preserves angles when projecting the earth's surface onto a plane surface.

To obtain the data for the budget programs, several preliminary steps were necessary. First, surface and upper air fields were plotted using DISSPLA, which is a software package available on the NPS IBM 3033 mainframe. The user must be aware that DISSPLA requires a rectangular region of latitude/longitude points to be specified. Because NORAPS output fields are specified in Lambert conformal coordinates, DISSPLA would perform what amounts to a double

transformation and produce a distorted and inaccurate field. Three separate steps are required in the program DISPLA NORAPS to produce a plot with correct positioning on the map projection. First, a subplot area is specified and a blanking routine is used to truncate the lower curved boundary which is standard for the Lambert conformal plot. This step merely serves to ensure a rectangular plot is produced. Second, the contouring and a border are drawn that is separate from the projection and geography routines. Third, the Lambert conformal projection, i.e., the latitiude and longitude lines, and the geography are added. Integral to each of these three separate steps is the statement, CALL ENDGR(0), which terminates that particular block of code. This statement ends a subplot but remains on the same physical page, which allows other plots, such as the contouring and projection in this case, to be drawn on the same physical page.

It is sometimes necessary to retrieve data from the output grid to determine the center of a low center in the (i,j) Lambert conformal coordinates. The NDATA FORTRAN program can be easily modified to retrieve output data for any user specified field and level. Once the appropriate data fields are obtained, a program called TRANS FORTRAN is used to transform the (i,j) Lambert conformal coordinate to a latitude and longitude on the earth's surface. The corresponding latitude and longitude of the low center are entered into an interactive program (called STORMO FORTRAN) at each time period to compute the speed and direction of the cyclone center. A forward difference is used to compute the speed for the first and last time periods, while a centered difference is used for the other time periods. The low center location, direction and speed are then entered at the end of the budget programs as required parameters for the budget calculations.

2. DESCRIPTION OF WIND ADJUSTMENT

Because all NORAPS output fields are given in Lambert conformal coordinates, the wind directions will be distorted from the true direction away from the central meridian of the conformal grid. This central or true meridian, which is 80°W in this case, is parallel to the y-axis in an x,y Cartesian coordinate system. A subroutine called WNDADJ makes the necessary transformations to provide the true wind direction on the earth's surface. The only information required to make this transformation are the Lambert conformal coordinates of the pole point, which are 52.0 (x-coordinate) and -37.986 (y-coordinate). Equations B.1 and B.2 are used to transform the Lambert conformal wind direction components, denoted u' and v' are:

$$U = u'\cos(\theta) - v'\sin(\theta); \text{ and} \qquad (B.1)$$

$$V = v'\cos(\theta) + u'\sin(\theta) , \qquad (B.2)$$

where U and V are the true horizontal wind direction components and the angle $\theta = \tan^{-1}(x_p - x/y - y_p)$, where x_p, y_p are the Lambert conformal pole point coordinates and x,y are the Lambert conformal (i,j) grid point that is being transformed. The convention for the angle (θ), which the Lambert conformal coordinate axes are rotated to become true directional axes, is positive for a counter-clockwise direction and negative for a clockwise rotation.

3. CONVENTIONS FOR NORAPS FIELDS AND BUDGET PROGRAMS

The NORAPS output fields are presented in a right-hand coordinate system with the (1,1) grid point being the southwest corner of the grid. The column value increases eastward and the row value increases northward. These NORAPS

data fields, however, are read in for the budget programs in a different manner. A left-hand coordinate system is used in the budget program and therefore, data fields have to be read in accordingly. The fields are read in using the HOJO subroutine with the (1,1) grid point at the northwest corner. The column value increases eastward and the row value increases downward. The pole point is referenced in this coordinate system since wind adjustments are performed after the data fields have been read in.

The latitude convention in the budget program is positive north and negative south; longitude is positive west of Greenwich and (360-longitude), east of Greenwich. The convention for the normal wind components in the budget programs are positive outward and negative inward. This likewise applies to the normal component of the cyclone velocity.

Another convention the user should be aware of is the method of defining latitude and longitude in the DISSPLA software package used in plotting the NORAPS output fields. Longitudes west of Greenwich are negative, while east of Greenwich they are positive. The latitudes are positive for north and negative for south. These are arguments to be included in the subroutines GRAF and MAPGR.

APPENDIX C

NORAPS MODEL RESULTS - CORRECTED VERSION

1. GENERAL

The incorrect specification of moistening and heating rates in the NORAPS model led to a poor comparison of budget results with the model-predicted diabatic heating and moistening rates as discussed in Chapter 5. The corrections to the specification of the heating and moistening rates in the prognostic equations were made in a test version of the NORAPS model and the forecast was re-run for the 28-29 March 1984 storm. Corrections to the calculation of the vertical fluxes of moisture and momentum were also made so that a linear (in pressure) interpolation scheme is used to estimate horizontal winds and specific humidity at levels of vertical velocity. An abbreviated discussion of the results in the corrected model run is presented. A brief synopsis is given for the track and intensity of the low center in the two versions of the model. The new residuals for the heat and moisture budgets are then compared with the updated model-predicted heating and moistening rates. These model-predicted heating and moistening rates are accumulated 6 h values converted to a daily rate rather than an instantaneous value obtained each 6 h during the integration of the model and converted to a daily rate. Results are presented for radius 4^{o} lat. as before and figures are placed at the end of this appendix.

2. SYNOPTIC DISCUSSION

The track and intensity of the surface low center during the first 24 h in the corrected NORAPS model run are very similar to the incorrect version (Fig. C.1a). A weaker intensity low center is predicted in the corrected model

during the last 12 h. A slightly greater cyclone speed is predicted in the revised model during the last 12 h, which reduces the position error at 12 GMT 29 March 1984 (Fig. C.1b).

During 00-06 GMT 29 March 1984, the sea-level pressure (SLP) tendency diminishes from 4.5 mb/6 h (old version) to 0.9 mb/6 h (new version). During 06-12 GMT 29 March 1984, the SLP tendency only slightly diminishes from 3.7 mb/6 h to 3.0 mb/6 h. Thus, the central SLP in the new version is 978 mb at 12 GMT 29 March 1984, whereas the intensity of the low center is 974 mb in the old version. By comparison, the NORAPS analysis at 12 GMT 29 March 1984 has a 973 mb center after a 8.5 mb/12 h SLP decrease, which is nearly double the SLP tendency for the new version. Although a weaker storm results from the incorporation of corrections to the NORAPS model, the position error improves at 36 h.

A noteworthy difference between the old and new forecast is the formation of a secondary low pressure center within the northeast quadrant of the major center of low pressure at 00 GMT 29 March 1984. This mesoscale feature has some similar characteristics as the coastal low that becomes the major low center during the last 12 h of the forecast period. The exact details of this mesoscale feature are not correctly predicted by the NORAPS model, but it presents a much more realistic picture of the actual situation as seen in the NMC analyses discussed in Chapter 3.

3. BUDGET RESULTS

1. Heat Budget

The terms in the heat budget for the new forecast have a similar vertical profile as in the old forecast. A noticeable difference in the new forecast is the greater oscillatory trend in time of the vertical temperature advection and energy conversion terms (not shown). This is a result of a stronger secondary maximum in the vertical

velocity field (Fig. C.2) at 09 GMT 28 March 1984 in the new forecast.

The residual (diabatic heating plus calculation error) diagnosed from the budget for the new forecast (Fig. C.3a) has two maxima: a 20°C/day center at 450 mb between 09 and 15 GMT 28 March 1984 and a 25°C/day center at 09 GMT 29 March 1984 near 350 mb. The magnitude of maximum heating is 5°C/day greater than in the old forecast and the level is 100-200 mb higher. The convective precipitation component does not increase substantially during the later stages of the storm and therefore can not account for this higher level of heating. It had been hoped that the diabatic heating would be at lower levels using the new forecast fields. The diagnosed heating rate (Fig. C.3a) in the new forecast is much closer to the actual model heating rate (Fig. C.3b). The magnitude of 20-25°C/day during the first strong heating period at 09 GMT 28 March 1984 agrees well with the actual rate in the model. Excellent agreement is also found in the phases and levels of maxima in the diagnosed and predicted heating rates. Stronger heating occurs at the last time period than is diagnosed in the heat budget. Other differences between the diagnosed and predicted rates are the higher level of heating (350 mb) diagnosed in the heat budget at 09 GMT 29 March 1984 and the strong heating (in the budget) below 850 mb between 09 and 21 GMT 28 March 1984 as opposed to cooling predicted by the model during this period.

The difference between the budget diagnosed heating rate and the model-predicted rate is given in Fig. C.4. Errors of less than 20-25% in the budget are acceptable and can be attributed to computational errors. If the errors are larger than this, then the validity of the particular budget must be questioned. Two regions have significant errors (greater than 10°C/day) in the diagnosed heating

rate. The first region occurs below 850 mb centered at 15 GMT 28 March 1984. The large surface heat flux ($10^{o}C$/day) at this time can explain this difference since this surface heat flux has not been included in the model-predicted diabatic heating rate. The second region of large errors (negative) occurs at the last time period in the middle troposphere. These errors are probably due to the fact that the largest heating rates are predicted by the model at this time and the time-averaging process in the budget tends to weaken the heating signal by spreading the maximum across two time periods. An alternate explanation is the strong vertical velocity diagnosed at the last time period is associated with excessive adiabatic cooling, which is not balanced by the other terms in the budget. Errors of 5-$10^{o}C$/day above 350 mb are due to unrealistically large values of horizontal and vertical temperature advection at the upper levels in the diagnostic calculations.

2. Moisture Budget

The moisture budget for the new forecast exhibits a similar structure as in the old version with the exception of the vertical moisture flux term. This term has much less vertical structure after 21 GMT 28 March 1984 (Fig. C.5) as a result of the corrections in the moistening rate. In particular, realistic values of specific humidity are now found in the middle to upper troposphere.

The budget residual for the new forecast (Fig. C.6a) has (negative) maxima in moistening at 09 GMT 28 March and 09 GMT 29 March 1984. These maxima at 700 mb and 600 mb, respectively, compare rather poorly with the levels of maximum diabatic heating (Fig. C.3a), which are diagnosed to be 200-300 mb higher. In the new forecast, the actual model moistening rate (Fig. C.6b) exhibits a peak magnitude in moistening at 450-500 mb. This compares rather poorly with the budget diagnosed results, which are 150-250 mb lower in

the troposphere. However, excellent agreement exists in the phases and maximum magnitudes of the moistening. The lower elevation of the residual in the moisture budget is distinctly different from the heat budget where the diagnosed maximum heating occurs at a higher level than in the model.

The differences between the budget diagnosed and model-predicted moistening rate are illustrated in Fig. C.7. Large errors (positive and negative) occur throughout the depth of the troposphere. The negative errors indicate an overestimation of the moisture sink in the budget residual, while positive values indicate an underestimation of the source. These errors in the moisture budget are on the order of the magnitude of the moistening rates, especially at 09 GMT 28 March and 09 GMT 29 March 1984. Evidently, there is another process in the forecast model which redistributes moisture in the vertical but is not included in the moistening rate we have output from the model. Other potential sources of error are the highly variable (horizontal and vertical) moisture fields, too coarse of a temporal resolution and unresolved processes in this rapidly varying situation.

The agreement between the column-integrated budget and model-predicted moistening rates is significantly improved in the new forecast. In the old forecast, a factor of two difference was found (Fig. C.8a) between the two rates. The diagnosed residual (Fig. C.8b) has a non-systematic error in the new forecast which is in much closer agreement with the model-predicted moistening rate. Thus, the correction to the prediction of the moistening rate in the model leads to consistent results between the budget diagnosed and model-predicted moistening rates in a column-averaged sense. Another pleasing result is the degree of coincidence of the actual model-moistening rate and the

model precipitation when accumulated values rather than instantaneous rates are calculated for both variables.

4. SUMMARY

In general, the heat budget captures rather well the major thermodynamic process of diabatic heating in comparison to the rates internally predicted within the model. The corrections to the heating and moistening rates in the the NORAPS model have yielded more consistent results in the column-integrated moisture budget. However, a discrepancy remains in the vertical distribution of moistening estimated from the budget and directly from the model prediction.

Problems still remain in the model and budgets which need to be resolved. The most serious problem is the difference in the elevation of the maximum heating/moistening rates between the budget and model-predicted calculation. Unrealistic vertical temperature profiles above 350 mb are found in the model output data. Unrealistically strong horizontal and vertical temperature advection above 350 mb is diagnosed in the heat budget. The moisture budget *may* be less reliable than the heat budget due to the higher degree of noise in the specific humidity field as compared to the temperature field.

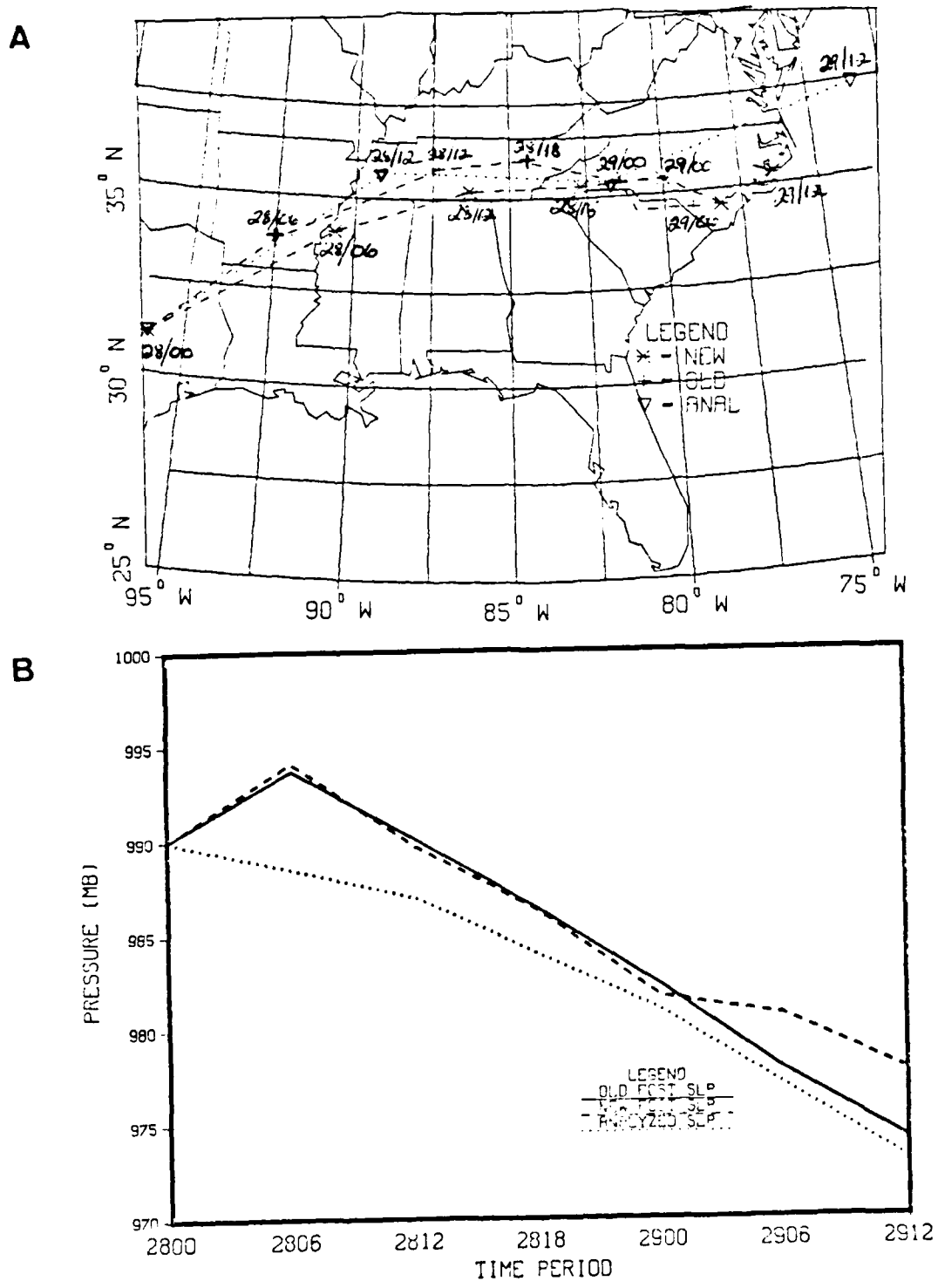

Fig. C.1 (A) Track of low center and (B) SLP tendency for the old (solid) and new (dashed) NORAPS forecast and analyses (dotted) for 28-29 March 1984.

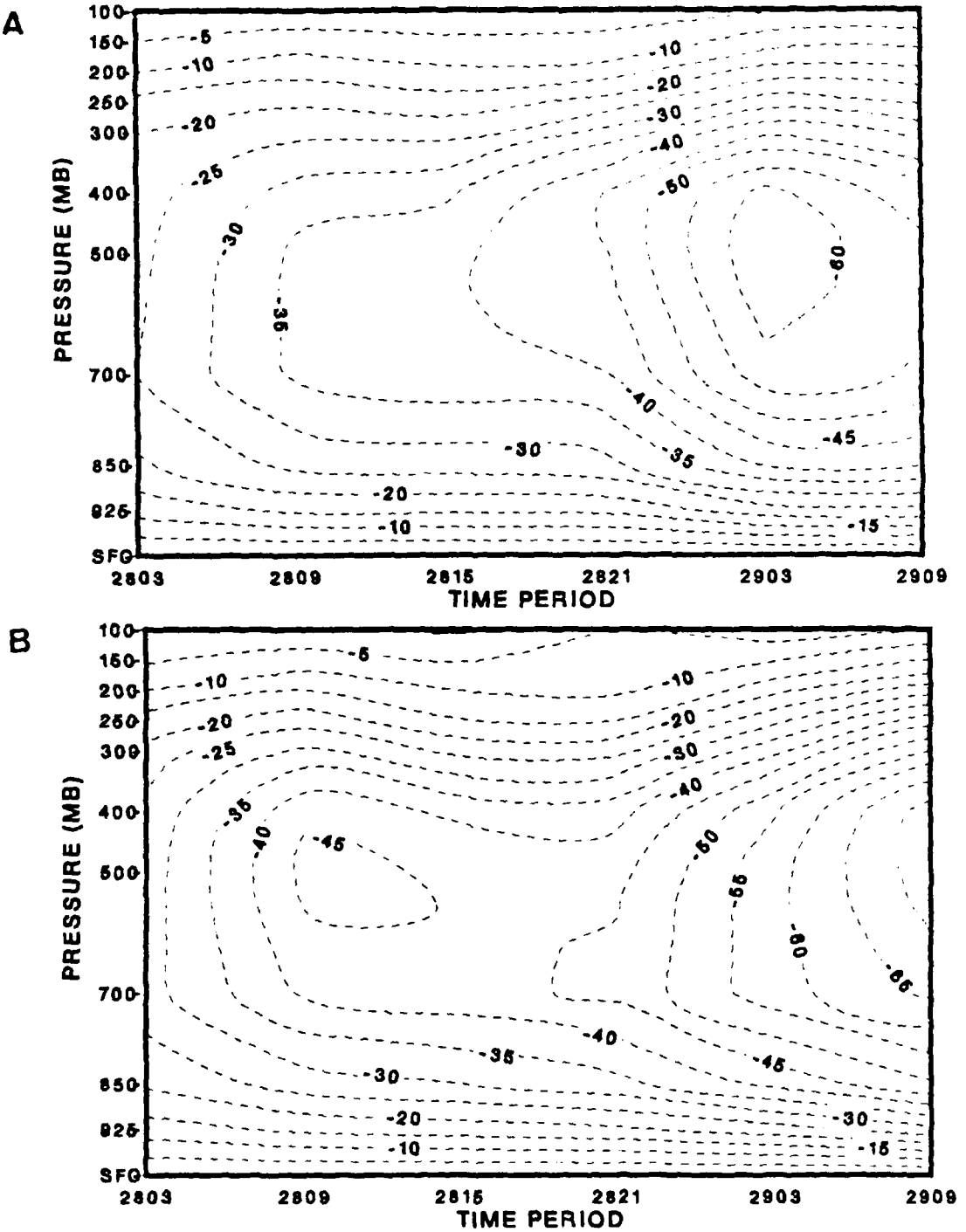

Fig. C.2 Area-averaged vertical velocity at radius 4 for (A) old forecast and (B) new forecast. Contour interval is 5 x 10**-4 mb/s. Negative values indicate upward vertical motion.

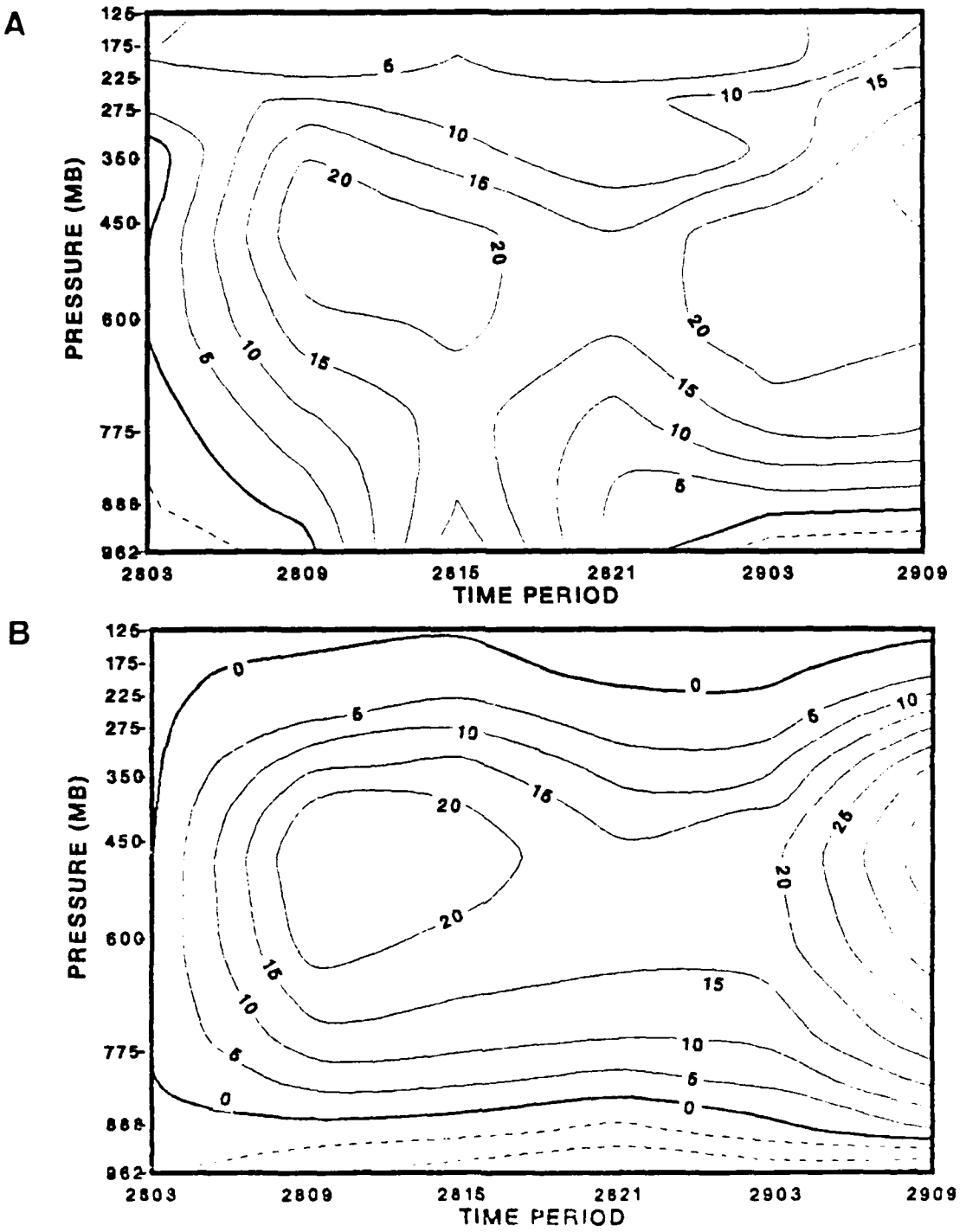

Fig. C.3 (A) Budget residual and (B) actual model heating rates in ^{o}C/day for the new forecast at radius 4.

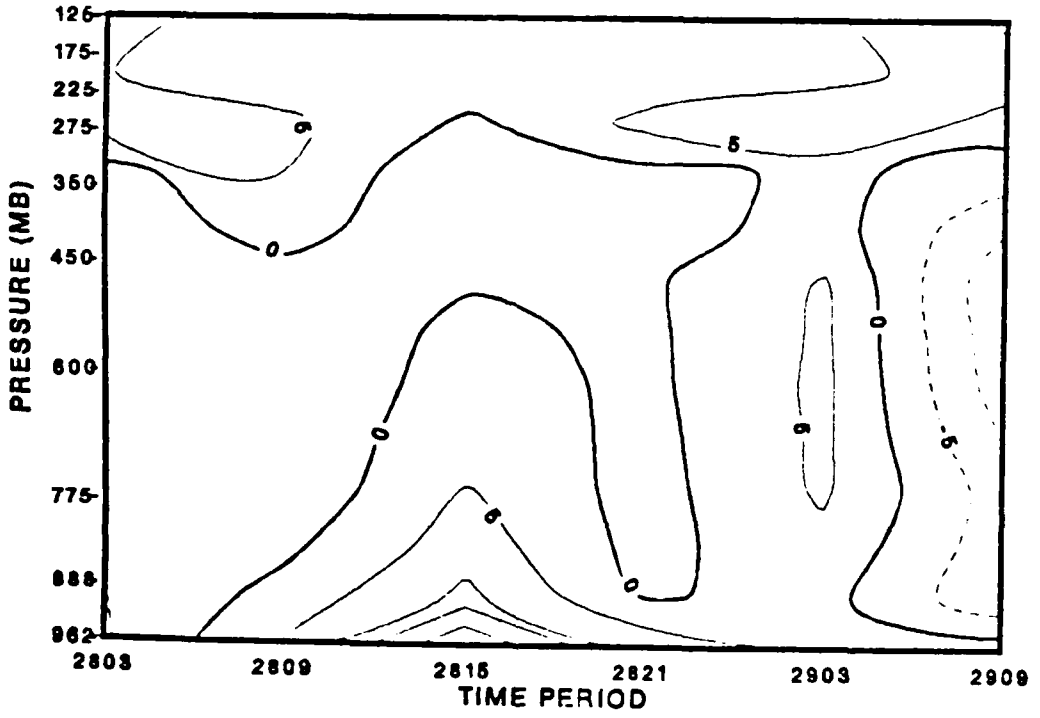

Fig. C.4 Differences (^{o}C/day) between the budget-diagnosed and model-predicted heating rate at radius 4 for the new forecast.

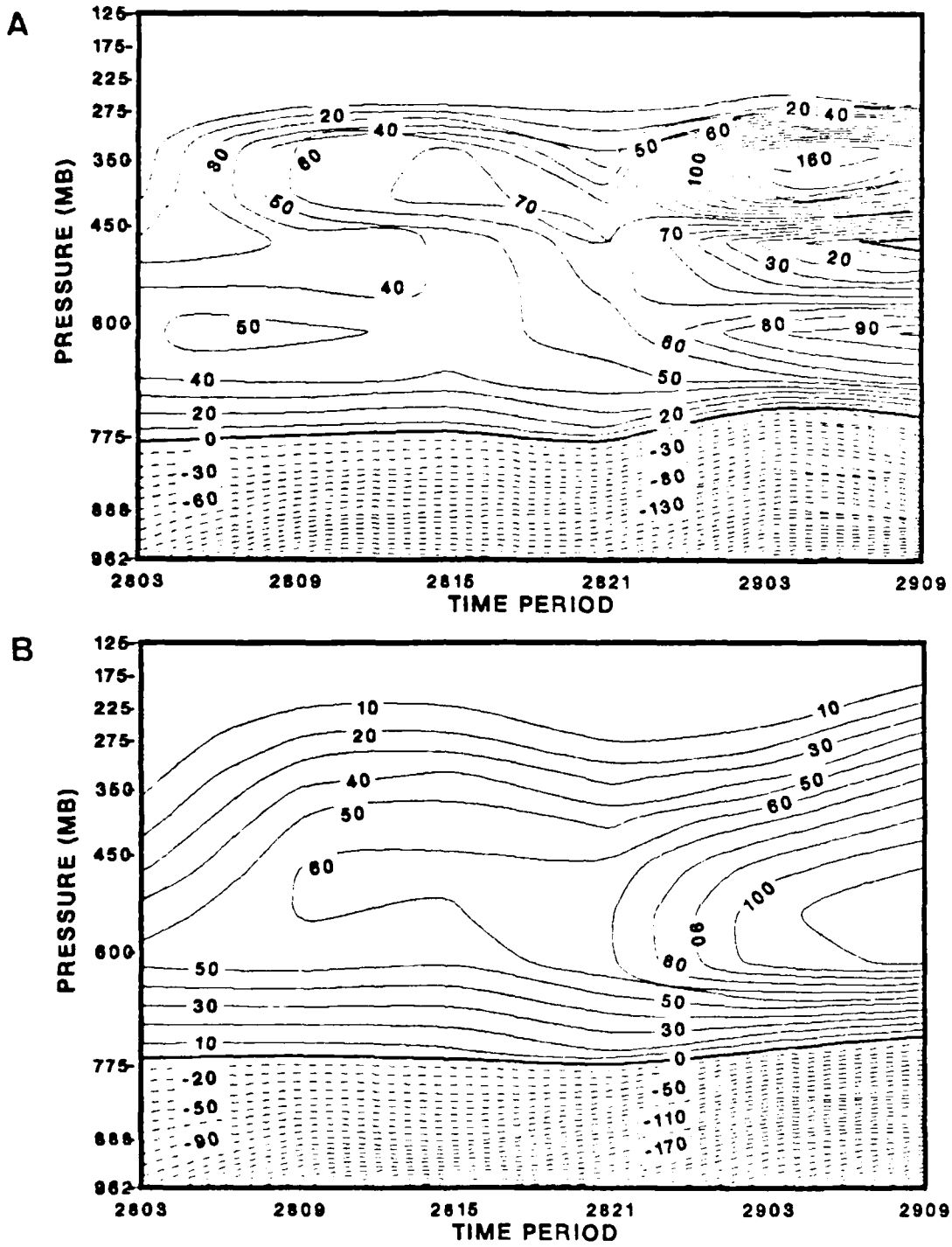

Fig. C.5 Vertical moisture flux for radius 4 in the (A) old forecast and in the (B) new forecast. Contour interval is 10 x 10**-4 g/g/day.

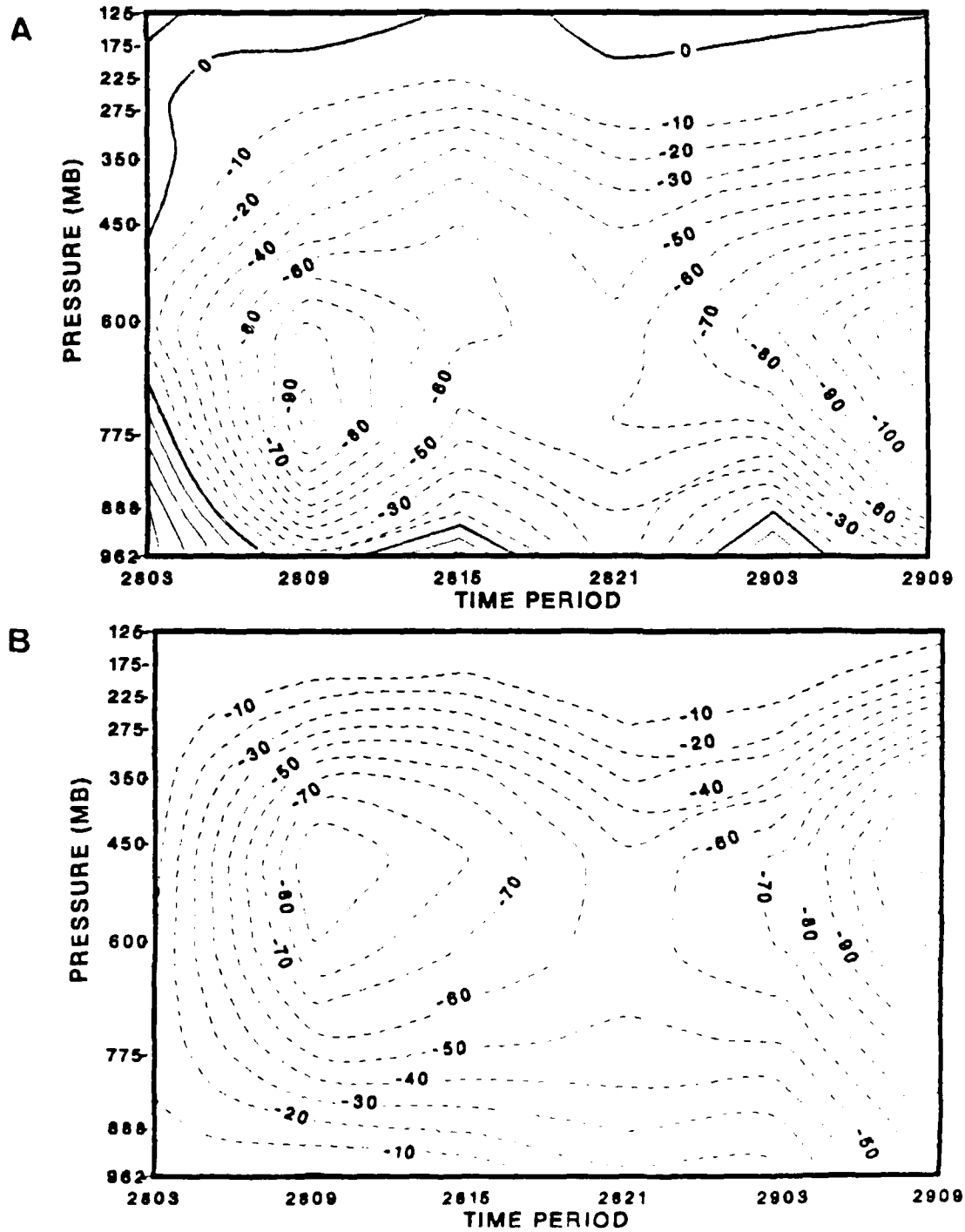

Fig. C.6 (A) Budget-diagnosed and (B) model-predicted moistening rates at radius 4 for the new forecast. Contour interval is 10 x 10**-4 g/g/day.

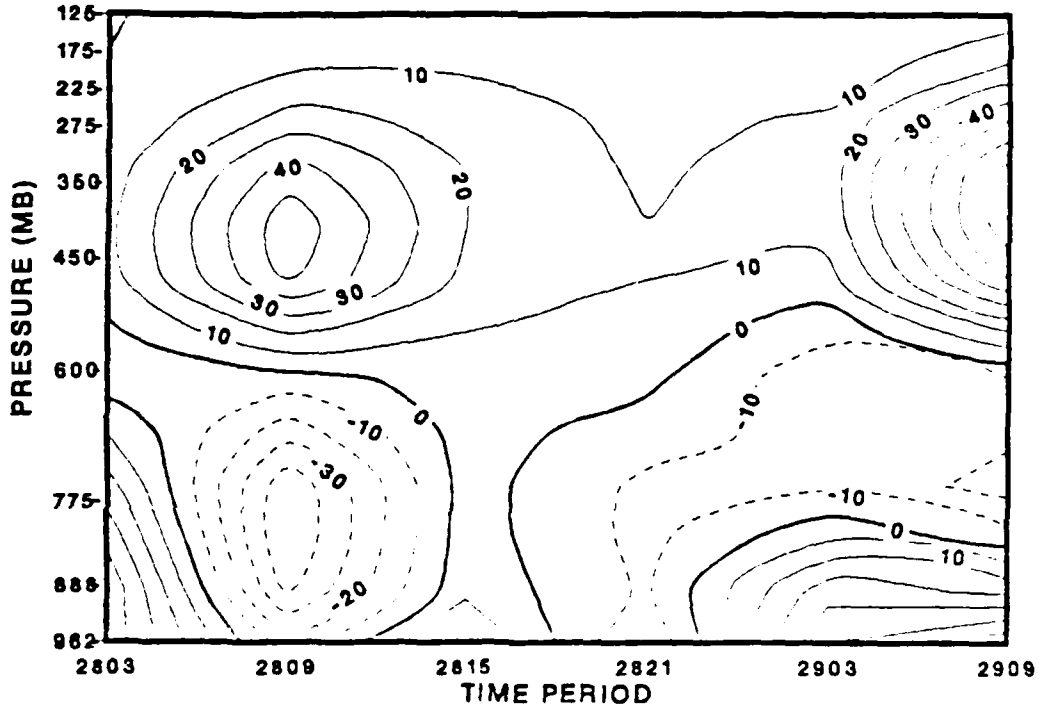

Fig. C.7 Difference in the budget-diagnosed and model-predicted moistening rate at radius 4 for the new forecast. Contour interval is 10 x 10**-4 g/g/day.

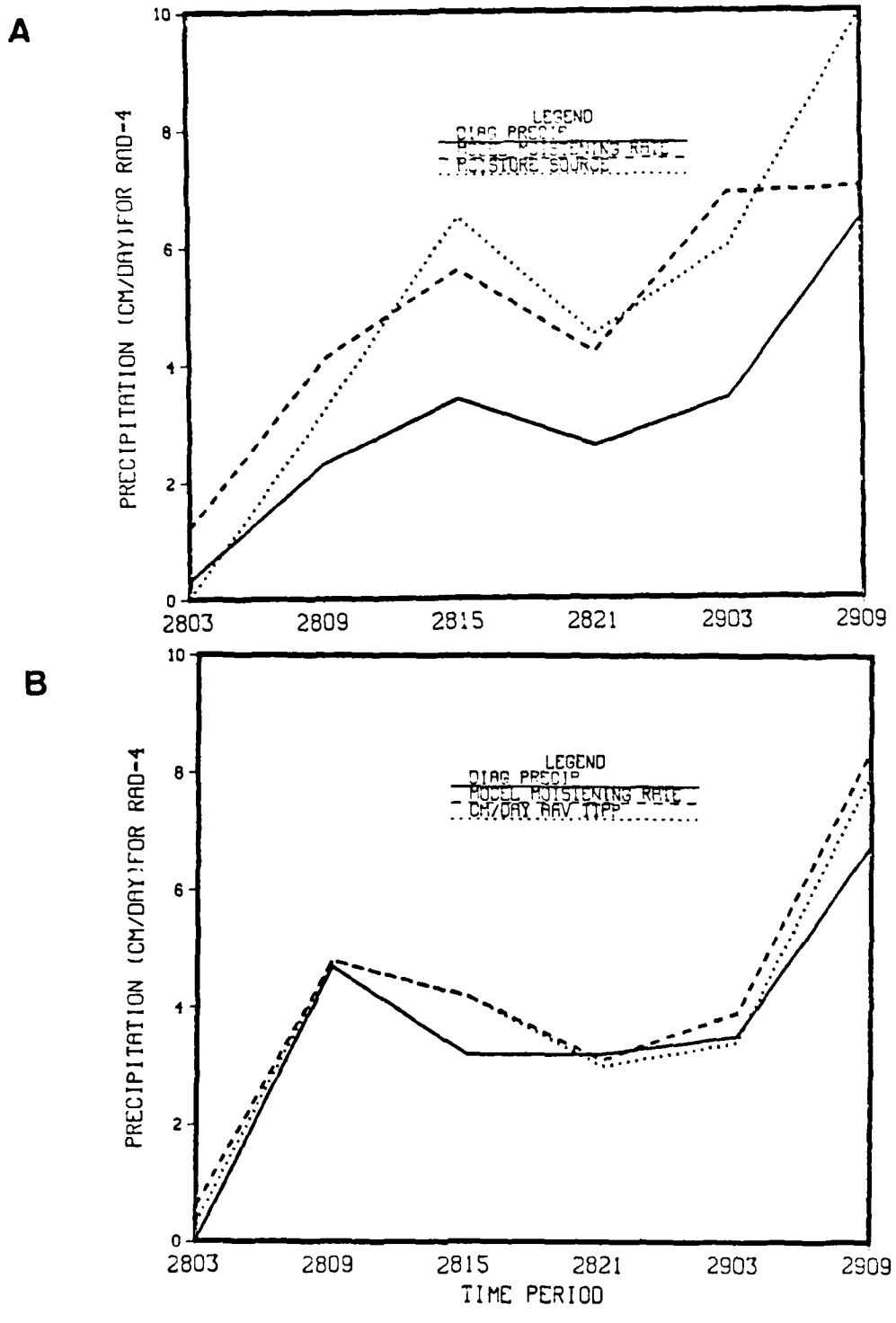

Fig. C.8 Column-integrated moisture budget results for radius 4 (A) old and (B) new forecast. Units are cm/day. Solid line represents the budget residual, dashed line is the model-predicted moistening rate (accumulated) and the dotted line is the model precipitation.

LIST OF REFERENCES

Anthes, R. A., Y. H. Kuo, and J. R. Gyakum, 1983: Numerical simulation of a case of explosive maritime cyclogenesis. *Mon. Wea. Rev., 100*, 1174-1188.

Arakawa, A., and V. R. Lamb, 1977: Computational design of the basic dynamic process of the UCLA general circulation models. *Methods in Computational Physics*, 17, Academic Press, 173-265.

Blackadar, A. K., 1979: High resolution models of the planetary boundary layer. *Advances in Environmental Science and Engineering, Vol. 1*, Gordon and Breach, 50-85.

Bosse, T. E., 1984: Estimations of diabatic heating for an explosively- developing maritime cyclone. M.S. Thesis, Naval Postgraduate School, 158 pp.

Calland, W. E., 1983: Quasi-Lagrangian diagnostics applied to an extratropical explosive cyclogenesis in the North Pacific. M.S. Thesis, Naval Postgraduate School, 152 pp.

Chang, C. B., D. J. Perkey, and C. W. Kreitzberg, 1982: A numerical case study of the effects of latent heating on a developing wave cyclone. *J. Atmos. Sci., 39*, 1555-1570.

--------, --------, --------, 1984: Latent heat induced energy transformations during cyclogenesis. *Mon. Wea. Rev., 112*, 357-367.

Charney, J.G., and A. Eliassen, 1964: On the growth of the hurricane depression. *J. Atmos. Sci., 21*, 68-75.

Cook, W. A., 1983: A quasi-Lagrangian diagnostic investigation of rapid cyclogenesis in a polar air stream. M.S. Thesis, Naval Postgraduate School, 147 pp.

Danard, M. B., 1964: On the influence of release latent heat on cyclone development. *J. Appl. Meteor., 3*, 27-37.

--------, 1966: On the contribution of released latent heat to changes in available potential energy. *J. Appl. Meteor., 5*, 81-84.

Deardorff, J. W., 1972: Parameterization of the planetary boundary layer for use in general circulation models. *Mon. Wea. Rev., 100*, 93-106.

Ferguson, E. W., F. P. Ostby, P. W. Leftwich, and J. E. Hales, 1986: The tornado season of 1984. *Mon. Wea. Rev., 114*, 624-635.

Fuelberg, H.E., Y.-J. Lin and H.-W. Chang, 1986: A moisture analysis of the meso-β scale thunderstorm environment during AVE-SESAME V (20-21 May 1979). *Mon. Wea. Rev., 114*, 534-545.

Gall, R. L., 1976: The effects of released latent heat in growing baroclinic waves. *J. Atmos. Sci., 33*, 1686-1701.

Gyakum, J. R., 1983a: On the evolution of the QE-II Storm. I: Synoptic aspects. *Mon. Wea. Rev., 111*, 1137-1155.

Gyakum, J. R., 1983b: On the evolution of the QE-II Storm. II: Dynamic and thermodynamic structure. *Mon. Wea. Rev., 111*, 1156-1173.

Haltiner, G. J., and R. T. Williams, 1980: *Numerical Prediction and Dynamic Meteorology, Second Edition*, John Wiley and Sons, 226-230.

Hodur, R. M., 1982: Description and evaluation of NORAPS: The Navy Operational Regional Atmospheric Prediction System. *Mon. Wea. Rev., 110*, 1591-1602.

--------, 1984: A numerical study of the Pacific polar low. Ph.D. Thesis, Department of Meteorology, Naval Postgraduate School, 130-143.

Johnson, D. R., and W. K. Downey, 1975: Azimuthally averaged transport and budget equations for storms: Quasi-Lagrangian Diagnostics. *Mon. Wea. Rev., 103*, 967-979.

Katayama, A., 1974: A simplified scheme for computing radiative transfer in the troposphere. Tech. Rep. *No. 6*, Dept. Met., UCLA, 77 pp.

Kocin, P.J., L. W. Uccelini, J.W. Zack, and M.L. Kaplan, 1984: Recent example of mesoscale numerical forecasts of severe weather events along the East Coast. *NASA Technical Memorandum, 86172* 57 pp.

Kuo, H. L., 1965: On formation and intensification of tropical cyclones through latent heat release by cumulus convection. *J. Atmos. Sci., 22*, 40-63.

Kuo, Y.-H., and R. A. Anthes, 1984: Accuracy of dianostic heat and moisture budgets using SESAME-79 field data as revealed by observing system simulation experiments. *Mon. Wea. Rev., 112*, 1465-1481.

Liou, C.-S., and R. L. Elsberry, 1985: Physical processes in prediction of explosive maritime cyclogenesis. *Preprints of Seventh Conference on Numerical Weather Prediction*, Amer. Meteor. Soc., Boston, MA, 212-218.

Mak, M., 1982: On moist quasi-geostrophic baroclinic instability. *J. Atmos. Sci., 39,* 2028-2037.

Nieuwstadt, F. T-M. and H. Tennekes, 1981: A rate equation for the nocturnal boundary layer height. *J. Atmos. Sci., 38,* 1418-1428.

O'Brien, J. J., 1970: Alternative solutions to the classical vertical velocity problem. *J. Appl. Meteor., 2,* 197-203.

Ooyama, K., 1964: A dynamical model for the study of tropical cyclone development. *Geofis. Int., 4,* 187-198.

Rasmussen, E., 1979: The polar low as an extratropical CISK-disturbance. *Quart. J. Roy. Meteor. Soc., 105,* 531-549..

Sanders, F., and J. R. Gyakum, 1980: Synoptic-dynamic climatology of the "Bomb". *Mon. Wea. Rev., 108,* 1589-1606.

Sardie, J. M., and T. T. Warner, 1983: On the mechanism for the development of polar lows. *J. Atmos. Sci., 40,* 869-881.

Sasamori, T., 1968: The radiative cooling calculation for application to general circulation models. *J. Appl. Met., 7,* 721-729.

Smith, P. J., P. M. Dare, and S.-J. Lin, 1984: The impact of latent heat release in synoptic-scale vertical motions and the development of an extratropical cyclone system. *Mon. Wea. Rev., 112,* 2421-2430.

Stull, R. B., 1976: Mixed-layer depth model based on turbulent energetics. *J. Atmos. Sci., 33,* 1268-1278.

Toll, R. F., 1986: A linear stability analysis of the rapid development of an extratropical cyclone. M. S. Thesis, Naval Postgraduate School, 108 pp.

Wash, C. H., 1978: Diagnostics of observed and numerically simulated extratropical cyclones. Ph.D. Thesis, Department of Meteorology, University of Wisconsin, 215 pp.

INITIAL DISTRIBUTION LIST

		No. Copies
1.	Defense Technical Information Center Cameron Station Alexandria, VA 22304-6145	2
2.	Library, Code 0142 Naval Postgraduate School Monterey, CA 93943-5000	2
3.	Chairman (Code 63Rd) Department of Meteorology Naval Postgraduate School Monterey, CA 93943-5000	1
4.	Chairman (Code 68Mr) Department of Oceanography Naval Postgraduate School Monterey, CA 93943-5000	1
5.	Professor R. Elsberry (Code 63 Es) Department of Meteorology Naval Postgraduate School Monterey, CA 93943-5000	4
6.	Professor C.-S. Liou (Code 63 Lq) Department of Meteorology Naval Postgraduate School Monterey, CA 93943-5000	2
7.	Professor C. Wash (Code 63 Wx) Department of Meteorology Naval Postgraduate School Monterey, CA 93943-5000	1
8.	LT Robert E. Rau 2952 Flameglow St. Louis, Mo. 63129	2
9.	Director Naval Oceanography Division Naval Observatory 34th and Massachusetts Avenue NW Washington, DC 20390	1
10.	Commander Naval Oceanography Command NSTL Station Bay St. Louis, MS 39522	1
11.	Commanding Officer Naval Oceanographic Office NSTL Station Bay St. Louis, MS 39522	1
12.	Commanding Officer Fleet Numerical Oceanography Center Monterey, CA 93943	1
13.	Commanding Officer Naval Ocean Research and Development Activity NSTL Station Bay St. Louis, MS 39522	1

14. Commanding Officer 1
Naval Environmental Prediction Research Facility
Monterey, CA 93943

15. Chairman, Oceanography Department 1
U.S. Naval Academy
Annapolis, MD 21402

16. Chief of Naval Research 1
Naval Ocean Research and Development Activity
800 N. Quincy Street
Arlington, VA 22217

17. Commanding Officer 1
Naval Eastern Oceanography Center
Naval Air Station
Norfolk, VA 23511

18. Commanding Officer 1
Naval Western Oceanography Center
Box 113
Pearl Harbor, HI 96860

19. Commanding Officer 1
Naval Oceanography Command Center, Rota
Box 31
FPO San Francisco, CA 09540

20. Commanding Officer 1
Naval Oceanography Command Center, Guam
Box 12
FPO San Francisco, CA 96630

21. LT Dan Soper 1
134 Brownell Circle
Monterey, CA 93940

22. Dr. R. Hodur 1
Naval Environmental Prediction Research Facility,
Naval Postgraduate School
Monterey, CA 93943

END

1-87

DTIC